Vol. 78, A, Part II (April to June) 2008 ISSN 0369-8203

Proceedings of the National Academy of Sciences, India

Section A - Physical Sciences

Published by

The National Academy of Sciences, India

5, Lajpatrai Road, Allahabad-211002

CONTENTS

Proc. Nat. Acad. Sci. India Sect. A, Vol. 78, Pt. II, 2008

We present a review of the derivation and properties of continuous and discrete Painlevé equations. We show that the properties of these systems exhibit a striking parallel.

Iodide ion–selective electrode was prepared by using silver iodide as an electroactive material. The characteristic of the electrode was studied for their possible use as an indicator electrode.

The phase diagram of acetanilide-benzoic acid system shows the formation of 1:2 addition compound followed by two side by side eutectic alloys whereas acetanilide-cinnamic acid system gives 1:1 addition compound followed by two eutectics.

Chemometric multivariate methods have been combined with synchronous fluorescence spectroscopy data to develop a reliable calibration for the estimation of kerosene fraction present in diesel.

Experiments on wastewater containing metanil yellow by photo-Fenton process were conducted at normal laboratory temperature and atmospheric pressure to examine the effect of operating variables like the concentration of ferric ion, concentration of metanil yellow, pH, hydrogen peroxide and light intensity on the reaction rate.

N

S NH$_2$

(i) $ClCOCH_2Cl$

(ii) $NH_2NH_2 . H_2O$

(iii) Ar_1 CHO

N

S NHCOCH$_2$NHN = CHAr$_1$

(3a-n)

2-Amino-4-phenyl-1,3-thiazole derivatives were synthesized and their antimicrobial activity were screened against *B. substilis, E. coli, S. aureus* and *K. pneumoneae bacteria* and *A. niger, A. flavus, F. oxisporium* and *T. viride* fungi respectively.

Recurrent almost Hermite manifolds with respect to a Riemannian connection and a semi-symmetric metric connection have been introduced and the necessary and sufficient condition for a recurrent almost Hermite manifold with respect to Riemannian connection to be recurrent almost Hermite manifold with respect to semi-symmetric metric connection has been obtained.

A mathematical model is proposed to study the effect of soil pollution on the growth dynamics of plant-herbivore system.

Using the theory of ultradifferentiable functions it is shown that there exist band-limited wavelets of infraexponential decay.

Thermally stimulated luminescence (TSL) from well synthesized crystals of $PbWO_4$, $CdWO_4$, Y_3 Al_5 O_{12}, Bi_4Ge_3 O_{12} and LiB_3O_5 characterized by XRD and DTA has been studied by TSL is found to be useful in detecting minute nonstoichiometry in these oxide crystals.

Formic Acid Monomer

Acetic Acid Monomer

Benzoic Acid Monomer

Formic Acid Dimer

Acetic Acid Dimer

Benzoic Acid Dimer

Absorption spectra of formic, acetic and benzoic acid's monomers and dimers are recorded by FTIR spectrometer. Assuming C_s point symmetry, vibrational assignments for the observed frequencies have been proposed.

PROCEEDINGS

OF THE

NATIONAL ACADEMY OF SCIENCES, INDIA

2008

VOL. LXXVIII SECTION–A PART II

Painlevé equations : from continuous to discrete

K.M. TAMIZHMANI*, A. RAMANI#, B. GRAMMATICOS** and T. TAMIZHMANI+

*Department of Mathematics, Pondicherry University, Kalapet,, Puducherry-605 014, India

#Centre de Physique Théorique, Ecole Polytechnique,CNRS, 91128 Palaiseau, France

**IMNC, Université Paris VII-Paris XI, CNRS, UMR 8165, Bât. 104, 91406 Orsay, France

+Department of Mathematics, Kanchi Mamunivar Centre for Postgraduate Studies, Puducherry, India

Received June 6, 2006; Accepted May 17, 2007

Abstract

We present a review of the derivation and properties of continuous and discrete Painlevé equations. We show that the properties of these systems exhibit a striking parallel. Thus these systems are indeed the analogues of each other.

(**Keywords** : Painlevé equations/discrete systems/integrability /discrete special functions)

Introduction

The revival of interest in integrable systems, some thirty years ago, did not follow the path traced by nineteenth and early twentieth century mathematicians who had focused mainly on the ordinary differential equations. Rather the first, seminal, modern studies concentrated on infinite-dimensional dynamical systems and the coherent structures which characterise their behaviour. The first system in which the existence of such a coherent structure was proven goes back again to the 19th century. Korteweg and de Vries[1], following the discovery of the solitary wave by Scott Russel, proposed a nonlinear evolution equation describing the propagation of long, one-dimensional, small amplitude, surface gravity waves in a shallow water channel. Written in nondimensional form this equation, known today as the KdV equation, has the form

$$u_t + uu_x + u_{xxx} = 0 \tag{1}$$

where subscripts denote partial differentiation. It was shown to possess a solitary wave solution of the form,

$$u(x, t) = 2\kappa^2 \operatorname{sech}^2(\kappa(x-\kappa^2 t-x_0)) \tag{2}$$

with κ, x_0 are constants, and thus provide the theoretical background for the interpretation of Scott Russell's observations.

Still this equation, together with most results from that era, were more or less forgotten till the advent of high-speed electronic computers which spurred the study of complex systems through numerical simulations. While investigating a model of a lattice with nonlinear interactions, Fermi, Pasta and Ulam (FPU)[2] made an astonishing discovery: instead of energy equipartition between the various modes, the system exhibited a recurrent behavior. This indicated that some stable structure persisted in the evolution of the system. Several years later, Kruskal and Zabusky[3] investigated an equation that could be interpreted as a continuous limit of the FPU model and which turned out to be the KdV equation[1]. A new astonishing discovery was made at this point: the solitary waves of KdV were stable even when interacting among themselves. This led

Kruskal and his collaborators to conjecture (and shortly afterwards to prove) the integrability of the KdV equation[4]. This integrability was of an unusual type. While the integrable partial differential equations (PDE's) known at the time were linearizable through a Cole-Hopf transformation, KdV was fundamentally different. As discovered by Gardner *et al.*[4], it could be written as the compatibility condition of an overdetermined linear system. The latter was subsequently called the Lax pair[5], a notion which became a cornerstone of the modern approach to integrability. The crucial step came with the realization that, given the Lax pair, the techniques of inverse scattering (for the reconstruction of the potential from scattering data), known also a spectral methods, could be used in order to solve the initial value problem for KdV. This discovery rekindled the interest in integrable systems, and hundreds of integrable evolution equations have been discovered since.

Another fundamental discovery was soon to follow. Ablowitz and Segur (in close collaboration with Kruskal)[6], and also Hastings and McLeod[7], made a remarkable observation. All the reductions of integrable PDE's that could be written as second order ordinary differential equations (ODE) were members of a family of equations discovered at the turn of the (previous) century by Painlevé and his school.

The aim of Painlevé was to investigate the integrability of ordinary, nonlinear, differential equations. According to Poincaré[8], to integrate a differential equation is to find, for the general solution, a finite expression, possibly multivalued, in terms of a finite number of functions. The word "finite" indicates that integrability is related to a global rather than local knowledge of the solution. However, this definition is not very useful unless one defines more precisely what is meant by function. By extending the solution of a given ordinary differential equation (ODE) in the complex domain one has the possibility, instead of asking for a global solution for an ODE, to look for solutions locally and obtain a more global result by analytic continuation. If we wish to define a function, we must find a way to treat branch points i.e. points around which two (at least) determinations are interchanged. This can be done through various uniformization procedures provided the branch points are fixed. Linear ODE's are such that all the singularities of their solutions are fixed and are thus considered integrable. In the case of nonlinear ODE's, the situation is not so simple due to the fact that the singular points in this case may depend on the initial conditions: they are movable. The intuition of Painlevé[9] was to look for those of the nonlinear ODE's the solutions of which were free from movable branch points. Painlevé managed thus to take up the challenge of Picard[10] and determine the functions defined by the solutions of second-order nonlinear equations. The success of this approach is well-known: the Painlevé transcendents have been discovered in that way and their importance in mathematical physics is ever growing.

To be more specific, Painlevé[9] studied second order differential equations of the form $x''=f(x',x,t)$, where f is rational in x', algebraic in x and analytic in t from the point of view of the singularity structure of their solutions. With the help of Gambier[11], he identified fifty equations, the solutions of which did not contain movable critical singularities. They have shown that the majority of these equations were integrable (or reducible to some other, simpler, equation among the fifty). However, six of these equations could not be integrated with the techniques available at that time. Here is the list :

*P*I $$x''=6x^2+t$$

*P*II $$x''=2x^3+tx+a$$

*P*III $$x''=\frac{x'^2}{x}-\frac{x'}{t}+\frac{1}{t}(ax^2+b)+cx^2+\frac{d}{x}$$

*P*IV $$x''=\frac{x'^2}{2x}+\frac{3x^3}{2}+4tx^2+2(t^2-a)x-\frac{b^2}{2x}$$

*P*V $$x''=x'^2\left(\frac{1}{2x}+\frac{1}{x-1}\right)-\frac{x'}{t}+\frac{(x-1)^2}{t^2}\left(ax+\frac{b}{x}\right)+\frac{cx}{t}+\frac{dx(x+1)}{x-1}$$

*P*VI $$x''=\frac{x'^2}{2}\left(\frac{1}{x}+\frac{1}{x-1}+\frac{1}{x-t}\right)-x'\left(\frac{1}{t}+\frac{1}{t-1}+\frac{1}{x-t}\right)+\frac{x(x-1)(x-t)}{2t^2(t-1)^2}$$

$$\left(a - \frac{bt}{x^2} + \frac{c(t-1)}{(x-1)^2} + \frac{(d-1)t(t-1)}{(x-t)^2}\right)$$

Here the dependent variable x is a function of the independent variable t while a, b, c, and d are parameters (constants). Painlevé's intuition led him to decide that these equations were integrable indeed, defining new transcendents. The derivation of 'Lax pairs' for the Painlevé equations did not take too long. Garnier[12] derived the linear systems that led, as compatibility conditions, to the Painlevé equations, but did not use them in order to integrate the latter. This was done for the first time by Ablowitz and Segur[13], using inverse scattering (spectral) techniques. They have shown in fact that the linearization of the Painlevé equations can be realized through integrodifferential equations.

The discoveries of Ablowitz and Segur led naturally to the formulation, in collaboration with one of us (A.R.), of the ARS conjecture[14]. Every nonlinear ODE obtained by an exact reduction of a nonlinear PDE solvable by inverse scattering techniques is of P-type. This means that all its solutions have the Painlevé property i.e. they are free of movable critical singularities. They also developed an efficient algorithm for the investigation of the Painlevé property (which has since been used with great success in the detection of integrability[15]).

We must stress one important point here. The Painlevé property as introduced by Painlevé is not just a predictor of integrability but practically a definition of integrability. As such it becomes a tautology rather than a criterion. It is thus crucial to make the distinction between the Painlevé property and the algorithm for its investigation. The latter can only search for movable branch points within certain assumptions[16]. The search can thus lead to a conclusion the validity of which is questionable: if we find that the system passes what is usually referred to as the Painlevé test (in one of its several variants) this does not necessarily mean that the system possesses the Painlevé property. Thus at least as far as its usual practical application is concerned, the Painlevé test may not be sufficient for integrability. The situation becomes further complicated if we consider systems that are integrable through quadratures and/or cascade linearisation. If we extend the notion of integrability in order to include such systems, it turns out that the Painlevé property is not related to it any more. Thus the criterion based on the singularity structure is not a necessary one in this case. Despite these considerations the Painlevé test has been of great heuristic value for the study of the integrability of continuous systems, leading to the discovery of a host of new integrable systems.

Singularity Analysis and the Painlevé Equations

As we have already hinted, singularities play an important role in determining the integrability of a given nonlinear ODE. Linear equations have only fixed singularities. Let us consider the second-order linear ODE,

$$\frac{d^2x}{dt^2} + p(t)\frac{dx}{dt} + q(t)x = 0. \tag{3}$$

A point t_0 in the neighbourhood of which p and q are analytic is called a regular point of the ODE and the solution $x(t)$ can be expressed as a Taylor series in the neighbourhood of t_0. The singular points of the solutions of the equation are located at the singular points of the coefficients p and q. A singular point t_0 is called regular if $(t-t_0)\ p(t)$ and $(t-t_0)^2\ q(t)$ are analytic in the neighbourhood of t_0[17], otherwise it is called irregular. An equation is called Fuchsian if every singular point is regular. The generalisation of these notions to a n-th order equation is straightforward.

Nonlinear equations have not only fixed singularities but movable singularities as well, i.e. singularities whose location depends on the integration constants. Various kinds of movable singularities can exist. Let us illustrate this through specific examples. (In what follows we are going to concentrate on equations that are mostly analytic, so our examples will be chosen from this class). We have:

$x' + x^2 = 0$ with solution $x = (t-t_0)^{-1}$,

$2x' + x^2 = 0$ with solution $x = (t-t_0)^{-1/2}$,

$xx'' - x' + 1 = 0$ with solution
$x = (t-t_0)\ln(t-t_0) + \alpha(t-t_0)$,

$\mu xx'' - (1 - \mu)x'^2 = 0$ with solution $x = \alpha(t-t_0)^{\mu}$,

$(xx'' - x'^2)^2 + 4xx'^3 = 0$ with solution $x = \alpha e^{(t-t_0)^{-1}}$,

$(1+x^2)x'' + (1-2x)x'^2 = 0$ with solution $x = \tan[\alpha + \ln(t-t_0)]$

where t_0 and α are the integration constants. Thus we have here as movable singularities a pole, an algebraic branch point, a logarithmic branch point, a transcendental singular point (for irrational μ) an isolated essential singularity and a nonisolated essential singularity. Everything but a pole is called a critical singularity.

The first application of singularity analysis was on first-order equations. Painlevé proved[18] that for equations of the form,

$$F(x', x, t) = 0 \tag{4}$$

with F polynomial in x' and x, and analytic in t, the movable singularities of the solutions are poles and/or algebraic branch points. Fuchs[19] showed that the only equation of the form,

$$x' = f(x, t) \tag{5}$$

where f is rational in x and analytic in t, with critical points that are all fixed, is the Riccati equation,

$$x' = a(t)x^2 + b(t)x + c(t) \tag{6}$$

Its integration is straightforward. If $a = 0$ equation (6) is linear, otherwise, the transformation

$$x = -\frac{u'}{au} \tag{7}$$

reduces the equation to a linear one of the second-order,

$$au'' - (a'+ab)u'+a^2cu = 0. \tag{8}$$

Binomial equations of the form $x'^n=f(x, t)$ have also been analysed by Briot and Bouquet[20]. They found that for $n > 1$ the following equations have the Painlevé property:

$$\left.\begin{array}{ll} x'^2 = 4x^3 + \lambda x + 1 & \text{integrable in terms of elliptic functions} \\ x'^2 = x(q(t)x + r(t))^2, & \text{reducible to a Riccati} \\ x'^3 = x^2(x-1)^2, & \text{elliptic function} \\ x'^4 = x^3(x-1)^3, & \text{elliptic function} \\ x'^6 = x^4(x-1)^3, & \text{elliptic function} \\ x'^n = q(t)x^{n-1}, & \text{integrable by quadratures.} \end{array}\right\} \tag{9}$$

Painlevé provided a systematic classification of equations of the form,

$$x'' = f(x', x, t) \tag{10}$$

with f a polynomial in x', rational in x and analytic in t, and also obtained new transcendents that appear regularly in physical applications. The starting point for Painlevé's approach was the observation that critical singularities of second-order equations can be branch points, both algebraic and logarithmic, as well as essential singularities. Painlevé developed his method (known as α – method) that made it possible to test an equation for the existence of all of these singularities in the solution. Moreover, since Painlevé was concerned by the integrability of his equations, he proposed his approach as a double method. The first part (based on the α – method) was the local study giving the necessary conditions for the absence of critical singularities. The second part was the proof of the sufficiency of the conditions and either the integration or the proof of the irreducibility of the equations. In order to illustrate the Painlevé's α – method we will examine the derivation of the first transcendental equation that bears his name and consider an equation of the form,

$$x'' = x^2 + f(t) \tag{11}$$

where $f(t)$ is analytic. This is the simplest nontrivial form of equation (10). In the spirit of ARS we can say that equation (11) does not have algebraic branch points and one need only investigate the existence of logarithmic singularities. Painlevé introduces a small parameter α by a scaling, $x = X/\alpha^2$, $t = t_0 + \alpha T$. We thus find :

$$\frac{d^2X}{dT^2} = 6X^2 + \alpha^4 f'(t_0) + \alpha^5 f'(t_0) + \frac{1}{2}\alpha^6 f''(t_0) + O(\alpha^7) \tag{12}$$

and seek a solution in the form of a power series in α,

$$X(T)=X_0(T)+\alpha X_4(T)+\alpha^5 X_5(T)+\alpha^6 X_6(T)+O(\alpha^7) \tag{13}$$

(There is no need to introduce terms proportional to (α, α^2, α^3). We find,

$$\frac{d^2X_0}{dT} = 6X_0^2 \tag{14}$$

and

$$\frac{d^2X_{r+4}}{dT^2} - 12X_0X_{r+4} = \frac{T^r}{r\,!}\frac{d^r f}{dt^r}(t_0) \tag{15}$$

for r = 0,1,2. The general solution of equation (14) is the Weierstrass elliptic function, $X_0 = \wp(T - T_0;\ 0, h)$ with h and T_0 as constants of integration. Thus the homogeneous part of equation (15) is a Lamé equation,

$$\frac{d^2Y}{dT^2} - 12\wp(T - T_0;\ 0, h)Y = 0 \tag{16}$$

and its general solution is

$$Y(T) = a\left(T\frac{d\wp}{dT} + 2\wp\right) + b\frac{d\wp}{dT} \tag{17}$$

with a,b integration constants. The solution of equation (15) is obtained by the method of variation of parameters,

$$X_{r+4} = U_{r+4}\left(T\frac{d\wp}{dT} + 2\wp\right) + V_{r+4}\frac{d\wp}{dT} \tag{18}$$

and the coefficients U, V are given by

$$\frac{d^2U_{r+4}}{dT^2} = \frac{T^r}{24r!}\frac{d^r f}{dt^r}(t_0)\frac{dX_0}{dT} \tag{19}$$

$$\frac{d^2V_{r+4}}{dT^2} = \frac{T^r}{24r!}\frac{d^r f}{dt^r}(t_0)\left(T\frac{dX_0}{dT} + 2X_0\right). \tag{20}$$

Integrating equation (19) and equation (20) we find that U and V are given in terms of elliptic functions for r=0, 1. For r=2, expanding the solution X_0 around the movable singularity at T_0, where $X_0 \approx (T - T_0)^{-2}$, we find that a logarithm appears. For the solution to be free of movable critical points it is necessary for the coefficient of the logarithm to vanish and the explicit calculation leads to

$$\frac{d^2 f}{dt^2}(t_0) = 0. \tag{21}$$

Since t_0 is arbitrary, this means that, for integrability, f must be linear in t. Apart from cases that are integrable in terms of elementary functions, one finds the PI equation,

$$x'' = 6x^2 + t \tag{22}$$

In practice, the Painlevé α- method requires the exact solution of a nonlinear ODE as well as that of inhomogeneous linear ODE's with the same homogeneous part and different inhomogeneous parts at each order. Thus, a particular solution is needed at each order for the integration. As a result the whole approach is somewhat cumbersome. This is probably the reason why Painlevé was not able to produce the total classification of second order ODE's and had to leave this task to Gambier. Gambier's approach looks very modern and is quite similar to the ARS method. He makes also the very interesting remark that the integration of the integrability condition is intimately related to the integration of the nonlinear equation itself. Let us illustrate the derivation of PI by Gambier's method. Starting with equation (11) we look for the dominant behaviour in the neighbourhood of a singularity t_0. We assume that

$$x \sim a\tau^p \tag{23}$$

where $\tau = t - t_0$ Substituting into equation (11) we find $p = -2$ and $a = 1$, corresponding to x'' and x^2 being dominant. Since p is an integer, we can

proceed further and look for the second integration constant t_0 being the first. We look in particular for the power of τ called the index according to Fuchs, or the resonance in the ARS terminology, at which this second constant appears. We introduce

$$x = \tau^{-2} + \gamma\tau^{r-2}$$

into the dominant part of equation (11). Linearizing for γ we find that

$$(r-2)(r-3) - 12 = 0, \qquad (25)$$

with roots $r = -1$, corresponding to the arbitrariness of t_0 and $r = 6$. Since this second resonance is integer we can proceed to a check of compatibility that will guarantee the absence of logarithmic branch points. We expand

$$x = \tau^{-2}\sum_{r=0}^{6} a_r \tau^r \qquad (26)$$

with $a_0 = 1$. The calculations are straightforward and we find as a condition $\frac{d^2 f}{dt^2} = 0$, i.e. f must be linear.

Gambier obtained all the equations of the Painlevé type and in particular produced a list of 24 fundamental ones[11] if one knows the solution of these 24 equations, then one can construct the solution of any other equation of the Painlevé type at order two. Here is the Gambier (t) list, where a, b, c, d, e are constants, q, r are free functions of t, and f_n, ϕ_n, ψ_n are definite functions of q and r:

G1 $x'' = 0$

G2 $x'' = 6x^2$

G3 $x'' = 6x^2 - \frac{1}{24}$

G4 $x'' = 6x^2 + t$

G5 $x'' = -3xx' - x^3 + q(x' + x^2)$

G6 $x'' = -2xx' + qx' + q'x$

G7 $x'' = 2x^3$

G8 $x'' = 2x^3 + ax + b$

G9 $x'' = 2x^3 + tx + a$

G10 $x'' = \frac{x'^2}{x}$

G11 $x'' = \frac{x'^2}{x} + ax^3 + bx^2 + c + \frac{d}{x}$

G12 $x'' = \frac{x'^2}{x} - \frac{x'}{t} + \frac{1}{t}(ax^2 + b) + cx^3 + \frac{d}{x}$

G13 $x'' = \frac{x'^2}{x} + q\frac{x'}{x} - q' + rxx' + r'x^2$

G14 $x'' = \left(1 - \frac{1}{n}\right)\frac{x'^2}{x} + qxx' - \frac{nq^2}{(n+2)^2}x^3 + \frac{nq'}{n+2}x^2$

G15 $x'' = \left(1 - \frac{1}{n}\right)\frac{x'^2}{x} + \left(f_n x + \phi_n - \frac{n-2}{nx}\right)x'$

$$-\frac{nf_n^2}{(n+2)^2}x^3 + \frac{n(f_n' - f_n\phi_n)}{n+2}x^2 + \psi_n - \phi_n - \frac{1}{nx}$$

G16 $x'' = \frac{x'^2}{2x} + \frac{3x^3}{2}$

G17 $x'' = \frac{x'^2}{2x} + \frac{3x^3}{2} + 4ax^2 + 2bx - \frac{c^2}{2x}$

G18 $x'' = \frac{x'^2}{2x} + \frac{3x^3}{2} + 4tx^2 + 2(t^2 - a)x - \frac{b^2}{2x}$

G19 $x'' = \frac{x'^2 - 1}{2x}$

G20 $x'' = x'^2\left(\frac{1}{2x} + \frac{1}{x-1}\right)$

G21 $x'' = x'^2\left(\frac{1}{2x} + \frac{1}{x-1}\right) + (x-1)^2\left(ax + \frac{b}{x}\right)$

$+cx + \frac{dx}{x-1}$

G22 $x'' = x'^2\left(\frac{1}{2x} + \frac{1}{x-1}\right) - \frac{x'}{t} + \frac{(x-1)^2}{t^2}$

$\left(ax + \frac{b}{x}\right) + c\frac{x}{t} + \frac{dx(x+1)}{x-1}.$

G23 $x'' = \frac{x'^2}{2}\left(\frac{1}{x} + \frac{1}{x-1} + \frac{1}{x-a}\right) + x(x-1)$

$(x-a)\left(b + \frac{c}{x^2} + \frac{d}{(x-1)^2} + \frac{e}{(x-a)^2}\right)$

G24 $x'' = \frac{x'^2}{2}\left(\frac{1}{x} + \frac{1}{x-1} + \frac{1}{x-t}\right) - x'\left(\frac{1}{t} + \frac{1}{t-1} + \frac{1}{x-t}\right)$

$+\frac{x(x-1)(x-t)}{2t^2(t-1)^2}\left(a - \frac{bt}{x^2} + c\frac{t-1}{(x-1)^2} + \frac{(d-1)t(t-1)}{(x-t)^2}\right)$

Third and fourth order equations were treated by Chazy and Garnier[21, 12] who attempted to obtain a Painlevé-Gambier classification at orders three and four. However, the difficulties are considerably higher and only partial classifications were obtained. Bureau[22, 23] was the only one who, before the appearance of integrable PDE's, pursued the singularity analysis approach. His method neither resembled Kovalev-skaya's nor Painlevé's. We shall not go into these details here. The two major problems that Bureau set out to solve were the analysis of the system :

$$x' = P(x,y,t), \quad y' = Q(x,y,t) \tag{27}$$

where P and Q are polynomial in x, y[22]. The rather disappointing result was that no new transcendents were found. The more general, and also more interesting, problem with P and Q rational was, unfortunately, not treated. Bureau's second problem was that of binomial equations[23],

$$x''^2 = f(x', x, t). \tag{28}$$

Although he obtained very interesting results the complete classification had to wait. Cosgrove[24,25] has given a classification of all the integrable binomial equations of the form

$$x''^n = f(x', x, t) \tag{29}$$

We list below his results, where we have tried to follow the same conventions as in the Gambier case:

SDI $x''^2 = q(t)R_3(tx' - x, x')$

SDII $x''^2 = (q(t)x' + r(t)x + s(t))^2 R_1(tx' - x, x')$

SDIII $x''^2 = (q(t)x + r(t))^2 R_2(tx' - x, x')$

SDIV $x''^2 = (q(t)x^2 + r(t)x + s(t))^2 R_1(tx' - x, x')$

SDV $x''^2 = (q(t)x + r(t))^2 R_1(tx' - x, x')$

SDVI $x''^2 = q(t)R_2(tx' - x, x')$

BPVII $x''^3 = q(t)(R_2(tx' - x, x'))^2$

BPVIII $x''^3 = (q(t)x + r(t))^3(R_2(tx' - x, x'))^2$

BPIX $x''^4 = q(t)(R_2(tx' - x, x'))^3$

BPX $x''^4 = q(t)(R_1(tx' - x, x'))^2(\tilde{R}_1(tx' - x, x'))^3$

BPXI $x''^6 = q(t)(R_1(tx' - x, x'))^4(\tilde{R}_1(tx' - x, x'))^5$

BPXII $x''^6 = q(t)(R_1(tx' - x, x'))^3(\tilde{R}_1(tx' - x, x'))^5$

BPXIII $x''^6 = q(t)(R_1(tx' - x, x'))^3(\tilde{R}_1(tx' - x, x'))^4$

BPXIV $x''^{n} = q(t)\left(R_1(tx' - x, x')\right)^{n+1}$

BPXV $x''^{n} = q(t)\left(R_1(tx' - x, x')\right)^{n-1}$

The R_i's correspond to the following expressions, where $a,b,c,\ldots$ are constants:

$$R_1 = d(tx' - x) + bx' + c$$

$$\widetilde{R}_1 = d(tx' - x) + ex' + f \tag{30}$$

$$R_2 = a(tx' - x)^2 + bx'(tx' - x) + cx'^2 + d(tx' - x) + ex' + f$$

$$R_3 = a(tx' - x)^3 + bx'(tx' - x)^2 + cx'^2(tx' - x) + dx'^3 + e(tx' - x)^2 + fx'(tx' - x) + gx'^2 + h(tx' - x) + kx' + l$$

The integration of these equations led to the following results.

SDI : This is the 'master' equation. Its solution can be given in terms of all Painlevé transcedents from PVI to PI depending on the parameter values.

SDII : can be reduced to a second-order linear equation,

SDIII : integrated in terms of PV or PIII,

SDIV : integrated in terms of PIV,

SDV : integrated in terms of PI,

SDVI : can be reduced to second-order linear equation,

BPVII : integrated in terms of PIV or PI,

BPVIII : integrated in terms of PII or Airy functions,

BPIX : integrated in terms of elliptic functions,

BPX : integrated in terms of PII or Airy functions,

BPXI : integrated in terms of elliptic functions,

BPXII : integrated in terms of elliptic functions,

BPXIII : integrated in terms of PI,

BPXIV : solved by quadratures,

BPXV : solved by quadratures.

The important remark here is that no new transcendent was found in this generalisation of Painlevé's work. In an unpublished work Cosgrove has completed the study of equations of the form

$$(x'')^2 + x''f(x', x, t) + g(x', x, t) = 0 \tag{31}$$

and, again, no new transcendent has been obtained. So it looks rather safe to assume that the only second-order transcendents are the ones defined by the six known Painlevé equations.

Properties of the Painlevé Equations

The Painlevé equations possess a host of properties which make them unique among second-order ODEs. In what follows we present a (non exhaustive) list of these properties.

(a) Degeneration cascade

The continuous Painlevé equations, through coalescence of singularities, form a degeneration cascade[17]. Starting from the highest we can, through appropriate limiting processes, obtain the lower ones (after some rescalings and changes of variables):

$$\begin{array}{ccccc} \text{PVI} & \to & \text{PV} & \to & \text{PIV} \\ & & \downarrow & & \downarrow \\ & & \text{PIII} & \to & \text{PII} \to \text{PI} \end{array}$$

Note that PIV and PIII are at the same level since they can both be obtained from PV. Moreover both PIV and PIII degenerate to PII with the appropriate coalescence. In fact, starting from PIV

$$X'' = \frac{X'^2}{2X} + \frac{3X^3}{2} + 4TX^2 + 2\left(T^2 - A\right)X - \frac{B}{X} \tag{32}$$

and putting $X = \frac{2}{\varepsilon^3} + \frac{x}{\varepsilon}$, $T = -\frac{2}{\varepsilon^3} + t\varepsilon, A = -\frac{2}{\varepsilon^6} + \mu$ and $B = \frac{8}{\varepsilon^{12}}$ we obtain, at the limit $\varepsilon \to 0$ the PII equation

$$x'' = 2x^3 + 8tx + 4\mu \tag{33}$$

in a slightly noncanonical form.

Similarly starting from PIII

$$X''=\frac{X'^2}{X}-\frac{X'}{T}+\frac{1}{T}\left(AX^2+B\right)+CX^2+\frac{D}{X}. \quad (34)$$

We put $X=1+2\varepsilon x$, $T=1+\varepsilon^2 t$, $A=-\frac{1}{2\varepsilon^6}$, $B=-A+\frac{2\mu}{\varepsilon^3}$, $C=\frac{1}{4\varepsilon^6}$, $D=-C$ and obtain again, at the limit $\varepsilon \to 0$ PII equation for x as a function of t

$$x''=2x^3+tx+\mu \quad (35)$$

in canonical form.

(b) Lax pairs

As we explained in the introduction the Painlevé equations can be obtained from the compatibility of a linear system of PDEs. Lax pairs are known for all six Painlevé equations. They have the general form :

$$\psi_\zeta = A\psi \quad (36)$$

$$\psi_t = B\psi \quad (37)$$

where ζ is the spectral parameter and A, B are matrices depending explicitly on ζ and the dependent as well as the independent variables w and t. The continuous P equation is obtained from the compatibility condition $\psi_{\zeta t}=\psi_{t\zeta}$ leading to :

$$A_t - B_\zeta + AB - BA = 0. \quad (38)$$

We illustrate this in the case of the PIV equation. Its Lax pair is[26] :

$$A=\zeta\begin{pmatrix}1 & 0\\ 0 & -1\end{pmatrix}+\begin{pmatrix} t & u\\ \frac{2}{u}(v-\theta_0-\theta_\infty) & -t\end{pmatrix}$$

$$+\zeta^{-1}\begin{pmatrix}\theta_0-v & -\frac{uw}{2}\\ \frac{2v}{uw}(v-2\theta_0) & -(\theta_0-v)\end{pmatrix} \quad (39)$$

$$B=\zeta\begin{pmatrix}1 & 0\\ 0 & -1\end{pmatrix}+\begin{pmatrix}0 & u\\ \frac{2}{u}(v-\theta_0-\theta_\infty) & 0\end{pmatrix} \quad (40)$$

The compatibility leads to:

$$\left.\begin{aligned}\frac{dw}{dt}&=-4v+w^2+2tw+4\theta_0\\ \frac{du}{dt}&=-u(w+2t)\\ \frac{dv}{dt}&=\frac{2v^2}{w}+\left(\frac{4\theta_0}{w}-w\right)v+(\theta_0+\theta_\infty)w\end{aligned}\right\} \quad (41)$$

which results to PIV

$$\frac{d^2w}{dt^2}=\frac{1}{2w}\left(\frac{dw}{dt}\right)^2+\frac{3w^3}{2}+4tw^2+2\left(t^2+a\right)w+\frac{b}{w}. \quad (42)$$

The parameters a, b are related to the monodromy exponents, θ_0, θ_∞ through:

$$a=1-2\theta_\infty, b=1-8\theta_0^2. \quad (43)$$

Similar results have been obtained for all the Painlevé equations.

(c) Miura and Bäcklund relations

The Painlevé equations possess several relations which either connect two different equations or the same equation for different values of the parameters. In the first case we have a Miura transformation while in the second one we have an auto-Bäcklund (or Schlesinger) transformation.

The (probably) best known Miura among the Painlevé equation is the one relating PII to the 34th equation in the canonical list of 50 established by Gambier and which is known as P34. The starting point is the Miura pair[27]

$$\left.\begin{aligned}aw&=u'+u^2+\frac{t}{2}\\ u&=\frac{w'+1}{2w}\end{aligned}\right\} \quad (44)$$

Eliminating w we obtain the PII equation

$$u'' = 2u^3 + tu - \left(\alpha + \frac{1}{2}\right) \tag{45}$$

while eliminating u we find P34

$$w'' = \frac{w'^2}{2w} + 2\alpha w^2 - tw - \frac{1}{2w}. \tag{46}$$

Miura transformations are also the starting point for the derivation of the auto-Bäcklund transformations of the Painlevé equations

We illustrate the auto-Bäcklund transformations by presenting the one of PV :

$$v'' = \left(\frac{1}{2v} + \frac{1}{v-1}\right)v'^2 - \frac{v'}{z} + \frac{(v-1)^2}{z^2}\left(\alpha v + \frac{\beta}{v}\right)$$

$$+ \frac{\gamma v}{z} + \frac{\delta v(v+1)}{v-1}. \tag{47}$$

Before giving the auto-Bäcklund transformations we introduce a new, more convenient parametrisation. First through the appropriate scaling of the independent variable z we put $2\delta = -1$. We write $2\alpha = (n-p)^2$, $2\beta = -(n+p)^2$, $\gamma = -2q$. Furthermore, introducing the two independent signs $\varepsilon = \pm 1$, $\eta = \pm 1$, we have $\sqrt{2\alpha} = \varepsilon(n-p)$, $\sqrt{-2\beta} = \eta(n+p)$. Thus every instance of PV is characterised by a triplet (n,p,q). We can now give the auto-Bäcklund[28]:

$$V = 1 - \frac{2zv}{zv' - \varepsilon(n-p)v^2 + (\varepsilon(n-p) - \eta(n+p) + z)v + \eta(n+p)} \tag{48}$$

which relate $v(n,p,q)$ and $V(N,P,Q)$ where (N,P,Q) are related to (n,p,q) through the following relations:

$$\left.\begin{aligned} N &= \sigma q \\ P &= \begin{cases} \sigma(1/2 - \eta n) & \text{if } \varepsilon\eta = 1 \\ \sigma(1/2 - \eta p) & \text{if } \varepsilon\eta = -1 \end{cases} \\ Q &= \begin{cases} -\eta p & \text{if } \varepsilon\eta = 1 \\ -\eta n & \text{if } \varepsilon\eta = -1 \end{cases} \end{aligned}\right\} \tag{49}$$

where $\sigma = \pm 1$ From equation (48) it is clear that the auto-Bäcklund introduces indeed four transformations depending on the signs ε, η.

(d) Particular solutions

The Painlevé equations possess special solutions, which exist only for specific values of the parameters and moreover involve only one (or zero) integration constants[29]. The simplest such case is that of PII

$$x'' = 2x^3 + tx + \mu \cdot \tag{50}$$

It is straightforward to check that when

$$\mu = \frac{\varepsilon}{2} \tag{51}$$

with $\varepsilon^2 = 1$ equation (50) possesses solutions given by the Riccati

$$x' = \varepsilon\left(x^2 + t/2\right). \tag{52}$$

The latter can be linearised by a Cole-Hopf transformation $x = \varepsilon u'/u$ leading to an Airy equation

$$u'' + \frac{t}{2}u = 0. \tag{53}$$

These special function solutions of Painlevé equations involve one integration constant.

Working with PII we shall profit in order to exhibit another type of solutions. The Painlevé equations have also rational solutions, under one constraint of the parameters, which involve no integration constant. In the case of PII we find by inspection that if $\mu = 0$, $x = 0$ is a solution. More solutions of this type can be easily constructed. We have for instance when $\mu = \varepsilon$ a rational solution is $x = -\varepsilon/t$. The other yet type of solutions exist for Painlevé equations which have at least two parameters. These solutions are expressed in terms of special functions and involve two constraints. We illustrate this in the case of the PIV equation :

$$x'' = \frac{x'^2}{2x} + \frac{3x^3}{2} + 4tx^2 + 2x\left(t^2 + \alpha\right) - \frac{2\beta^2}{x} \tag{54}$$

has linearisable solutions whenever the constraint :

$$\varepsilon_1\alpha + \varepsilon_2\beta = 1 \tag{55}$$

holds[6]. They are given by the solutions of the Riccati:

$$x' = \varepsilon_1\left(x^2 + 2tx\right) - 2\varepsilon_2\beta \tag{56}$$

Clearly, if $\beta = 0$ in which case $\alpha = \varepsilon_1$ the Riccati becomes a linear equation for $u=1/x$:

$$u' = -\varepsilon_1(2tu + 1) \tag{57}$$

The integration of equation (57) is straightforward. We find:

$$u = \left(c - \varepsilon_1 \int e^{\varepsilon_1 t^2} dt\right) e^{-\varepsilon_1 t^2} \tag{58}$$

with c an integration constant, i.e. u, or equivalently w, can be expressed in terms of the error function (of t for $\varepsilon_1 = -1$ and of it for $\varepsilon_1 = 1$).

It has been shown that the particular solutions of the Painlevé equations can be expressed as Wronskian determinants the elements of which are special functions.

(e) Contiguity relations

The contiguity relations of the Painlevé equations are a direct consequence of their auto-Bäcklund transformations. Their interest lies in the fact if we view them as mappings, they introduce discrete Painlevé equations. Let us give an example, which, if identified at the time, would have opened the domain of the discrete Painlevé equations a decade earlier. The starting point is the auto-Bäcklund of PII

$$u'' = 2u^3 + tu + m \tag{59}$$

Starting from u we compute the quantity

$$\overline{u} = -u - \frac{2m+1}{2u' + 2u^2 + t} \tag{60}$$

which is also a solution of PII with parameter $m+1$ instead of m i.e. $\overline{u} \equiv u(m+1)$. Using equation (60) and the symmetry of PII, $u(m) = -u(-m)$, we can construct also the solution $\underline{u} \equiv u(m-1)$. It suffices then to eliminate u' which leads to

$$\frac{m+1/2}{u_{m+1} + u_m} + \frac{m-1/2}{u_{m-1} + u_m} = -2u_m^2 - t \tag{61}$$

This is the contiguity relation of the solutions of PII, obtained by Jimbo and Miwa[30]. On the other hand viewed as a mapping, under the evolution of m, this is just a discrete form of PI, as can be shown by the continuous limit. Indeed, by putting $u = \rho\left(1 + \varepsilon^2 x\right), t = -6\rho^2, m = \rho^3\left(4 + \varepsilon^4 z\right)$, $\rho^3\varepsilon^5 = 1$, we find at the limit $\varepsilon \to 0$ the equation

$$x'' = 6x^2 + z \tag{62}$$

i.e. precisely PI.

The Discrete Painlevé Equations

In the past fifteen years the domain of discrete integrability has undergone a real revolution. First, physicists started realizing that discrete systems were more fundamental than continuous ones. Second, integrable discrete systems had started appearing[31], replacing the previous scarcity by a body of examples that would allow the formulation and testing of conjectures on integrability. It was in this context that we proposed[32] the singularity confinement method that has proven its efficiency as an integrability detector. The principle is in fact simple. In a rational mapping, singularities may appear spontaneously due to a particular choice of initial condition. In analogy to the continuous case we call these singularities movable. Our conjecture states that, in systems integrable by spectral methods, these singularities must disappear after a few iterations. The implementation of this method has been reviewed in detail[33]. More discrete integrability detectors appeared over the years. Most prominent among them is the method based on the computation of algebraic entropy[34]. A rigorous approach related to the Nevanlinna theory[35] should also be mentioned in this context. Since the Painlevé equations turned out to be of the utmost usefulness in the study of physical problems, it was natural to try to establish the

analogous results in the case of discrete equations. As we have mentioned in the previous section Jimbo and Miwa[30] had already obtained a discrete form of d-PI,

$$\frac{z_n}{x_{n+1}+x_n}+\frac{z_{n-1}}{x_n+x_{n-1}}=-x_n^2+a \tag{63}$$

but, its analogy to the continuous Painlevé equation was not established. The first unambiguous reference to a discrete Painlevé equation is made in the work of Brézin and Kazakov[36] who have shown (by computing the continuous limit) that a recursion relation derived in a two-dimensional model of quantum gravity, was the standard form of d-PI,

$$x_{n+1}+x_{n-1}=-x_n+\frac{z_n}{x_n}+1. \tag{64}$$

Shortly afterwards, d-PII was also obtained[37,38] and the introduction of singularity confinement allowed us to derive[39] the remaining d-P's obtaining, for the first time, q-discrete forms of Painlevé equations.

Over the years various methods for the derivation of discrete Painlevé equations have been proposed. These approaches can be cast roughly into four major classes :

(i) The ones related to some inverse problem : The discrete AKNS method, the methods of orthogonal polynomials, of discrete dressing, of non-isospectral deformations, etc. belong to this class.

(ii) The methods based on some reduction : Similarity reduction of integrable lattices is the foremost among them but this class contains the methods based on limits, coalescences and degeneracies of d–P's as well as stationary reductions of nonautonomous differential-difference equations.

(iii) The contiguity relations approach : Discrete P's can be obtained from the auto-Bäcklund, Miura and Schlesinger transformations of both continuous and discrete Painlevé equations.

(iv) The direct, constructive, approach : Two methods fall under this heading. One is the construction of discrete Painlevé equations from the geometry of some affine Weyl group. The other is the method of deautonomisation using some discrete integrability criterion like singularity confinement or algebraic entropy.

Here is the full list of standard d-P's[40]:

δ – PI $$x_{n+1}+x_{n-1}=-x_n+\frac{z_n}{x_n}+1$$

δ – PII $$x_{n+1}+x_{n-1}=\frac{z_n x_n+a}{1-x_n^2}$$

δ – PIII $$x_{n+1}x_{n-1}=\frac{(x_n-aq_n)(x_n-bq_n)}{(1-cx_n)(1-x_n/c)}$$

δ – PIV $$(x_{n+1}+x_n)(x_n+x_{n-1})=\frac{(x_n^2-a^2)(x_n^2-b^2)}{(x_n-z_n)^2-c^2}$$

q– PV $$(x_{n+1}x_n-1)(x_nx_{n-1}-1)=\frac{(x_n-a)(x_n-1/a)(x_n-b)(x_n-1/b)}{(1-cx_nq_n)(1-x_n q_n/c)}$$

δ – PV $$\frac{(x_{n+1}+x_n-z_n-z_{n+1})(x_n+x_{n-1}-z_n-z_{n-1})}{(x_n+x_{n+1})(x_n+x_{n-1})}=\frac{(x_n-z_n-a)(x_n-z_n+a)(x_n-z_n-b)(x_n-z_n+b)}{(x_n-c)(x_n+c)(x_n-d)(x_n+d)}$$

q – PVI $$\frac{(x_{n+1}x_n-q_nq_{n+1})(x_nx_{n-1}-q_nq_{n-1})}{(x_nx_{n+1}-1)(x_nx_{n-1}-1)}=\frac{(x_n-aq_n)(x_n-q_n/a)(x_n-b_n)(x_n-q_n/b)}{(x_n-c)(x_n-1/c)(x_n-d)(x_n-1/d)}$$

$z_n=\alpha n+\beta$, $q_n=q_0\lambda^n$ and a, b, c, d are constants. We distinguish difference and multiplicative equations through the use of the prefixes δ and q.

The Properties of the Discrete Painlevé Equations

The properties of the discrete Painlevé equations are in perfect analogy with those of the continuous ones. In what follows we present a (non exhaustive) list of these properties.

(a) Degeneration, through coalescence, cascades

As we have shown earlier the continuous Painlevé equations, through coalescence of singularities, form a degeneration cascade. We have shown[40] that the discrete P's follow also a degeneration cascade but the pattern may be more complicated in the discrete case.

In order to illustrate the process, let us work out in full detail the case d–PII $\rightarrow$ d–PI. We start with the equation

$$X_{n+1}+X_{n-1}=\frac{ZX_n+A}{1-X_n^2} \tag{65}$$

We put $X=1+\delta x$ whereupon the equation becomes

$$4+2\delta(x_{n+1}+x_{n-1}+x_n)=-\frac{Z(1+\delta x_n)+A}{\delta x_n} \tag{66}$$

Now, clearly, Z must cancel A up to order δ and this suggests the ansatz $Z=-A-2\delta^2 z$. Moreover, the $O(\delta^0)$ term in the right-hand side must cancel the 4 of the left-hand side and we are thus led to $A=4+2\delta a$. Using these values of Z and A we find (at $\delta\rightarrow 0$)

$$x_{n+1}+x_{n-1}+x_n=\frac{z}{x_n}+a \tag{67}$$

i.e. precisely d-PI.

Mapping equation (67) is not the only coalescence limit of d–PII. Putting $X=x/\delta$, $Z=-\frac{z}{\delta^2}$, $c=-\gamma/\delta^3$ we recover an alternate d–PI at the limit d$\rightarrow$0.

$$x_{n+1}+x_{n-1}=\frac{\gamma}{x_n^2}+\frac{z}{x_n} \tag{68}$$

On the other hand the alternate d–PI equation (68) does not belong to the same cascade but comes from an alternate d–PII[41],

$$\frac{z_{n+1}}{x_{n+1}x_n-1}+\frac{z_n}{x_n x_{n+1}+1}=-x_n+\frac{1}{x_n}+z_n+\mu. \tag{69}$$

Similar results hold for the other known discrete Painlevé equations.

(b) Lax pairs

The ultimate proof of the integrablity of the d–P's is their effective linearization, i.e. their transcription as the compatibility condition for a linear isospectral deformation problem. For the discrete Painlevé equations which are contiguities of continuous ones the Lax pair is known[42].

Let us start with the Lax pair of a continuous Painlevé equations. It has the general form :

$$\psi_\zeta=A\psi \tag{70}$$

$$\psi_z=B\psi \tag{71}$$

where ζ is the spectral parameter and A, B are matrices depending explicitly on ζ and the dependent as well as the independent variables w and z. The continuous Painlevé equation is obtained from the compatibility condition $\psi_{\zeta z}=\psi_{z\zeta}$ leading to :

$$A_z-B_\zeta+AB-BA=0. \tag{72}$$

In general, the Painlevé equation depends on parameters (α,β....) which are associated to the monodromy exponents θ_i appearing explicitly in the Lax pair. The Schlesinger transform relates two solutions Ψ and Ψ' of the isomonodromy problem for the equation at hand corresponding to different sets of parameters (α,β....) and (α',β'....). The main characteristic of these transforms is that the monodromy exponents (at the singularities of the associated linear problem), related to the sets (α,β....) and (α',β'....) differ by integers (or half-integers). The general form of a Schlesinger transformation is :

$$\Psi'=R\Psi \tag{73}$$

where R is again a matrix depending on, ζ, w, z and the monodromy exponents θ_i. The important remark is that equation (70) together with equation (73) constitute the Lax pair of a discrete equation. The latter is obtained from the compatibility conditions:

$$R_\zeta + RA - A'R = 0 \tag{74}$$

A most interesting result is the isospectral problem associated to q–PIII[43]. Here a q-difference scheme is necessary instead of a differential one,

$$\left.\begin{aligned}\Phi_n(q\zeta) &= L_n(\zeta)\Phi_n(\zeta)\\ \Phi_{n+1}(\zeta) &= M_n(\zeta)\Phi_n(\zeta)\end{aligned}\right\} \tag{75}$$

leading to

$$M_n(q\zeta)L_n(\zeta) = L_{n+1}(\zeta)M_n(\zeta). \tag{76}$$

The resulting Lax pair is written in terms of 4x4 matrices.

(c) Miura and Bäcklund relations

Just as in the continuous case[28], the d–Ps possess (auto-) Bäcklund and Miura transformations that allow to establish a dense net of relationships among them. Let us illustrate this point with the example of d–PII, written as

$$x_{n+1} + x_{n-1} = \frac{x_n(z_n + z_{n-1}) + \delta + z_n - z_{n-1}}{1 - x_n^2}. \tag{77}$$

We introduce the Miura transformation[27],

$$y_n = (x_n - 1)(x_{n+1} + 1) + z_n \tag{78}$$

and we obtain,

$$(y_n + y_{n+1})(y_n + y_{n-1}) = \frac{-4y_n^2 + \delta^2}{y_n - z_n}. \tag{79}$$

Equation (79) is d- P34, i.e. the discrete form of equation (34) in the Gambier classification, in perfect analogy to what happens in the continuous case.

An example of auto-Bäcklund transformation will be given in the case of d–PIV[44]. It is written as the pair of equations,

$$y_n = -\frac{x_n x_{n+1} + x_{n+1}(\tilde{z} + \kappa) + x_n(\tilde{z} - \kappa) + \mu}{x_n + x_{n+1}} \tag{80}$$

$$x_n = -\frac{y_n y_{n-1} + y_n(z - \tilde{\kappa}) + y_{n-1}(z + \tilde{\kappa}) + \lambda}{y_n + y_{n-1}} \tag{81}$$

where $\tilde{z} = z + \alpha/2$, $\tilde{\kappa} = \kappa + \alpha/2$ and α is the lattice spacing in the discrete variable n. The meaning of these equations is that, when one eliminates either x or y between the two he/she ends up with d–P_{IV} in the form

$$(x_n + x_{n+1})(x_n + x_{n-1}) = \frac{(x^2 - \mu)^2 - 4\kappa^2 x^2}{(x + z)^2 - \tilde{\kappa}^2 - \lambda} \tag{82}$$

$$(y_n + y_{n+1})(y_n + y_{n-1}) = \frac{(y^2 - \lambda)^2 - 4\tilde{\kappa}^2 y^2}{(y + \tilde{z})^2 - \kappa^2 - \mu} \tag{83}$$

The important remark here is that equation (82) and equation (83) are not on the same lattice (since in equation (82) the quantity $\tilde{z}$ figures in the denominator, instead of z) but, rather, on staggered lattices.

(d) Particular solutions

As mentioned already the continuous Painlevé equations PII to PVI possess elementary solutions for specific values of their parameters. Some of them are in terms of special functions (Airy, Bessel, Weber-Hermite, Whittaker and hypergeometric but also beta, gamma and error functions), while the others are just rational ones. Quite remarkably the discrete P's have the same property and, in fact, their "special function" type solutions are solutions of linear difference equations that are discretizations of the corresponding equations for the continuous special functions[45]

In order to obtain particular solutions of a d-P we first reduce the equation to a discrete Riccati, i.e. a homographic transformation, which is subsequently linearized and reduced to the equation for some special function. We shall present here the case of q-PV,

$$(x_{n+1}x_n - 1)(x_n x_{n-1} - 1) = \frac{pr(x_n - u)(x_n - 1/u)(x_n - v)(x_n - 1/v)}{(x_n - p)(x_n - r)}. \quad (84)$$

We propose the following factorization:

$$x_{n+1}x_n - 1 = \frac{pr(x_n - u)(x_n - v)}{uv(x_n z - p)} \quad (85)$$

$$x_n x_{n-1} - 1 = \frac{uvr(x_n - 1/u)(x_n - 1/v)}{(x_n z - r)}. \quad (86)$$

The two equations are compatible only when the following condition holds,

$$uv = p/r\lambda. \quad (87)$$

In this case, equations (85-86) can be cast in a more symmetric form that is in fact a discrete Riccati,

$$z(x_{n+1}x_n - 1) = px_{n+1} + \lambda r(x_n - u - v). \quad (88)$$

We can easily show that this equation is indeed related to the confluent hypergeometric/Whittaker equation. For the continuous limit we must take $\lambda = 1 + \varepsilon$, $p = 1/\varepsilon + p_0$, $r = -1/\varepsilon + p_0$, $u = 1 + \varepsilon u_1$, $v = -1 + \varepsilon v_1$, $z = e^{-n\varepsilon}$. We thus obtain at the $\varepsilon \to 0$ limit the Riccati (where $'$ denotes the z derivative),

$$x' = -x^2 + \frac{2p_0 - 1}{z}x + \frac{\kappa}{z} + 1. \quad (89)$$

where κ is related to u_1 and v_1. Next we linearize, introducing the Cole-Hopf transformation $x = a'/a$ and obtain

$$a'' = \frac{2p_0 - 1}{z}a' + \left(\frac{\kappa}{z} + 1\right)a. \quad (90)$$

Finally, we transform once more $a = we^{-z}$ and obtain a confluent hypergeometric equation for w,

$$zw'' = (2p_0 - 1 - 2z)\,w' + (\kappa + 2p_0 - 1)\,w. \quad (91)$$

We can also show that equation (88) can indeed be linearized. Solving for x_{n+1} we rewrite it as

$$x_{n+1} = \frac{\lambda r(x_n - u - v) + z}{zx_n - p}. \quad (92)$$

We introduce the discrete equivalent of a Cole-Hopf, $x = B/A$, and obtain the system,

$$\left.\begin{aligned} B_{n+1} &= \lambda r B_n + (z_n - \lambda r(u+v))\,A_n, \\ A_{n+1} &= z_n B_n - pA_n. \end{aligned}\right\} \quad (93)$$

Eliminating B we get the linear three-point mapping,

$$A_{n+2} = (p - r)\,A_{n+1} - (z_n z_{n+1} - z_n r(u+v) + pr))\,A_n = 0, \quad (94)$$

which in view of our analysis above is indeed a discrete form of the confluent hypergeometric equation, up to some straightforward transformations.

Another type of solutions do exist for discrete Painlevé equations just as in the continuous case. They are expressed in terms of special functions under two constraints. Here we shall illustrate this in the case of the d−PIV :

$$(x_{n+1} + x_n)(x_n + x_{n-1}) = \frac{(x_n^2 - a^2)(x_n^2 - b^2)}{(x_n - z_n)^2 - c^2} \quad (95)$$

where a, b, c are constants and $z_n = \delta n + z_0$. The linearisability condition is :

$$2c - a - b = \delta. \quad (96)$$

and the corresponding homographic mapping is :

$$x_{n+1} = \frac{x_n(a + b - c - z_n) - ab}{-x_n + c + z_n}. \quad (97)$$

This mapping can obviously be made linear for $y \equiv 1/x$ provided we take $ab = 0$. Taking, for instance, $b = 0$ and implementing relation (96) we obtain :

$$y_{n+1} = \frac{y_n(c+z_n)-1}{c - z_{n+1}} . \qquad (98)$$

The homogeneous part of this equation can be solved simply in terms of gamma functions whereupon the general solution of relation (98) is given in terms of a discrete quadrature. This special solution has been shown to be the discrete equivalent of the error function solution of the continuous PIV.

The discrete Painlevé equations have yet another type of solutions, namely rational ones. We shall examine them in the case of q – PIV. One obvious solution of this type is $x = \pm 1$ which exists whenever either u or v takes the value ± 1. Nontrivial solutions also exist. We have, in fact two families of such rational solutions. The first has a most elementary member,

$$x = \pm 1 \ + \ (p+r)/z \qquad (99)$$

provided u(or $1/u$) $\mp 1/\lambda$ v(or $1/v$) $\mp p/r$ (or $u \leftrightarrow v$). For the second we find

$$x = (p+r)/z \qquad (100)$$

which exists for $u = \sqrt{\lambda}$, $v = -\sqrt{\lambda}$. These rational solutions exist only on a codimension-two submanifold and, moreover, they do not contain any free integration constants.

The Geometrical Description of Discrete Painlevé Equations

As pointed out before discrete (difference) Painlevé equation can be obtained from continuous ones. In this section we are going to focus on a most interersting consequence of this construction. We start from the derivation of the alternate-d – PII equation obtained through the auto-Bäcklund transform[46] of the (continuous) PIII equation:

$$w'' = \frac{w'^2}{w} - \frac{w'}{t} + \frac{1}{t}\left(aw^2 + \beta\right) + \gamma w^2 + \frac{\delta}{w} \qquad (101)$$

Assuming $\gamma \neq 0$, $\delta \neq 0$ one can use scaling of both w and t to get $\gamma = 1$, $\delta = -1$. We have the following relations:

$$w(-\alpha, -\beta) = -w(\alpha, \beta) \qquad (102)$$

$$w(-\beta, -\alpha) = w^{-1}(\alpha, \beta) \qquad (103)$$

$$w(-\beta-2,-\alpha-2) = w(\alpha,\beta)\left(1 + \frac{2+\alpha+\beta}{t\left(\frac{w'}{w} + w + \frac{1}{w}\right) - 1 - \beta}\right) \qquad (104)$$

We assume further that $\alpha \neq \beta$. Using these relations, starting from $w(-\beta,-\alpha)$ which leads to $w(\alpha-2, \beta-2)$ we can eliminate w' and obtain a relation in $w(\alpha-2, \beta-2)$, $w(\alpha,\beta)$ and $w(\alpha+2, \beta+2)$ i.e. a one-dimensional 3-point mapping on the (α,β)-plane. We introduce the independent variable $z = (\alpha + \beta + 2)/4$ (so as to have $\Delta z = 1$) and the two parameters κ, μ through $\mu = (\beta - \alpha - 2)/4$, $\kappa = -it/2$. We choose as $x = i/w$ as the mapping variable and find :

$$\frac{z_n}{x_{n+1}x_n + 1} + \frac{z_{n-1}}{x_n x_{n-1} + 1} = \kappa\left(-x_n + \frac{1}{x_n}\right) + z_n + \mu . \qquad (105)$$

It is, moreover, straightforward to put $\kappa = 1$ through scaling (at the price of changing Δz).

One interesting question that arises naturally is whether one can play the same game with the Schlesinger transformations of the discrete equations. In other words, can we derive further discrete equations by considering the evolution along the parameters, induced by the discrete Schlesinger's? Let us examine once again the alternate d-PII[41]. The Schlesinger transform of alt-d-PII is :

$$\underset{\sim}{x}_n = \frac{1}{x_n} + \frac{\mu(1 + x_n x_{n-1})}{1 + x_n x_{n-1} - z_{n-1}x_n} . \qquad (106)$$

where $\underset{\sim}{x}$, satisfies the alt-d-PII equation with parameter $\underset{\sim}{\mu} = \mu - \Delta z$. Following the construction[41] we have also $\tilde{x}_n$ which satisfies the equation for a value of the parameter $\mu + \Delta z$. We find thus :

$$\underset{\sim}{x}_n = \left(x_n + \frac{(-\mu + \Delta z)(1 + x_n x_{n-1})}{1 + x_n x_{n-1} - z_{n-1}x_{n-1}}\right)^{-1} . \qquad (107)$$

The final step consists in eliminating x_{n-1} between equation (106) and equation (107). We obtain thus the dual equation of alt-d-PII, i.e. the equation where the parameter μ is now the independent variable ($x_n, \underset{\sim}{x}_n, \tilde{x}_n$ are associated to $\mu, \mu + \Delta z$, $\mu - \Delta z$ respectively):

$$\frac{\mu + \Delta z}{x\tilde{x} - 1} + \frac{\mu}{x\underset{\sim}{x} - 1} = x + \frac{1}{x} - \mu - z\,. \qquad (108)$$

Here we have dropped the index n, and $z \equiv z_n$ is just a parameter. We remark that equation (108) is alt-d-PII itself. The only significant change is the fact that x of the dual equation is multiplied by i with respect to the initial one.

This is a most remarkable result. The discrete equation we obtain is the same whether we consider it along the independent variable or along the parameter μ. This is the property of self-duality and we have shown that it is a general feature of discrete, difference equations[47]. It is at the origin of what we have dubbed the grand scheme which provides a unified description of discrete equations together with their Schlesinger transformation. The explanation of the self-duality for difference Painlevé equations is not difficult to grasp. A δ-Painlevé equation is obtained from the Schlesinger transformations of the parameters of a continuous one. When the latter possesses several parameters, which, in general, play the same role, one can perform the transformation to a recurrence along any of these parameters while the Schlesinger's of the remaining parameters carry over as Schlesinger's of the discrete equation. Since all these transformations are equivalent it is natural to obtain the same difference equation as a recurrence from the application of the Schlesinger's. This relation between continuous and difference Painlevé equations is also most useful for the classification of the latter. The best way of dealing with the proliferation of the difference Painlevé equations is to classify them according to geometrical criteria. Their common origin leads to a natural description in terms of Weyl groups[48].

While the case of δ-Painlevé equations appears to be settled, there remains the question of q-Painlevé equations. These are genuinely discrete equations with no relation whatsoever to the continuous Painlevé equations. So, the question is whether these equations are also self-dual. It turns out that although this is not true in general some equations are self-dual indeed. But this is immaterial. Self-duality has served its purpose, leading to the geometrical description of discrete Painlevé equations. Once this has been realised it was natural to seek a global geometrical description for all the discrete Painlevé equations.

The Sakai approach and the classification of d-P's

While in a series of works[49–52] we have undertaken the classification of d-P's based on a geometrical description, another approach has tackled the same problem and presented a global answer[50]. Our approach has been essentially constructive: starting from a given d-P equation we worked out in detail its geometric description. Sakai's[53] approach is complementary: he started from the geometry and obtained the d-P equations in the end. The approach of Sakai also draws its inspiration from the work of Okamoto[54] on continuous P's. The two key notions are the space of initial conditions and the symmetries under affine Weyl groups. Let us make these notions a little more precise.

The continuous P's are second-order differential equations. Thus one would expect the space of their initial conditions to be C^2 since for a given value t_0 of the independent variable the solution is specified by the data of the function and its derivative at this point (with some precautions concerning the points at which the coefficients of the equation become singular). However there exist solutions which diverge at t_0. Thus we must compactify C^2. Once this is done; it may happen that several solutions pass through the point at infinity. We must then separate them. The procedure is through a blowing-up of the space (i.e. through the introduction of local coordinates which make the divergence disappear).

The second idea of Okamoto, pertinent to the work of Sakai, is that of the symmetries of continuous P's under affine Weyl groups. As Okamoto has shown the auto-Bäcklund (Schlesinger) transformations of the continuous P's generate

extended affine Weyl groups and he has provided the following correspondence between equations and symmetries: PII– $A_1{}^1$, PIII – $(2A_1{}^1)$, PIV – $A_2{}^1$, PV – $A_3{}^1$, PVI – $D_4{}^1$ (equation PI has no parameters and thus no auto-Bäcklund transformation). We must point out here that Okamoto's methodology was, in spirit, closer to ours, in the sense that he started from a given equation and obtained the space of initial conditions as well as the affine Weyl group corresponding to each equation.

Sakai's approach consisted in studying rational surfaces in connection to extended Weyl groups. Surfaces obtained by successive blow-ups of P^2 or $P^1 \times P^1$ have been studied through the connections between Weyl groups and the groups of Cremona isometries on the Picard group of the surfaces. (The Picard group of a rational surface X is the group of isomorphism classes of invertible sheaves on X and it is isomorphic to the group of linear equivalent classes of divisors on X. A Cremona isometry is an isomorphism of the Picard group such that (a) it preserves the intersection number of any pair of divisors, (b) it preserves the canonical divisor K_X and (c) it leaves the set of effective classes of divisors invariant). In the case where 9 points (for P^2, or 8 points for $P^1 \times P^1$) are blown up, if the points are in a generic position, the group of Cremona isometries becomes isomorphic to an extension of the Weyl group of type $E_8{}^{(1)}$. When 9 points are not in a generic position, the classification of connections between the group of Cremona isometries and the extended affine Weyl groups was studied in full generality by Sakai. Birational (bi-meromorphic) mappings on P^2 (or $P^1 \times P^1$) are obtained by interchanging the procedure of blow-downs. Discrete Painleveé equations are recovered as birational mappings corresponding to translations of affine Weyl groups. We shall not go into the presentation of the work of Sakai. We urge the interested reader to seek out this excellent piece of work and study it carefully.

The net result of the Sakai approach is a complete classification of the d- P's in terms of affine Weyl groups. Starting from the exceptional Weyl group $E_8{}^{(1)}$ he obtained the systems corresponding to the degeneracy pattern below :
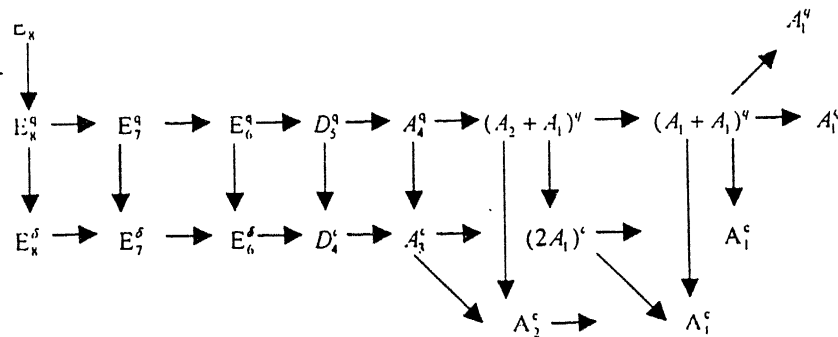
In this diagram, we assign to a Weyl group an upper index e if it supports a discrete equation involving elliptic functions, an upper index q if the equation is of q-type, an upper index δ if it is a difference equation not explicitly related to a continuous equation, and an upper index c if it is a difference equation which is explicitly the contiguity relation of one of the (continuous) Painlevé equations, namely PVI for D_4, PV for A_3, PIV for A_2 (full) PIII for $2A_1$ (which means the direct product of twice A_1 in a self-dual way), PII for the A_1 on the last line and finally the one-parameter PIII for the A_1 on the line above last. Neither PI nor the zero-parameter PIII appear here, since having no parameter they have no contiguity relations, hence no discrete difference equation related to them. Explicit expressions for the equations of this degeneration cascade have been presented in previous works of ours, up to and including, examples of elliptic-discrete Painlevé equations[55].

Conclusion

In this paper we have reviewed results on the continuous and discrete Painlevé equations. What is amazing is that even for the continuous systems, which have been known for over a century, new results keep appearing. One fundamental (and highly

nontrivial) result, due to Kruskal and collaborators[56] is the proof that the Painlevé equations do have indeed the Painlevé property. The discrete domain is the theater on an ongoing and intense activity. Still we can confidently claim that by now the discrete analogue of the whole Painlevé-Gambier classification has been established. This means that we possess today not only the discrete analogues of the Painlevé equations but also of another large class of integrable systems, that of linearisable equations.

Several extensions of the Painlevé equations can be, and have been, proposed. We have given fermionic extensions of the (continuous) Painlevé equations.[57] We have presented a first study towards the derivation of delay Painlevé equations, a domain largely unexplored[58]. The cellular-automaton analogue, based on the ultra-discretisation procedure, of discrete Painlevé equations has been the object of several studies [59]. At each step one is amazed by the richness of these simple systems, the genesis of which is due to the inspired approach of Painlevé.

References

1. Korteweg DJ & de Vries. On the change of form of long waves advancing in a rectangular canal, and on a new type of long stationary waves. *Philos Mag Ser* 1895; 5(39): 422-443.
2. Fermi E Pasta J & Ulam S. Studies of nonlinear problems, *Los Alamos Report LA*1940, 1955.
3. Zabusky NJ & Kruskal MD. Interaction of solitons in a collisionless plasmas and the recurrence of initial states. *Phys Rev Lett* 1965; **15**:240-243.
4. Gardner CS, Greene JM, Kruskal MD & Miura R. Method of solving the Korteweg-de-Vries equation, *Phys Rev Lett* 1967; **19** : 1095-1097.
5. Lax PD. Integrals on nonlinear equations of evolution and solitary waves. *Commun Pure Appl Math* 1968; **21**:467-490.
6. Ablowitz MJ & Segur H. Exact asymptotic solutions of the Korteweg-de Vries equations. *Stud Appl Math* 1977; **57**:13-44.
7. Hastings SP & McLeod JB. A boundary value problem associated with the second Painleve transcendent and the Korteweg-de Vries equation. *Arch Rat Mech Anal* 1980; **73**: 31-51.
8. Poincaré H. Les méthodes nouvelles de la Mécanique Céleste, Paris : Gauthier Villars, 1892.
9. Painlevé P. Sur les equations differentielles du second ordre et d'ordre superieur dont l'integrale generale est uniforme. *Acta Math* 1902; **25**: 1-85.
10. Picard E. Mémoire sur la thérie des functions algébriques de deux variables. *J de Math* 1889; 5(4) : 135-319.
11. Gambier B. Sur les équations differentielles du second ordre et du premier degree dont l'intégrale générale est a points critiques fixes. *Acta Math* 1909; **33**: 1-55.
12. Garnier *R.*. Sur des équations differentielles du troisiéme ordre et dont l'intégrale générale est uniforme et sur une classe d' équations nouvelles d'ordre d'ordre supérieur dont l'intégrale générale a ses points critiques fixes. *Ann Sci Ecole Norm. Sup.* 1912; **29** : 1-126.
13. Ablowitz MJ & Segur H. Exact linearization of a Painlevé transcendent. *Phys Rev Lett* 1977; **38** : 1103-1106.
14. Ablowitz MJ, Ramani A & Segur H. Nonlinear evolution equations and ordinary differential equations of Painlevé type. *Lett Nuov Cim* 1978; **23** : 333-338.
15. Ramani A, Grammaticos B & Bountis T. The Painlevé property and singularity analysis of integrable and non-integrable systems. *Phys Rep* 1989; **180**: 159-245.
16. Kruskal MD. Flexibility in applying the Painlevé test. In Levi D. and Winternitz P. editors, Painlevé Transcendents-their Aymptotics and Physical Aplications, New York : *NATO ASI, Plenum* 1992; **B278**: 187-195.
17. Ince EL. Ordinary Differential Equations, London : Dover 1956.
18. Painlevé P. Sur les équations differentielles du premier order *C R. Acad Sc Paris* 1888; **107**: 221-224 ,320-323, 724-726.
19. Fuchs L. Uber differentialgleichungen deren integrale feste verzweigungspunkte besitzen, *Sitz Akad Wiss Berlin* 1884; **32**: 669-719.
20. Briot C & Bouquet JC. Properties des functions definies par des equations differentielles *J école Imp Polytech* 1856; **36**: 133-198.
21. Chazy J. Sur des équations differentielles du troisiémeordre et d'ordre supérieur dont l'intégrale générale a ses points critiques fixes. *Acta Math* 1911; **34**: 317-385.
22. Bureau F, Garcet A & Goffar J. Transformées algébraiques des equations du second ordre dont l'intégrale générale est a points critiques fixes. *Ann Math Pura Appl* 1972; **92**: 177-191.
23. Bureau F. Equations différentielles du second ordre en y et du second degree en y dont l'intégrale généale est a points critiques fixes. *Ann Math Pura Appl* 1972; **91**: 163-281.
24. Cosgrove C & Scoufis G. Painlevé classification of a class of differential equations of the second degree. *Stud Appl Math* 1993; **88**: 25-87.
25. Cosgrove CM. All binomial-type Painlevé equations of the second order and or higher. *Stud Appl Math* 1993; **90**: 119-187.
26. Mugan U & Fokas AS. Schlesinger transformations of Painlevé II-V. *J Math Phys* 1992; **33** : 2031-2045.

27. Ramani A & Grammaticos B. Miura transforms for discrete Painlevé equations. *Jour Phys A* 1992; **25** : L633-L637

28. Fokas AS & Ablowitz MJ. On a unified approach to transformations and elementary solutions of Painlevé equations. *J Math Phys* 1982; **23**: 2033-2042.

29. Gromak VA & Lukashevich NA. The analytic solutions of the Painlevé equations *(in Russian)* :Universitetskoye Publishers, Minsk 1990.

30. Jimbo M & Miwa T. Monodromy preserving deformation of linear ordinary differential equations with rational coefficients II. *Physica D,* 1981; **2** : 407-448.

31. Quispel GRW, Roberts JAG & Thompson CJ. Integrable mappings and soliton equations II. *Physica D* 1989; **34** : 183-192.

32. Grammaticos B, Ramani A & Papageorgiou VG. Do integrable mapping have the Painlevé property? *Phys Rev Lett* 1991; **67:** 1825-1828.

33. Ramani A, Grammaticos B, & Papageorgiou V. Singularity Confinement. In Levi D, Vinet L. Winternitz P. editors. Symmetries and Integrability of Difference Equations. *CRM Lecture Notes* 1996; **9** : 303-318.

34. Hietarinta J & Viallet C. Singularity confinement and chaos in discret systems. *Phys Rev Lett* 1998; **81** : 325-328.

35. Ablowitz MJ, Halburd R & Herbst B. On the extension of the Painlevé property to difference equations. *Nonlinearity* 2000; **13 :** 889-905.

36. Brézin E & Kazakov VA. Exactly solved field theories and closed strings. *Phys Lett* B 1990; **236 :** 144-150.

37. Nijhoff FW & Papageorgiou VG. Similarly reductions and integrable lattices and discrete analogues of the Painlevé II equations. *Phys Lett* A 1991; **153** : 337-344.

38. Periwal V & Shevitz D. Ultra-matrix models as exactly solvable string theories. *Phys Rev Lett* 1990; **64** : 1326-1329.

39. Ramani A, Grammaticos B & Hietarinta J. Discrete versions of the Painlevé equations. *Phys Rev Lett* 1991; **67 :** 1829-1832.

40. Grammaticos B, Ramani A. Discreté Painlevé equations : A review. In Basil Grammaticos, Yvette Kosmann-Schwarzbach, Thamizharasi Tamizhmani, Discrete Integrable Systems. Berlin : Springer. *Lect Notes Phys* 2004; **644 :** 245-321.

41. Nijhoff F, Satsuma J, Kajiwara K, Grammaticos B & Ramani A. A study of the alternate discrete Painlevé II equations. *Inv Probl* 1996; **12:** 697-716.

42. Grammaticos B & Ramani A. Integrability in discrete world. *Chaos, Solitons & Fractals* 2000; **11 :** 7-18.

43. Papageorgiou VG, Nijhoff FW, Grammaticos B & Ramani A. Isomonodromic deformation problems for discrete analogues of Painlevé equations. *Phys Lett* A 1992; **164** : 57-64.

44. Tamizhmani KM, Grammaticos B & Ramani A. Schlesinger transforms for discrete Painlevé IV equation. *Lett Math Phys* 1993; **29 :** 49-54.

45. Tamizhmani KM, Tamizhmani T, Grammaticos B & Ramani A. Special solutions for discrete Painlevé equations. In Basil Grammaticos, Yvette Kosmann-Schwarzbach, Thamizharasi, editors, Discrete Integrable Systems, Berlin; Springer. *Lect Notes Phys* 2004; **644 :** 323-382.

46. Fokas AS, Grammaticos B & Ramani A. From continuous to discrete Painlevé equations. *J Math An and Appl* 1993; **180 :** 342-360.

47. Ramani A & Grammaticos B. The Grand Scheme for discrete Painlevé equations, Lecture at the Toda 96 symposium.

48. Okamoto K. The Painlevé equations and the dynkin diagrams. In : Decio Levi, Pavel Winternitz, editors, Painlevé Transcendents : Their Asymptotics and Physical Applications New York. *NATO ASI series* B 1992; **278 :** 299-313.

49. Ramani A, Ohta Y, Satsuma J & Grammaticos B. Self-duality and Schlestinger chains for the asymmetric dP II and qP III euqations. *Comm Math Phys* 1998; **192 :** 67-76.

50. Ramani A, Grammaticos B & Ohta, Y. Geometrical description of the discrete Painlevés VI and V equations. *Comm Math Phys* 2001; **217 :** 315-329.

51. Ramani A, Grammaticos B & Ohta Y. The q-Painlevé V equation and its geometrical description. *J Phys A* 2001; **34** : 2505-2513.

52. Ohta Y, Ramani A & Grammaticos B. An affine Weyl group approach to the 8-parameter discrete Painlevé equations. *J Phys A* 2001; **34** : 1052310532.

53. Sakai H. Rational surfaces associated with affine root systems and geometry of the Painlevé equations. *Commun Math Phys* 2001; **220** : 165-229.

54. Okamoto K. Sur les feuilletages associé aux equations du second ordre a points critiques fixes de P. Painlevé *Japan J Math* 1979; **5** : 1-79.

55. Ohta Y, Ramani A & Grammaticos B. Elliptic discrete Painlevé equations. *J Phys A* 2002; **35** : L653-L59.

56. Kruskal MD, Tamizhmani KM, Joshi N & Costin O. The Painlevé property: a simple proof for Painlevé equation III, in preparation.

57. Ramani A, Carstea S & Grammaticos B. Fermionic extensions of Painlevé equations. *Phys Lett A* 2001; **292** : 115-119.

58. Grammaticos B, Ramani A & Moreira IC. Delay-differential equations and the Painleve transcenents. *Physica A* 1993; **196** : 574-590.

59. Grammaticos B, Ohta Y, Ramani A, Takahashi D & Tamizhmani KM. Cellular automata and ultra-discrete Painlevé equations. *Phys Lett A* 1997; **226** : 53-58.

Application of precipitation based iodide ion-selective electrode in pharmaceutical analysis

ANITA SINGH and V.S. TRIPATHI

Electrochemical Sensors Laboratory, Department of Chemistry, University of Allahabad, Allahabad-211002 (U.P.) INDIA.

Email : anita.singh.01@gmail.com

Received January 10, 2007; Finally Revised June 1, 2007; Accepted July 11, 2007

Abstract

Ion–selective electrodes find wide applications in direct or indirect determination of analytes because they give real time analysis. Iodide ion-selective electrode was prepared by using silver iodide as an electroactive material. The characteristic of the electrode was studied for their possible use as an indicator electrode. The iodide selective electrode exhibits Nernstian behavior with a slope of 57.0 mV per decade .The electrode has a linear dynamic range between 1×10^{-1} – 1×10^{-6} M. The response time of sensor is 80 seconds and can be used in pH range of 3 – 9. The membrane sensor was successfully applied to the determination of iodide in water samples as well as in pharmaceutical products.

(**Keywords** : iodide ion-selective electrode/potentiometric titration/pharmaceutical products)

Introduction

Determination of minute quantities of analytes by simple methods is of special interest in analytical chemistry. Iodine is an essential micronutrient and plays an important role in many biological activities such as brain function, neurological activities and thyroid function. Several analytical methods have been developed for its determination including gas chromatography[1], ion chromatography[2,3], polarogrphy[4], chemiluminescence[5], cathodic[6] and anodic stripping voltammetry[7]. However, most of these methods require expensive instrumentation. A very interesting development in the field of ion selective electrodes is the construction of electrodes that is chemically selective for anions or cations and offer potentiometric responses that differ from classical exchange based membranes. For example, Ross and Drust[8] reported a homogeneous iodide ion selective electrode based on pressed Ag_2S/AgI. Some authors also reported modified iodide ion selective electrode based on Ag_2S/AgI[9-11]. HgS/Hg_2I_2 based homogeneous iodide ion selective electrode have been developed by Sekerka and Lechner[12] . Different types of heterogeneous iodide ion selective electrodes were also proposed by some authors[13-15] .

In recent years, there has been a growing need for constructing chemical sensors for the fast and economical monitoring of pharmaceutical compounds. Potentiometric detection based on ion- selective electrodes offers the advantages of speed and ease of preparation and procedure, relatively fast response, reasonable selective of the membrane, active materials, wide linear dynamic range and low cost. In the present work simple precipitation based potentiometric membrane sensors have been reported for determination of iodide and iodide containing drugs.

Materials and Methods

Potassium iodide (BDH), silver nitrate (Thomas Baker), sodium sulphide (CDH), iodine (SRL), methanol (Merck), sulphuric acid (Merck), epoxy-resin (Araldite), sodium hydroxide (Thomas Baker), and distilled water.

Apparatus : A Philips pH meter PR 9405 M (input impedance $\geq 5 \times 10^{11}$ Ω) was used for the potential measurements. All emf measurements were carried out with the following assembly :
Hg | Hg_2Cl_2 | solution of I^- | membrane | sample solution | Hg_2Cl_2 | Hg.

pH of the solution was monitored with a convetional pH glass electrode.

Electrode preparation : A yellow precipitate of AgI was used as an electro-active material. The general procedure to prepare master membrane was to mix AgI, Ag_2S and epoxy resin (Araldite-Ciba Geigy) in 1:1:4 ratio to obtain a paste. The resulting paste was spread uniformly over a Whatman filter paper, which was kept to dry in air for 24 hours. The resulting membrane was used as a master membrane. Then the membrane was fixed at the taper end of a barrel shaped glass tube. The electrode was finally conditioned by dipping it in 1.0×10^{-1} M KI solution. A saturated calomel electrode was used as external reference electrode to maintain electrical contact

Results and Discussion

In preliminary experiments, the potential response of iodide ion-selective electrode was recorded at the concentration range of $1 \times 10^{-1} - 1 \times 10^{-7}$ M. The electrode response of sensor shows that a linear relationship exists over a concentration range $1 \times 10^{-1} - 1 \times 10^{-6}$ M. The iodide selective indicator electrode shows Nernstian slope of 57 mV per decade change in concentration of iodide ions (as shown in Fig. 1). After 1×10^{-6} M concentration potential remains constant because beyond this concentration iodide ion (I^-) selective electrode does not sense the iodide ions present in the solution.
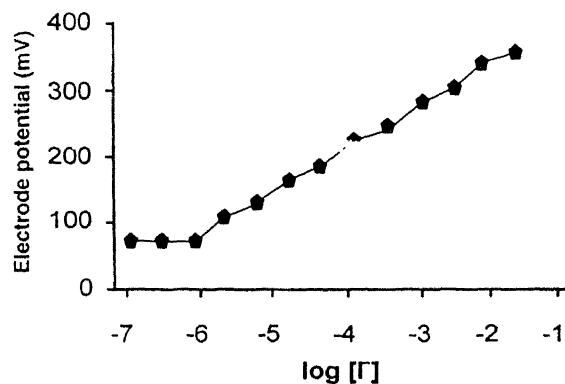
Fig. 1 – Electrode response of iodide selective electrode with change in concentration.

The electrode response time is an important factor for an ion selective electrode. In this study the electrode potential was also recorded by immediate changing of I^- concentration from 0.01 to 0.001M at different intervals of time and was found that electrode potential becomes stable after 80 seconds, which means that the response time of electrode is 80 seconds (as shown in Fig. 2). The time to reach equilibrium value depends on the direction of concentration change.
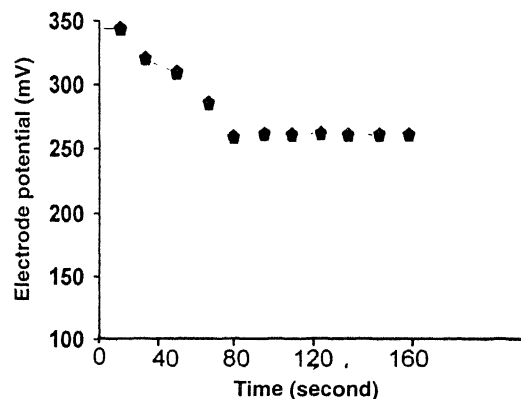
Fig. 2 – Electrode response *vs* Time.

The influence of pH of the test solution on the potential response of iodide indicator electrode was tested at 0.01 M dm^{-3} concentration of KI over a pH range of 2.0 – 13.0. It was observed that the electrode potential remained constant over a pH range of 3.0 to 9.0 as shown in Fig.3. It was observed that when the test solution contains ions other than those to which electrode is essentially reversible a change in the electrode potential depends upon the selectivity of the membrane. It is an important characteristic of ion selective electrode. The calculated selectivity coefficients are summarized in Table 1.
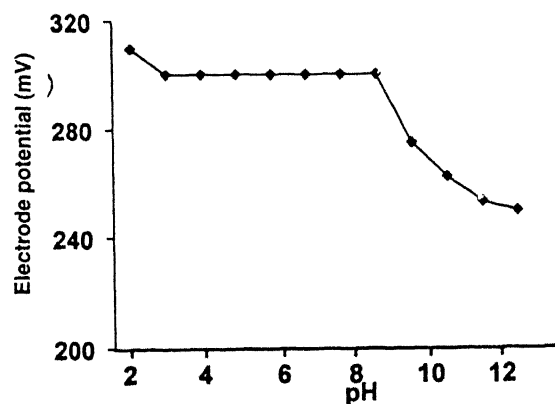
Fig. 3 – Electrode response *vs* pH.

The proposed detection system was found to be stable. The calibration slope did not change more than ± 0.5 over 6 weeks. The potentiometric selectivity coefficient reflects the relative response of the membrane sensor for the primary ion over

other ions present in the solution. Hence, it is one of the most important characteristics of an ion selective electrode. From the table it is observed that Br^- ion has highest selectivity or more interfering ion than the other ions.

Table 1 – Selectivity coefficient Ksel of several interfering anions.

X^-	Ksel
F^-	0.01
Cl^-	0.015
Br^-	0.10
NO_3^-	0.01
SCN^-	0.01
CH_3COO^-	0.035
SO_4^{2-}	0.0058
ClO_4^-	0.015

Analytical Application

The resulting electrode was applied successfully as an indicator electrode in the determination of iodide ion.

Titration of iodide solution with a standard silver nitrate solution : The proposed electrode was used as an indicator electrode in the direct titration of 50 ml of 1.0×10^{-2} M iodide solution with 0.1 M silver nitrate solution as shown in Fig. 4. From the graph it is observed that the amount of iodide ion
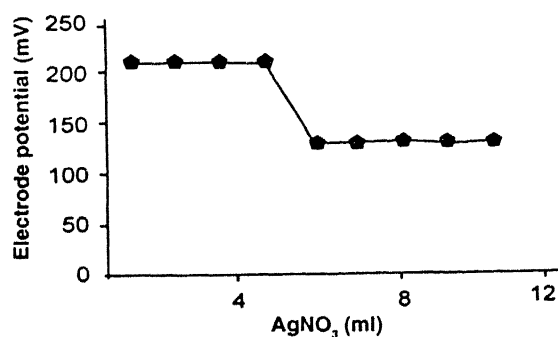
Fig 4 Titration of 50 ml of I^- (10^{-2} M) with a standard solution of silver nitrate.

can be determined from the potentiometric titration by using iodide ion selective electrode as an indicator electrode.

Determination of iodide ion in water sample : The resulting electrode was used for the determination of iodide ion added to tap water samples. The direct potentiometric titration of silver and iodide ions was carried out using the standard addition technique. The result for the determination of iodide ion at several concentrations was in good agreement with the added amount of iodide ion in water sample. The results are shown in Table 2 which indicates that the recovery of iodide ion is almost quantitative.

Table 2 – Recovery of iodide from water sample.

Water samples	added (M)	found (M)	% Recovery
Tap water	0.10	9.7×10^{-2}	97
	0.01	9.5×10^{-3}	95

Determination of iodide in drugs : The resulting electrode was also used for the determination of iodine containing drugs. For example a sample of L-thyroxin was prepared by fusing drug sample with sodium in a fusion tube. The iodide released from decomposition of the drug was determined by potentiometric titration using standardized silver nitrate solution and electrode was used as an indicator electrode. The sample of povidone-iodine (Win-Medcare Pvt. Ltd.) was prepared by refluxing 5 ml of the drug preparation in concentrated sodium hydroxide solution in the presence of zinc powder for 30 min. After cooling the resulting mixture was filtered. The filterate was acidified with sulphuric acid and diluted with water. The iodide content of the resulting mixture was determined potentiometrically by the standard addition method and electrode was used as an indicator electrode. The results are summarized in Table 3. As can be seen, in both cases, there is a satisfactory recovery of iodide from drugs sample.

Table 3 – Recovery of iodide from drugs.

Drug	taken (M)	found (M)	% recovery
L-thyroxin	1 g	0.96 g	96%
	2 g	1.89 g	93%
povidone-iodine	0.5 % w/v	0.47% w/v	94%

Conclusion

Silver iodide based ion selective electrode can be used successfully for the determination of iodide content in a wide variety of samples. The selectivity coefficient for the I^- should be very high and that for other interfering ions be negligibly small.

References

1. Shin HS, Shin YS, Kim JH & Ryu JK. Trace level determination of iodide, iodine and iodate by gas chromatography-mass spectrometry *J Chromatogr A* 1996; **732** : 327 - 333.
2. Bichsel Y & Von-Gunten U. Determination of iodide and iodate by ion chromatography with postcolumn reaction and UV/visible detection. *Anal Chem* 1999; **71** : 34 - 38.
3. BuchbergerW & Ahrer W. Combination of suppressed and non-suppressed ion chromatography with almospheric pressure ionization mass spectrometry for the determination anions. *J Chromatogr A* 1999; **850**: 99 - 106.
4. Turner JA, Abel RH & Osteryoung RA. Normal pulse polarographic analysis based on mercury anodization. sulfide and iodide. *Anal Chem* 1975; **47** : 1343 - 1347.
5. Fujiwara T, Mohammadzai H, Inoue H & Kumamaru T. Chemiluminescence determination of iodide and/or iodine using a luminol-hexadecylltrimethylammonium chloride reversed micelle system following on-line oxidation and extraction. *Analyst* 2000; **125** : 759 - 763
6. Prost RC. Cathodic pulse stripping analysis of iodine at the parts-per-billion level. *Anal Chem* 1977; **49** : 1199 - 1205.
7. Svancara I, Konvalina J, Schachl K & Vytras K. Vytras K stripping voltammetric determination of iodide with synergistic accumulation at a carbon paste electrode. *Electroanalysis* 1998; **10** : 435 - 441.
8. Ross(Jr) JW & Drust RA. Ion Selective Electrodes, NBS No. 314, 1969.
9. Orion Res. Brit Patent 1150698 [vide, Vesely, J & Stulik, K. Analyst With Ion Slective Electrodes, Ellis Horwood, Chichester 1978; p. 210], 1967.
10. Czaban JD & Rechnitz GA. Solid state ion-selective microelectrodes for heavy metals and halides. *Anal Chem* 1973; **45** : 471 - 475.
11. Wawro R & Rechnitz GA Split crystal ion selective membrane electrodes. *Anal Chem* 1974; **46** : 806 - 808.
12. Sekerka I & Lechner JF. Preparation and evaluation of halide ion-selective electrodes based on HgS matrices. *Electroanal Chem* 1976; **69** : 339 - 344.
13. Rechnitz GA, Kresz MR & Zanochnick SB. Analytical study of an iodide-sensitive membrane electrode. *Anal Chem* 1966; **38** : 973 - 976.
14. Pungor E. Theory and application of anion selective membrane electrodes. *Anal Chem* 1967; **39** : 28-45.
15. Janosova J, Senkyr J & Bartusek M. *Chem Listy* 1973; **67** : 836 [Vide, Vesely J & Stulik K. Analyst With Ion Slective Electrodes, Ellis Horwood, Chichester, 1978; p. 210].

Proc. Nat. Acad. Sci. India Sect. A, Vol. 78, Pt. II, 2008

Some studies on acetanilide based binary organic alloys

H.SHEKHAR* and K.B.PANDEY

Department of Chemistry V.K.S.University ARA-802301, India

Received May 30, 2007; Accepted July 21, 2007

Abstract

With a view to elucidate the physical organic chemistry of transparent binary eutectic and noneutectic alloys and addition compounds which are organic analogues of metal eutectic and noneutectic alloys and intemetallic compounds, respectively, the phase diagram of acetanilide based binary organic systems with benzoic acid, cinnamic acid and succinonitrile was studied. The phase diagram of acetanilide-benzoic acid system shows the formation of 1:2 addition compound whereas acetanilide-cinnamic acid system gives 1:1 addition compound followed by two eutectics. The heat of fusion data were used to compute the entropy of fusion, interfacial energy, interfacial roughness and excess integral thermodynamic functions. These thermodynamic parameters highlight the nature of interaction, stability, structure and ordering in the binary melt.

(**Keywords:** phase diagram/eutectic alloy/excess thermodynamic function)

Introduction

The evergrowing demand of materials to cater the needs of modern civilization has been compelling the chemists, physicist and metallurgists to develop new materials with specific properties at low cost. The fundamental understandings of growth from melt process and properties of multiphase materials have been a subject of extensive theoretical and experimental investigation of current interest. In recent years to study the physical organic chemistry of eutectic alloys and addition compound of organic origin, the transparent binary alloy model[1-3] has been the area of special interest to a number of research groups due to low melting and transformation temperature, good capacity of supercooling, transparency, ease in purification and minimized convection effects. In the present binary systems of acetanilide (ACT) with benzoic acid (BA) cinnamic acid (CA) and succinonitrile (SCN), the first two systems in which each component have high enthalpy of fusion are organic analogue of faceted (non metal)-faceted (non metal) systems and due to low enthalpy of fusion of SCN, ACT-SCN system belongs to faceted-nonfaceted system. These systems are selected to study their phase diagram and thermochemistry.

Experimental

The phase diagram of the binary systems was determined by thaw melt method[4-5]. Heat of fusion of materials was determined by DTA method[6].

Results and Discussion

Phase diagram

The phase diagram of ACT-BA and ACT-CA systems shows the formation of 1:2 and 1:1 addition with congruent melting point surrounded by two eutectic alloys E_1 and E_2 respectively and shown in Fig. 1 and 2. The melting temperature of 1:2 addition compound and its eutectic alloys E_1 and E_2 are 89°C, 70°C, and 80°C respectively and corresponding compositions are 0.675, 0.475 and 0.785 mole fraction of ACT whereas 1:1 addition compound and its eutectic alloys E_1 and E_2 having mole fraction 0.50, 0.30, and 0.72 of ACT respectively, correspond to melting temperature 96°C, 84°C and 65°C respectively. On addition ACT in BA or CA, the melting temperature decreases and attains as E_1 (the first eutectic alloy of the system) and then rises to maximum where the composition of solid and liquid phase is identical. A further addition of ACT causes a decrease in melting temperature till the minimum at E_2 (the second eutectic alloy of the system) is attained. A flatness at top of the curve in the phase diagram suggests that the addition compound is dissociated[7] in molten state. At the congruent point the reaction can be expressed as
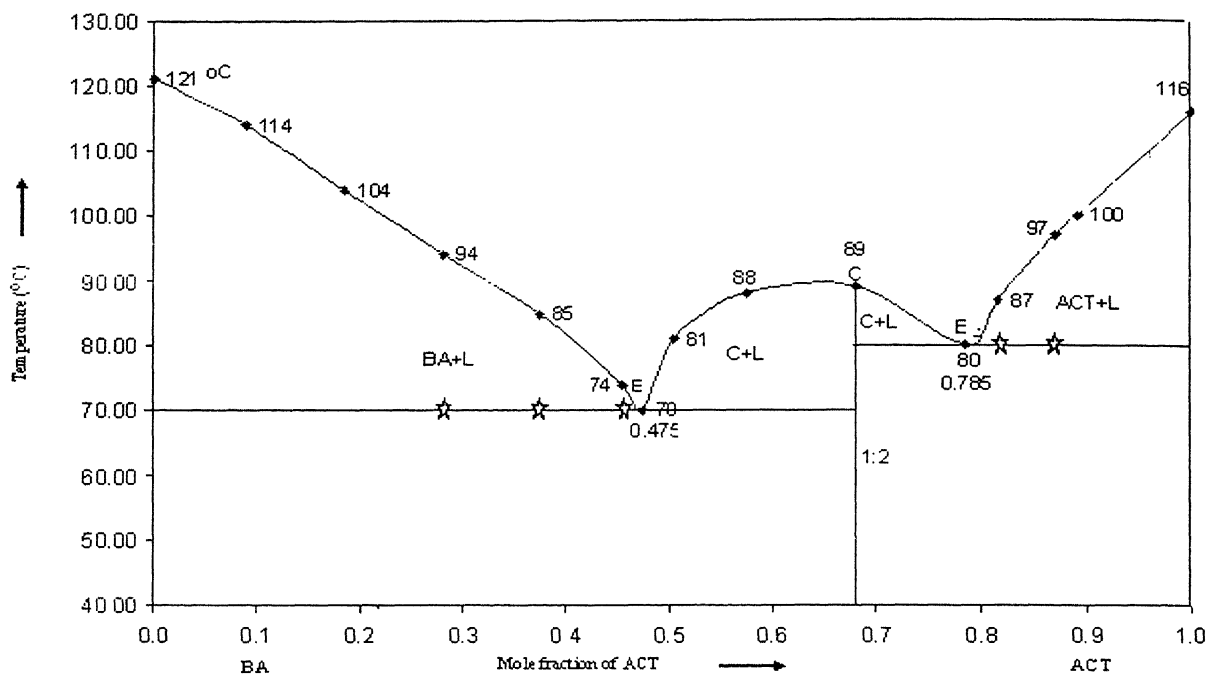
Fig.1 – Phase diagram of ACT-BA system. ★ thaw temperature. ◆ melting temperature.
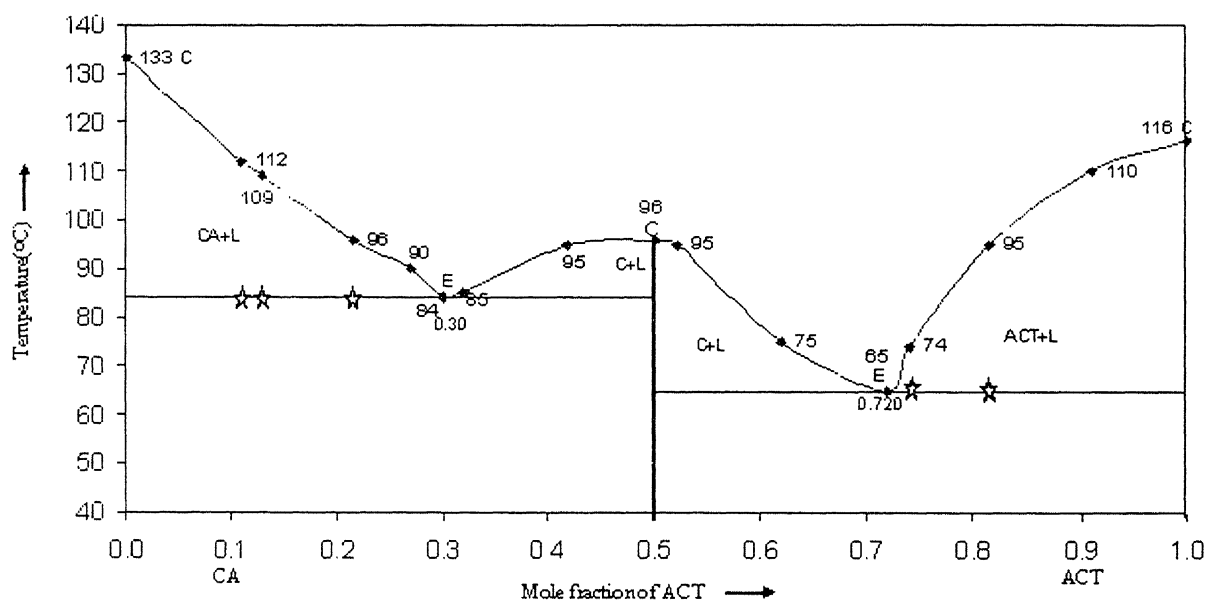
Fig.2 – Phase diagram of ACT-CA system. ★ thaw temperature. ◆melting temperature.

$$mA(solid) + nB(solid) \rightleftharpoons A_mB_n(L) \rightarrow AB(solid)$$
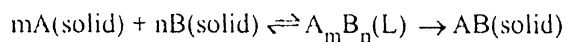
when the solid addition compound melts, the components still remain in the associated form. At the eutectic point the solid-liquid equilibrium can be represented by the reaction

$$L \rightleftharpoons S_1 + S_2$$
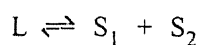
The eutectic alloy below its melting point both components (S_1 and S_2) separate out from the liquid phase (*L*) at a constant composition until the entire liquid phase disappears. The temperature-composition data of ACT-BA / ACT-CA and ACT-SCN system have been reported in Table 1. The organic alloys and compounds having good interaction between components, are confirmed earlier on the basis of magnitude of heat of mixing.

Table 1 – Mole fraction, melting temperature (M.P), heat of fusion (ΔH), entropy of fusion (ΔS), roughness parameter α ($\Delta S/R$) and interfacial energy (σ).

Alloys	Mole fraction of ACT	M.P (°C)	ΔH (kJ/mol)	ΔS (J/mol/K)	$\alpha(\Delta S/R)$	$\sigma \times 10^3$ (J/m²)
ACT-BA System						
A_2	0.090	114	17.71	45.76	5.50	29.52
A_2	0.185	104	17.96	47.63	5.73	29.89
A_3	0.280	94	18.07	49.23	5.92	30.27
A_4	0.375	85	18.29	51.81	6.23	30.66
E_1	0.475	70	18.50	53.93	6.49	31.06
Addition (1:2)	0.680	89	18.91	52.23	6.28	31.88
E_2	0.785	80	19.15	54.2	46.52	32.31
A_5	0.815	87	19.21	53.37	6.42	32.34
A_6	0.890	100	19.35	51.88	6.24	32.77
ACT-CA System						
A_1	0.110	102	22.99	59.72	7.18	35.19
A_2	0.215	96	22.59	61.22	7.36	34.92
E_1	0.300	84	22.27	62.39	7.50	34.73
Addition (1:1)	0.505	96	21.47	58.19	6.10	34.28
E_2	0.720	65	20.67	61.15	7.36	33.80
A_3	0.815	95	20.31	55.19	6.64	33.59
A_4	0.910	110	19.95	52.37	6.30	33.38
ACT-SCN System						
A_1	0.840	107	17.05	44.90	5.40	29.50
A_2	0.705	101	14.80	39.50	4.75	26.50
A_3	0.580	97	12.75	34.50	4.15	23.15
A_4	0.470	92	11.00	30.10	3.60	20.35
A_5	0.370	88	4.40	26.00	3.15	18.00
A_6	0.285	82	7.90	22.30	2.70	15.50
A_7	0.205	72	6.60	19.15	2.30	13.00
A_8	0.130	65	5.40	16.00	1.90	11.00

Thermochemistry

The growth of solid liquid interface of alloy from liquid phase is governed by interfacial energy, which is calculated from heat of fusion data. The interface morphology of material is governed by entropy and interfacial roughness factor and the thermal environment of solidification process is also the deciding factor. Heat of fusion value of ACT/ BA/CA and SCN determined by DTA method was already reported earlier[8]. Using these data in mixture law[9] the heat of fusion of binary eutectic, noneutectic alloys and addition compounds of systems of ACT with BA /CA and SCN have been computed. And with the help of heat of fusion data the entropy of fusion, interfacial energy, interfacial roughness and excess thermodynamic functions are calculated to throw light on the growth behavior and the nature of interaction between the components forming the binary alloys and compounds and are reported in Table 1.

Interfacial energy

Interfacial energy affects the magnitude of heat of fusion by interfacial tension and responsible for generating stable critical size of nucleus for the growth of the crystal. The interfacial energy (σ) is

given by the expression.

$$\sigma = C\Delta H \,/\, N^{1/3}\ V_m^{\ 2/3} \quad (1)$$

where N is Avogadro number, V_m is the molar volume and parameter C lies between 0.30 and 0.33.

Interfacial roughness

The shape, size and topology of the growing interface depend on entropy of fusion and interfacial roughness factor, which can be defined as

$$\alpha = \Delta\xi\, H \,/\, RT = \xi\, \Delta\, S/R \quad (2)$$

where ξ is crystallographic factor depending upon geometry of the molecule and the value is 1 or less than 1 and R is gas constant. The value $\alpha < 2$ for non eutectic alloys A_7 and A_8 of ACT-SCN system predicts nonfaceted growth in the alloys. The value of α except the above alloys, all the eutectic alloys and noneutectic alloys and addition compounds of all the systems being greater than 2 indicates that they solidify by faceted mechanism.

Excess thermodynamic function

The deviation from ideality originates[5] excess thermodynamic functions in integral or partial form. The excess integral free energy (g^E), excess integral enthalpy (h^E) and excess integral entropy (s^E) were calculated using the following equations[10].

$$g^E = RT\,(X_1 \ln \gamma_1^1 + X_2 \ln \gamma_2^1) \quad (3)$$

$$g_1^{-E} = RT \ln \gamma_1^1 \quad (4)$$

where g_1^{-E} is the excess partial molar free energy of component 1

$$h^E = -RT^2 (X_1\, \partial \ln\gamma_1^1 / \partial T + X_2\, \partial \ln\gamma_2^1 / \partial T) \quad (5)$$

$$s^E = -R(X_1 \ln\gamma_1^1 + X_2 \ln\gamma_2^1 + X_1 T\, \partial \ln \gamma_1^1 / \partial T + X_2 T\, \partial \ln\gamma_2^1 / \partial T) \quad (6)$$

Table 2 – Excess integral thermodynamic functions for eutectic alloys, noneutectic alloys and compounds.

Alloys	g^E (J/mol)	h^E (kJ/mol)	s^E (J/mol/K)
ACT-BA system			
A_1	698.2	7.21	16.85
A_2	787.0	5.68	12.99
A_3	662.3	– 3.16	-10.43
A_4	159.3	– 2.75	-8.24
E_1	– 274.7	1.05	3.85
Addition (1:2)	709.0	2.46	66.04
E_2	– 208.3	2.23	63.75
A_5	39.5	– 8.44	23.56
A_6	338.1	– 4.00	-11.63
ACT-CA system			
A_1	9.0	– 10.69	-27.78
A_2	– 0.0	– 0.06	0.16
E_1	– 0.1	9.52	26.68
Addition (1:1)	611.1	2.38	62.82
E_2	– 0.1	– 11.17	33.04
A_3	279.0	– 9.05	–25.35
A_4	672.1	4.444	9.84
ACT-SCN system			
A_1	1079.8	16.01	39.22
A_2	1499.8	31.73	80.83
A_3	1718.1	78.26	206.87
A_4	1731.7	33.36	86.64
A_5	1669.7	34.10	89.83
A_6	1500.5	22.73	59.81
A_7	1140.4	9.37	23.86
A_8	848.5	75.22	220.03

The activity coefficient of a component i present in the eutectic binary melt is given by

$$-\ln X_i\, \gamma_i^1 = \Delta H \,/\, R(1/T - 1/T_i^0) \quad (7)$$

where X_i, γ_i^1, ΔH, T_i^0 are the mole fraction, activity coefficient, heat of fusion and melting temperature of the component i respectively. R is gas constant and T is melting temperature of the alloys. The values of $\partial \ln \gamma_i^1 / \partial T$ can be determined by taking the slope of the liquidus curve near the binary melt in the phase diagram. The values of excess integral functions of alloys and compounds in the above manner are reported in Table 2.The positive value of g^E predicts[11] that the interaction between like molecules is stronger than between unlike molecules.

The interaction in alloys A_2, E_1, E_2 of ACT-CA system and eutectic alloys E_1 and E_2 of ACT-BA system exists between dissimilar molecules. The values h^E and s^E correspond to the excess integral free energy and are the measure of excess integral enthalpy of mixing and excess integral entropy of mixing respectively.

Acknowledgement

Thanks are due to Prof. R.K.Singh, Head, Department of Chemistry, V.K.S. University, Ara, Bihar for providing research facility.

References

1. Liu J & Elliott R. Review in molecular diversity and solid phase organic synthesis. *J Cryst Growth* 1995; **148** : 406-410.
2. Glicksman ME, Koss, MB & Winasa EA. Dendritic growth velocities in microgravity. *Phys Rev Lett* 1994; **73** : 573-580
3. Bassi PS & Sharma RP. Some physicochemical studies on binary organic eutectic and monotectic alloys. *J Ind Chem Soc* 1996; **35A** : 133-136
4. Rastogi RP & Verma KTR. Solid-liquid equilibria in solutions of non-electrollytes. *J Chem Soc* 1956; 2097-2103
5. Sangstar J. Calculation of phase diagram and thermodynamic properties of binary alloys. *J Phys Chem Ref Data* 1994; **23** : 295-317
6. Dodd JW & Togne KH. Thermal methods. In Currel BT, editor. Analytical chemistry by open learning series. Chichester : J Wiley Sons, 1987; pp. 120-127
7. Shukla BM & Singh NP. Physicochemical studies on organic eutectics and the 1:1 adition. *Mol Cryst Liq Cryst* 1984; **104** : 265-273
8. Rai US & Shekhar H. Chemistry of organic eutectics : phenanthrene-benzoic acid and phenanthrene-cinnamic acid system. *Cryst ResTechnol* 1990; **25** : 771-779
9. Rai US & Shekhar H. Direct observation on solidification of binary organic eutectic alloys. *J Therm Analys* 1993; **39** : 415-428
10. Rai US & Pandey Pinki. Physicochemical studies on organic eutectic and monotectic alloys. *J Therm Analys and Colorim* 2003; **74** : 141-150
11. Wisniak J & Tamir A. Mixing and Excess Thermodynamic Properties. First Edition, Elsevier: New York, 1978; pp. 21-34.

Proc. Nat. Acad. Sci. India Sect. A, Vol. 78, Pt. II, 2008

Development of an analytical method combining chemometrics and synchronous fluorescence: analysis of diesel-kerosene mixtures

O. DIVYA and ASHOK. K. MISHRA*

Department of Chemistry, Indian Institute of Technology-Madras, Chennai-36, India.

**Author for correspondence : Tel : (+91) 44-22574207;Fax : (+91) 44-22574202.*

E-mail :_mishra@iitm.ac.in

Received: June 27, 2007; Accepted: July 21, 2007

Abstract

Synchronous fluorescence spectroscopy (SFS) is a widely accepted technique for the analysis of multifluorophoric samples. Petroleum products are multifluorophoric since they contain a mixture of variety polycyclic aromatic compounds (PACs). In this work, chemometric multivariate methods have been combined with SFS data to develop a reliable calibration for the estimation of kerosene fraction present in diesel. Efficient and robust models are created using multivariate techniques such as principal component analysis (PCA), principal component regression (PCR) and partial least square regression (PLSR). The models developed by these methods are able to perceive very low level of kerosene contamination with low prediction error.

(**Keywords:** SFS/synchronous fluorescence/ principal component regression/ partial least squares regression)

Introduction

For multifluorophoric systems, conventional fluorescence methods are inefficient due to the extensive overlapping of excitation and emission bands. Synchronous fluorescence scan (SFS), developed by Lloyd[1], is known to be a method of choice for the simultaneous determination of multifluorophoric samples without a pre treatment. The method is simple, selective, and sensitive and has been successfully applied to simultaneous analysis of polycyclic aromatic compounds (PACs)[2,3] and petroleum products[4], thus enhancing the analytical potential of fluorescence spectroscopy. An SF spectrum is obtained by the simultaneous scanning of both the excitation and emission monochromators with a constant wavelength difference ($\Delta\lambda$) between them. Parameters needed to be optimized in the synchronous fluorescence scan based analytical methods are $\Delta\lambda$ and λ_{SFS}^{max}

Hydrocarbon fuels, generally used in automobiles, have been known to be the main source of environmental pollution. These fuels like diesel, petrol and kerosene are mixtures of various types and kinds of PACs, which are highly fluorescent. Therefore fluorescence, in contrast to conventional methods, can be used to analyze them directly[4,5]. The fluorescence studies of these hydrocarbon fuels are quite different from their origin (crude oils) as well as from each other. Development of fluorescence based method could therefore offer interesting possibilities for analysis. At higher concentrations complex energy-degrading interactions exist between the fluorophores making the analysis difficult, still petroleum products show a systematic behavior with respect to the fluorescence parameters.

Adulteration of petroleum products especially diesel has become a serious problem, particularly in Southeast Asia[6]. Common adulterants used in diesel are kerosene, industrial solvents, used lubricants and aliphatic and aromatic mixture, most common being kerosene. Easy availability of kerosene and ease in blending with diesel make the adulteration a common routine which consequently degrades the exhaust quality and deposits may degrade the engine performance[7]. Adulteration of diesel by kerosene can be monitored by various processes such as the filter test, checking properties like density, flash point and viscosity, odour based method[6], ultrasonic techniques[8], titration techniques[9] and optical techniques[10]. These techniques based on common physical properties

suffer from limitations in terms of accuracy and sensitivity in determining the adulteration level.

SFS based analytical techniques are fairly sensitive[4,5,11,12]. However, the sequence of procedure is long drawn out which involves much longer time. It requires management of a large body of data and appreciably long time for data analysis. Chemometrics, a chemical discipline which makes use of mathematical and statistical methods to chemical measurements, is very efficient in handling large bodies of data with appreciable reduction in processing time[13]. Management of large amount of the data can be made fast and efficient by combining chemometrics with SFS. Level of reliability and sensitivity can also be maintained by chemometrics methods in less time. The increasing use of chemometrics applied to the various regions of the electromagnetic spectrum is explained by its capability of treating large quantities of information. In the food and beverage industries, chemometrics along with fluorescence was applied in many instances, such as monitoring process like cheese ripening[14], bitterness in beer[15] and classification of vegetable oil according to its quality[16]. We have recently reported the determination of quantitative amounts of kerosene and petrol present in their mixture using the multivariate methods combined with SFS data[17]. In this work, synchronous fluorescence spectroscopic data in conjunction with multidimensional chemometric techniques such as PCA (principle component analysis), PCR (principal component regression) and PLSR (partial least square regression) for the classification of diesel kerosene mixtures are being reported.

Theory

A chemometric technique is an approach to analytical and measurement science that uses mathematical, statistical and other methods of formal logic to determine the properties of substances that otherwise would be very difficult to measure directly[18]. It is a powerful technique for the simultaneous determination of analytes in a mixture without any separation or extraction methods. It extracts maximum information from the data and develops a mathematical model that relates a property, such as concentration to absorbance or fluorescence intensity of a set of known reference samples at more than one wavelength. The first step is calibration which estimates the relationship between spectra and component concentrations from a set of reference samples, followed by prediction step in which the calibration plot is used to estimate the component concentrations from an unknown sample spectrum[19]. The various multivariate calibration tools adopted in this work are PCA, cluster analysis, PCR and PLSR.

Principal Component Analysis : The method which is most commonly used with multivariate data is principal component analysis[20], which is a statistical tool used for data compression and information extraction. The main aim of PCA is to reduce the large number of variables to a lesser number of principal components (PCs) that explains majority of variance in the data. This reduces the dimensionality of the data considerably enabling effective visualization, regression and classification of multivariate data.

If X is a data matrix with m rows and n columns, and with each variable being a column and each sample a row, PCA decomposes X as the sum of r, t_i and p_i, where r is the rank of the matrix X,

$$X = t_1 p_1^T + t_2 p_2^T + \dots t_k p_k^T + \dots t_r p_t^T \qquad (1)$$

Here r must be less than or equal to the smaller dimension of X, i.e., $r \leq \min\{m,n\}$. The t_i, p_i pairs are ordered by the amount of variance captured. The t_i vectors are known as scores and contain information on how the samples relate to each other. The p_i vectors are known as loadings and contain information on how the variables relate to each other. Thus the measured variables (e.g. SFS intensity at different wavelengths) are converted into new ones (scores on latent variables).

Cluster analysis : Cluster analysis is an exploratory data analysis tool for solving classification problems that involves the assessment of similarity between objects based on their measured properties (variables)[21]. It groups objects of similar kind into respective categories in a way that the degree of association between two objects is maximal if they belong to the same group and minimal otherwise. Objects are grouped in clusters in terms of their nearness in the multidimensional space. The elements

or clusters are joined with the criterion that the sum of heterogeneities of all clusters should increase as little as possible.

Principal Component Regression (PCR) and Partial Least Squares Regression (PLSR) : PCR is a two-step multivariate calibration method. In the first step, PCA of the data matrix is performed. The measured variables (e.g. absorbances at different wavelengths) are converted into new ones (scores on latent variables). This is followed by a multiple linear regression step (MLR) on the scores obtained in the PCA step. PLSR is another quantitative spectral decomposition technique that generalizes and combines features from principal component analysis and multiple regression and perform the data analysis in one step. PLSR is based on the simultaneous decomposition of two blocks of variables, X and Y which may contain spectral and concentration data respectively. Thus, in PLSR which is a single step decomposition and regression, scores are directly related to constituents of interest, whereas PCR, being a two step process scores are related to the largest common spectral variation[22-24].

Using the regression model the correlation coefficient R^2 and the parameter root mean square error of calibration (RMSE), a measure of the variabilty of the difference between the predicted and reference values for a set of samples are evaluated. RMSE is defined as

$$\mathrm{RMSE} = \sqrt{\frac{\sum_{i=1}^{n}\left(y_{\mathrm{pred}} - y_{\mathrm{ref}}\right)^2}{n}} \quad (2)$$

where y_{pred} and y_{obs} are the predicted and reference values respectively of sample i in the calibration set (or validation set or prediction set) and n is the number of samples used. RMSEC is the root mean square error of calibration, which explains how good the model is. The ability of a model to predict new sample is expressed in terms of root mean square error of cross validation (RMSECV) and that explains the ruggedness of the model. When the model is applied to a new set of data it is possible to calculate a root mean square error of prediction (RMSEP) provided the reference values for the new data set are known[23].

Materials and Methods

Apparatus : Fluorescence spectra were recorded on a Hitachi F-4500 spectrofluorimeter. For synchronous fluorescence measurement, the scan speed was 240 nm/sec and PMT voltage 700 V. Band pass for both excitation and emission monochromators were kept at 5 nm. Excitation source was 100 W xenon lamp. The corrected fluorescence spectrum was recorded in the range 200 – 600 nm and synchronous fluorescence spectra were plotted in the excitation scale. In a study of the effect of sample geometry on synchronous fluorescence characteristics of petroleum products Patra and Mishra[5] have recently shown that right angle geometry provides greater uniqueness of spectral response to a particular composition of petroleum products in a mixture.

Reagents and procedure : Diesel and kerosene were collected from the authorized local vendors in Chennai. Diesel samples with different relative kerosene fractions (in % v/v) were prepared by adding appropriate volumes of neat kerosene to neat diesel. A calibration set of 35 samples and an independent validation set of 8 samples containing varying amounts of diesel and kerosene were prepared. Relative kerosene fraction (in % v/v) in the samples varied from 0% to 100%. For 0% to 10% and 90% to 100% kerosene fraction in diesel, the interval maintained was 1% and for the range 10% to 90% the interval was 5%. Method was developed for the entire concentration range (0-100 % kerosene fraction in diesel).

Data Analysis : Preprocessing of the raw data obtained from fluorimeter and all calculations were performed on a Pentium 4 personal computer using the algorithms from the PLS_Toolbox 4.0 written on a MATLAB platform.

Results and Discussions

Synchronous fluorescence data: Synchronous fluorescence spectra of samples containing various compositions of diesel and kerosene were recorded and plotted in Fig. 1. The parameter $\Delta\lambda$ was optimized for diesel sample and was 40 nm. The peaks at 393 and 444 nm wavelengths show a gradual variation. On increasing the relative kerosene fraction (in % v/v) the peak positions get slightly blue shifted.
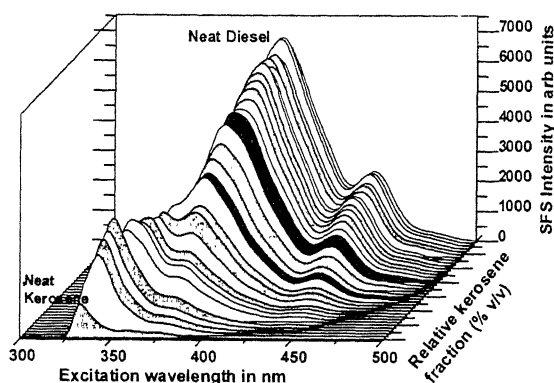
Fig. 1 – Synchronous fluorescence spectra of diesel kerosene mixtures at $\Delta\lambda$ 40 nm.

Preprocessing the SFS data : The SFS data thus obtained were arranged into a matrix characterized by samples as rows and synchronous fluorescence intensities as columns. The data were used for further analysis after preprocessing. Different preprocessing methods adopted were AUTO (auto scaling), MNCN (mean centering) and SAVGOL (Savitzky-Golay smoothing method) combined with SNV (standard normal variate scaling)[25]. SAVGOL essentially performs a local polynomial regression to determine the smoothed value for each data point on a matrix of row vectors y. At each increment a polynomial of order 2 is fitted to the number of points with width 21 surrounding the increment. An estimate for the value of the function (deriv = 0) at the increment is calculated from the fit resulting in a smoothed function y_1, where

$$y_1 = \text{savgol}\ (y,\ \text{width},\ \text{order},\ \text{deriv})$$

SAVGOL was performed with various window widths like 5, 7, 11, 15, and 21. With each output the model was built and the RMSEP values were compared and it was observed that there was a remarkable reduction in RMSEP for the window width 21. SNV, scales rows of the matrix y_1 to mean zero with unity standard deviation

$$x = \text{snv}\ (y_1)$$

Table 1 gives the RMSEP values obtained for PCR and PLSR method with different preprocessing techniques. Since SAVGOL and SNV produce the lowest RMSEP value, this was chosen as the best preprocessing method. The preprocessed data thus obtained was used for the multivariate analysis.

Table 1 – The RMSEP values of PLSR and PCR method with 5 LVs and 5 PCs respectively

Preprocessing method	PLSR (RMSEP)	PCR (RMSEP)
Auto scaling	1.08	1.71
Mean centering	1.68	1.62
SAVGOL and SNV	0.77	0.82

Multivariate methods employed : Various multivariate methods like PCA, PCR and PLSR were performed on the preprocessed data to obtain a reliable calibration model.

Principal Component Analysis (PCA) : The first step involved for the development of a reliable model is the determination of optimum number of factors that allow the system to be modeled without over fitting the data. A cross-validation method, leaving out one sample at a time, was used for this purpose. For a calibration set with N standards, the calibration was carried out with N-1 standards, and the data thus obtained were used to calculate the concentration of the left out samples. This process was repeated for N standards and the prediction error sum of squares (PRESS) was calculated. The number of components giving a minimum PRESS is the right number of factors that give optimal prediction. PRESS plot represents the RMSEV value against number of factors and is given in Fig. 2. The optimum number of factors obtained is 6 for the PCA method.
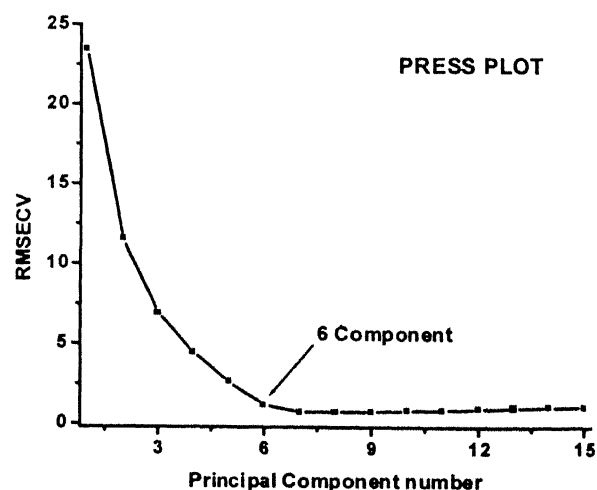
Fig. 2 – Value of PRESS *vs* the number of factors of PCA model.

PCA was performed on the preprocessed fluorescence data obtained from a batch of 35 samples. The first 3 PCs explained 98.03% of the variance in the spectra (69.72 % PC1, 23.77 % for PC2 and 4.54 % of PC3). The first 2 PC scores are plotted in a scatter diagram shown in Fig. 3. Clear discrimination of samples having more diesel like spectral character from samples having more kerosene like spectral character was achieved which can not be easily interpreted from the SFS spectra alone.
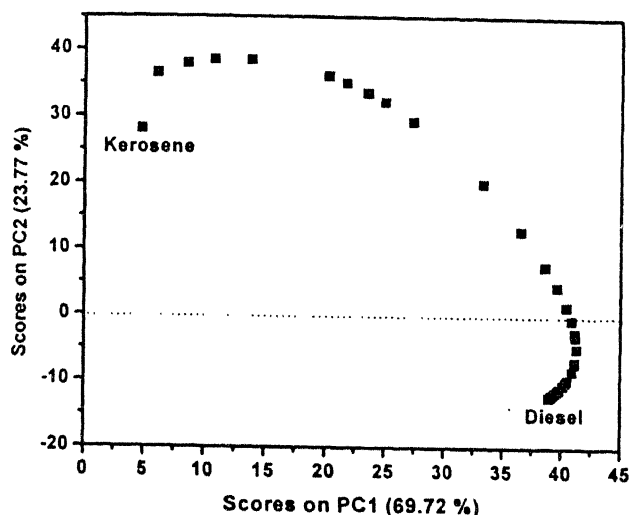
Fig. 3 – First two principal component scores plot for PCA model

Cluster Analysis : Fig. 4 shows a dendrogram obtained from a dataset of 35 samples of varying concentrations of kerosene. This method sorts out the samples in such a way that the degree of association is strong between members of the same cluster and weak between members of different clusters. Objects are grouped in clusters in terms of their nearness in the multidimensional space. From the distance matrices the dendrograms were created. In Fig. 4, the number 1 represents neat diesel and 35 represents neat kerosene. Dendrogram cluster analysis performs a clear grouping between the samples of same group.
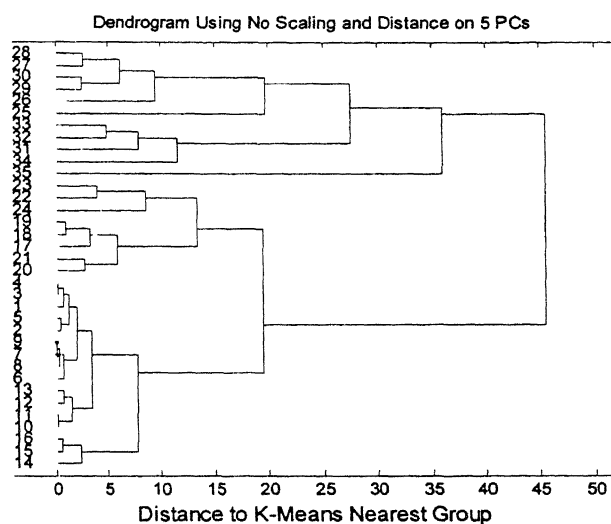
Fig. 4 – Dendrogram obtained on cluster analysis of a dataset of 35 samples of varying concentrations of kerosene

Multivariate regression methods (PCR and PLSR) : PRESS plots of PCR and PLSR are given in Fig. 5. The optimum number of factors to model the system was lesser compared to PCA analysis. Here the maximum variation can be explained by 5 factors while for PCA it was 6. This may be due to the additional concentration information provided for the building of model.
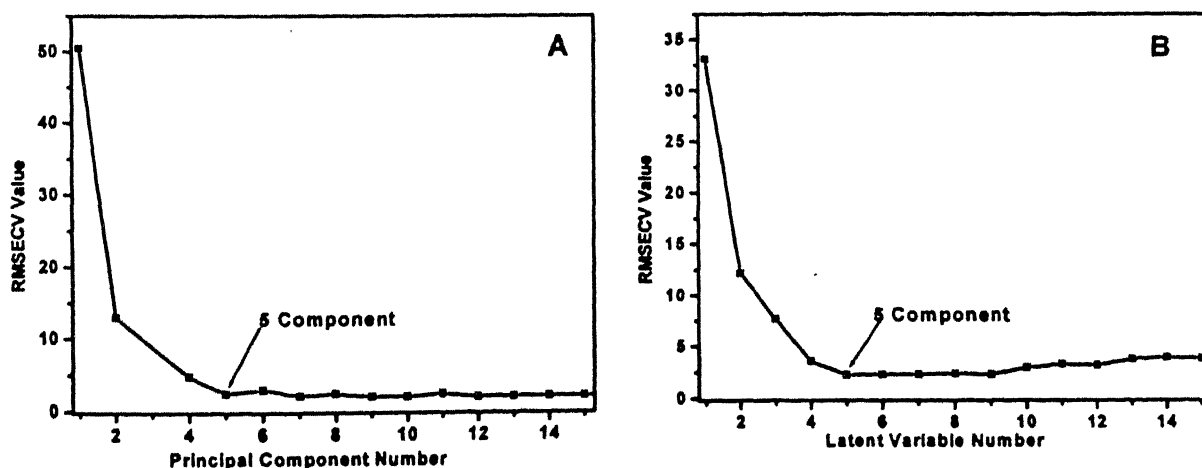
Fig. 5 – Value of PRESS versus the number of factors (A) PCR (B) PLSR model.

So, further analysis and development of model are carried out by taking into account that maximum information is carried by first 5 PCs. The scores plot for PCR model is same as in Fig. 3. Fig. 6 shows the scores plot for PLSR method. PLSR describes the variation in an efficient way with increased resolution among samples, which shows the effectiveness of PLSR method over PCR method. PLSR explained 95.75 % of the variance in the spectra (62.57% LV1, 30.90% for LV2 and 2.28% of LV3). The first 2 LV scores are plotted in a scatter diagram shown in Fig. 6.
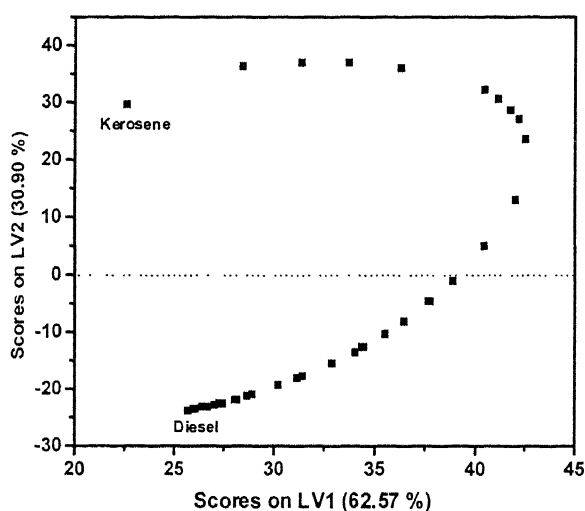
Fig. 6 – Scores plot of the 5 component PLS model calculated from SF spectra of 35 samples.

Scores plots provide information about the variation in spectra of samples. When the spectra were projected (using their scores as coordinates) in the space of the first and second components, the natural grouping of the samples into two groups was observed. The group in the negative quadrant represents the samples with more of diesel like character (less kerosene contamination) and the group in the positive quadrant contains samples with more of kerosene like character (more kerosene contamination).

Differentiation of samples in the less kerosene concentrated area (negative quadrant) is not as efficient by the PCR method as in PLSR method. From the experimental data (SF spectra) it is not possible to differentiate diesel from (1%-10%) kerosene adulterated diesel (Fig. 7). With PLSR method even 1 % contamination of kerosene in diesel is easily discriminated from diesel.
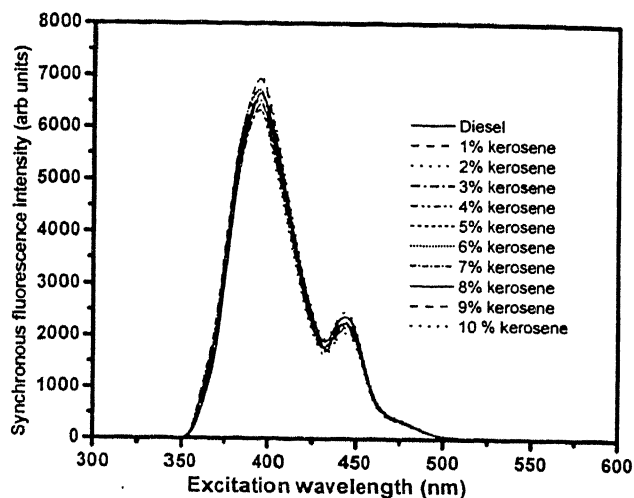
Fig. 7 – Synchronous fluorescence spectra of diesel and (1-10%) kerosene-adulterated diesel

Accuracy and prediction ability of the model : In order to determine the accuracy and robustness of the model a calibration plot was made where the reference values of concentration has been plotted against the concentration values predicted by the model. Fig. 8 is a linear calibration plot of the reference concentration *vs* the model predicted concentration. Both PCR and PLSR methods show good correlation between the measured and predicted concentrations with correlation coefficients of 0.997 (Fig. 8). The RMSEC values for PLSR and PCR are 1.92 and 1.97 respectively.

To evaluate the prediction ability of the model a test set of 8 samples of known concentrations were used. The amount of kerosene present in the mixture was determined, which is in very close agreement with the reference value (Table 2). The error values of prediction RMSEP for PLSR and PCR methods, are 0.77 and 0.82 respectively. RMSEP values obtained are low showing the predictive ability of the model.
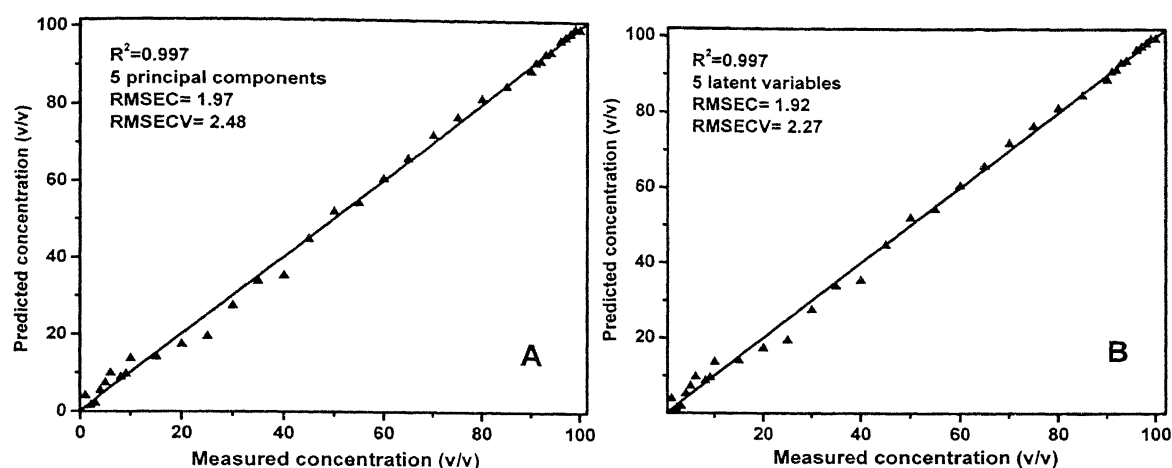
Fig. 8 – Measured versus predicted concentrations of diesel kerosene mixtures based on full cross validation (A) PCR model (B) PLSR model.

Table 2 – Reference value and predicted value of relative kerosene fraction present in the adulterated mixture using PLSR and PCR models.

Relative kerosene fraction (in % v/v) (reference value)	PLSR		PCR	
	Predicted concentration	Prediction error	Predicted concentration	Prediction error
0	-0.48	0.48	−0.31	0.31
2	1.32	0.68	1.45	0.55
8	8.77	0.77	8.80	0.80
15	14.04	0.96	14.01	0.99
65	65.78	0.78	65.80	0.80
80	81.14	1.14	81.38	1.38
92	91.29	0.71	91.21	0.79
98	98.28	0.28	98.36	0.36
Average RMSEP	0.77		0.82	

Conclusion

In this paper the SFS data were combined with various chemometric multivariate methods, such as PCA, PCR, PLSR and cluster analysis for the qualitative and quantitative analysis of kerosene fraction present in kerosene adulterated diesel samples. The developed models were robust and reliable with low prediction errors and were sensitive to detect low contamination of kerosene (1% relative kerosene fraction (in % v/v) in mixture.

Acknowledgement

O.D. acknowledges Council of Scientific and Industrial Research (CSIR) New Delhi for the SRF scholarship. The authors gratefully acknowledge Council of Scientific and Industrial Research, New Delhi, for the financial support to carry out this work. The authors would like to thank Mr. V. Venkataraman, Scientist (CEERI Centre, CSIR complex, Chennai) for valuable suggestions and help.

References

1. Lloyd JBF. Synchronized excitation of fluorescence emission spectra, *Nature Phys Sci* 1971; **231** : 64-65.
2. Vo-Dinh T & Martinez PR. Direct determination of selected polynuclear aromatic hydrocarbons in a coal liquefaction product by synchronous luminescence techniques, *Anal Chim Acta* 1981; **125** : 13-19.
3. Patra D & Mishra AK. Multivariate fluorimetric determination of mixtures of pyrene, perylene and triphenylene in water sample, *Anal Lett* 2000; **33** : 2293-2304.
4. Patra D & Mishra AK. Concentration dependent red shift : qualitative and quantitative investigation of motor oils by synchronous fluorescence spectra, *Talanta* 2001; **53** : 783-790.
5. Patra D & Mishra AK. Effect of sample geometry on synchronous fluorimetric analysis of petrol, diesel, kerosene and their mixtures at higher concentration, *Analyst* 2000; **125** : 1383-1386.
6. Gupta AA, Swami KK, Mishra AK, Henagar AK & Mukhopadhaya PK. Marker-R & D : a new marker system for kerosene, *Hydrocarbon Technology* 1992; **15** : 137-151.

7. Watson RT, Zinyyoweru MC & Moss RH. Technologies, policies and measures for mitigating climate change, *IPCC working group II, Technical Paper* 1996; **1** : 21-30.

8. Bhatnagar VP. An ultrasonic method to find liquid fuel adulteration, *J Acoust Soc India* 1981; **9** : 19-23.

9. Bahari MS, Criddle WJ & Thomas JDR. Determination of the adulteration of petrol with kerosene using rapid phase titration procedure, *Analyst* 1990; **115** : 417-419.

10. Roy S. Fiber optic sensor for determining adulteration of petrol and diesel by kerosene, *Sensor Actuat B* 1999; **55** : 212-216.

11. Patra D, Lakshmi Sireesha K & Mishra AK. Determination of synchronous fluorescence scan parameters for certain petroleum products, *J Scient Ind Res* 2000; **59** : 300-305.

12 Patra D & Mishra AK. Recent developments in multicomponent synchronous flourescence scan analysis, *Trends Anal Chem* 2002; **21** : 787-798.

13. Kowalski B. Chemometrics, *Anal Chem* 1980; **52** : 112R-122R.

14. Dufour E, Mazerolles G, Devaux MF, Duboz G, Duployer MH & Mouhous Riou N.Phase transition of triglycerids during during semi-hard cheese ripening, *Int Dairy J* 2000; **10** : 81-93.

15. Christensen J, Ladefoged AM & Norgaard L. Rapid determinnation of bitterness in beer using flourescence spectroscopy and chmometrics, *J Inst Brew* 2005; **111** : 3-10.

16. Poulli KI, Mousdis GAC & Georgiou A. Ckassification of edible and lampante virgin olive oil based on cynchronous flourescence and total luminescence spectroscopy, *Anal Chim Acta* 2005; **542** : 151-156.

17. Divya O & Mishra AK.Combining synchronous flourescence spectroscopy with multivariate methods for the analysis of petrol-kerosene mixtures, *Talanta* 2007; **72** : 43-48.

18. Lavine BK & Brown SD. Winning at Chemometrics, *Managing Mod Lab* 1998; **3** : 9-14.

19. Martens H & Naes T. Multivariate calibration, Wiley, Chichester, 1989.

20. Jackson JE. Principal components and factor analysis : part 1-principal components, *J Qual Tech* 1980; **12** : 201-213.

21. Sharaf MA, Illman DL & Kowalski BR. Chemometrics, John Wiley & Sons, NewYork, 1986.

22. Brereton RG. Chemometrics Data Analysis for the Laboratory and Chemical Plant, Wiley, Chichester, 2003.

23. Kramer R. Chemometric techniques for quantitative analysis, Marcel Dekker, New York, 1998.

24. Geladi P & Kowalski B.Partial Least Squares Regression : A Tutorial, *Anal Chim Acta* 1986; **185** : 1-17.

25. Wise BM, Gallagher NB, Bro R & Shaver JM. PLS-Toolbox 4.0, Eigenvector research, 2005.

Proc. Nat. Acad. Sci. India Sect. A, Vol. 78, Pt. II, 2008

Use of photo-Fenton's reagent for the photochemical bleaching of metanil yellow

ANIL KUMAR, MUKESH PALIWAL, RAMESHWAR AMETA and SURESH C. AMETA

Photochemistry and Solar Energy Laboratory, Department of Chemistry, University College of Science, M.L. Sukhadia University, Udaipur -313001, India

Email: ameta_sc@yahoo.com

Received April 12, 2007; Revised September 18, 2007; Accepted September 26, 2007

Abstract

Experiments on wastewater containing metanil yellow by photo-Fenton process were conducted at normal laboratory temperature and atmospheric pressure to examine the effect of operating variables like the concentration of ferric ion, concentration of metanil yellow, pH, hydrogen peroxide and light intensity on the reaction rate. The results showed that the metanil yellow was completely oxidized and degraded into CO_2 and H_2O. A suitable tentative mechanism for photochemical bleaching of metanil yellow by photo-Fenton's reaction has been proposed.

(**Keywords:** photochemical degradation/photo-Fenton/metanil yellow/advance oxidation processes)

Introduction

Inspite of many uses, the dyes are toxic and carcinogenic in nature, but bleached dye solutions are non-toxic and harmless. The technology to treat hazardous and toxic wastes is undergoing a transformation on discharge limits. Use of conventional oxidation and active charcoal as an adsorbent have served industry well for decades but now, it cannot meet the more stringent regulations, and as a consequence, innovative technologies such as the advance oxidation processes (AOP) have emerged for the destruction of organic compounds[1]. The hydroxyl radical is the active species, which attacks and destroys the undesired compounds. These radicals can be produced by homogeneous and heterogeneous processes.

The Fenton's reaction[2] produces hydroxyl radicals by interaction of H_2O_2 with ferrous salts.

$$Fe^{+2}+H_2O_2+h\nu \rightarrow Fe^{+2}+{}^{\bullet}OH+H^+ \qquad (1)$$
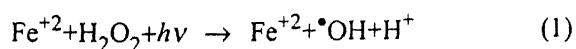
In dark, the reaction is retarded after complete conversion of Fe^{+2} to Fe^{+3}. Recently, it has been found that illumination of the Fe^{+2} – Fe^{+3} – H_2O_2 system increases the degradation rate of many organic substances e.g. TNT and RDX[3], orange II dye, nitrophenols[4] and p-chloroaniline[5]. The reason for this positive effect on the rate of degradation is the photoreduction of Fe^{+3} to Fe^{+2} ions, which produces new $^{\bullet}OH$ radicals with H_2O_2 according to the following mechanism

$$Fe^{+3}+H_2O_2+h\nu \rightarrow Fe^{+2}+{}^{\bullet}OH+H^+ \qquad (2)$$
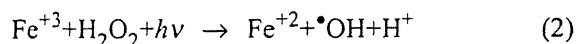
The direct photolysis of H_2O_2 also generates $^{\bullet}OH$ radicals.

$$H_2O_2+h\nu \rightarrow 2\ {}^{\bullet}OH\ (\lambda < 400\ nm) \qquad (3)$$
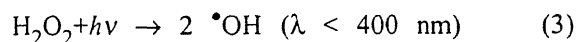
Liou *et al.*[6] studied the photochemical degradation of azo dyes, namely red MX-5B, reactive black-5 and orange-G using low iron concentrations in Fenton and Fenton like systems. Daneshvar and Khataee[7] decolorized the solution containing a common textile and leather dye, C.I. acid red 14 (AR14), at pH 3 using Fenton, $UV/H_2O_2/O_2$, $UV/H_2O_2/Fe^{2+}$, $UV/H_2O_2/Fe^{3+}$ and $UV/H_2O_2/Fe^{+3}$/oxalate processes. The influence of alizarin violet 3B dye on the Fenton reaction of organic compounds under visible irradiation ($\lambda > 450$ nm) was examined by Ma *et al.*[8] Dutta *et al.*[9] also chemically oxidized the methylene blue using a Fenton like reaction. Prousek *et al.*[10] reported the utilization of Fenton reaction for the degradation of dyes present in colored waste water. Photodegradation of malachite green in the presence of Fe^{+3}/H_2O_2 under visible irradiation has been observed by Wu *et al.*[11] Ruppert *et al.*[12] studied the

photo-Fenton reaction as an effective photochemical process to treat the polluted water. Mogra *et al.*[13,14] reported the photochemical degradation of p-dichlorobenzene and o-chlorobenzoic acid by photo-Fenton's reagent. Walling[15] studied intermediates in the reaction of Fenton's type reagents. The present study shows the photochemical degradation of metanil yellow by photo-Fenton's reagent using visible range of light.

Materials and Methods

Metanil yellow (Sisco), $FeCl_3$ (CDH) and H_2O_2 (30%, Merck), were used in the present investigations. The dye solution of metanil yellow was prepared in doubly distilled water. The photochemical degradation of metanil yellow was studied in the presence of Fe^{3+} ion, H_2O_2 and visible light. 0.0375 g of metanil yellow was dissolved in 100 ml of doubly distilled water (1.0×10^{-4} M) and 0.4055 g of $FeCl_3$ anhydrous was dissolved in 500 ml of doubly distilled water so that the concentration of $FeCl_3$ solution was 5.0×10^{-3} M. These were used as stock solutions. The photochemical degradation of metanil yellow was observed taking 30 ml of dye solution (2.4×10^{-5} M) and 2.0 ml of $FeCl_3$ solution (1.0×10^{-3} M). The reaction mixture was exposed to light (intensity 80.0 mW cm^{-2}). A 200 W tungsten lamp was used for irradiation purpose. Sunlight was used for higher intensities of light. The intensity of light was measured by Suryamapi (CEL Model SM 201). A water filter was used to cut off thermal radiations. The pH of the solution was measured by a digital pH meter (Systronics Model 106). The desired pH of the solution was adjusted by the addition of previously standardized hydrochloric acid and sodium hydroxide solutions. The necessary conditions for the correct measurement of optical density is that the solution must be free from suspension and therefore centrifuge machine (Remi-1258) and Whatmann filter paper was used to remove the suspension but both were not found suitable. Thus, G-3 sintered glass crucible was used for filtration to obtain the desired accuracy in measurement of optical density at different time intervals, whereas λ_{max} of the dye was determined with the help of ultraviolet-visible recording spectrophotometer (Shimadzu U.V. 240).

Results and Discussion

The photochemical degradation of metanil yellow was observed at λ_{max} = 545 nm. The results for a typical run are given in Fig. 1. It was observed that optical density of metanil yellow solution decreases with the increase in the time of irradiation; thus, indicating that metanil yellow is consumed on irradiation. A plot of 1 + log OD against time was linear and it followed pseudo-first order kinetics. The optimum rate constant k for this reaction was determined to be 9.60×10^{-4} s^{-1}.
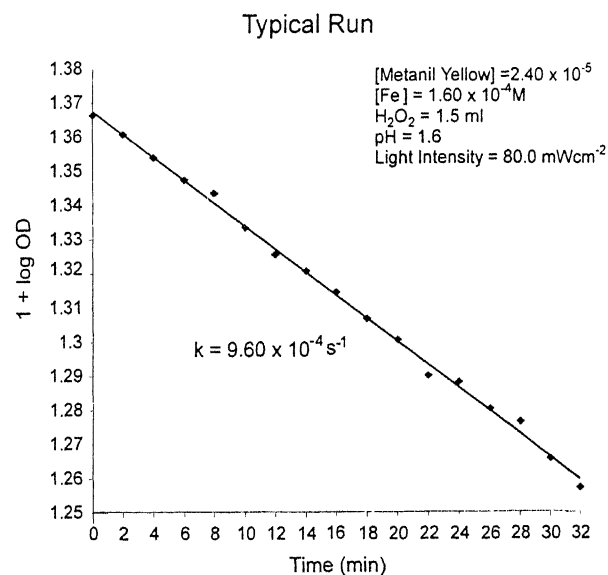
Fig 1 – Variation of optical density with time.

Effect of pH: The effect of pH on the rate of degradation of metanil yellow was investigated in the pH range (1.3 to 1.8). The results are reported in Table 1.

Table 1 – Effect of pH.

[Metanil Yellow] = 2.4×10^{-5} M = 80.0 $mWcm^{-2}$ pH	H_2O_2=1.5ml Light Intensity $[Fe^{3+}] = 1.60 \times 10^{-4}$ M $k \times 10^4$ (s^{-1})
1.3	6.98
1.4	7.35
1.5	8.53
1.6	9.60
1.7	8.35
1.8	6.40

The photochemical degradation depends strongly on the pH of the reaction medium as it is evident from the data in Table 1 that the rate of photochemical degradation of metanil yellow increases with increase in pH upto 1.6 and then the rate of reaction decreases with increasing pH. The hydroxyl radicals are generated by two steps–

(i) The reaction between ferrous ions with hydrogen peroxide.

(ii) Photochemical reaction of ferric ions and water.

The increase in the pH of the medium favours the step, (i) where OH^- ions are formed alongwith hydroxyl radicals, whereas protons are generated in step (ii); thus, it may be concluded that the step (i) dominates over step (ii) in the pH range below 1.6. However, retardation of the reaction above pH 1.6 suggests the dominance of step (ii) over step (i).

Effect of metanil yellow concentration : Effect of variation of dye concentration on rate of reaction was also studied by taking different concentrations of metanil yellow solutions. The results are tabulated in Table 2.

Table 2 - Effect of metanil yellow concentration.

pH = 1.6 $[Fe^{3+}] = 1.60 \times 10^{-4}$ M [Metanil Yellow] $\times 10^5$ M	H_2O_2 = 1.5 ml Light Intensity = 80.0 $mWcm^{-2}$ $k \times 10^4$ (s^{-1})
1.0	1.71
1.2	2.31
1.4	3.22
1.6	.3.83
1.8	4.54
2.0	5.12
4.0	4.72
6.0	4.39
8.0	3.79
10.0	2.79
12.0	1.36
14.0	1.00
16.0	1.05
18.0	0.97

The rate of photochemical degradation was found to increase with increasing concentration of metanil yellow upto 2.4×10^{-5} M. On further increasing its concentration, a sudden decrease in the rate of degradation was observed. This may be explained on the basis that on increasing the concentration of metanil yellow, more molecules of metanil yellow are available for degradation. However, on increasing the concentration above 2.4×10^{-5} M, the reaction rate was found to decrease. It may be attributed to the fact that as the concentration of metanil yellow was increased, it may start acting like a filter for the incident light, where its larger concentration will not permit the desired light intensity to reach the dye molecule in the bulk of the solution and thus, decrease in the rate of photochemical bleaching of metanil yellow was observed.

Effect of ferric ion concentration: The effect of concentration of Fe^{3+} ions on the rate of photochemical degradation of metanil yellow was observed by keeping all other factors identical. The results are summarized in Table 3.

Table 3 – Effect of ferric ion concentration.

[Metanil Yellow] = 2.4×10^{-5} M H_2O_2 = 1.5 ml $[Fe^{+3}] \times 10^5$M	pH = 1.6 Light Intensity = 80.0 $mWcm^{-2}$ $k \times 10^4$ (s^{-1})
1.0	3.83
1.2	4.79
1.4	4.86
1.6	4.94
1.8	5.14
2.0	5.45
2.2	8.06
2.4	9.60
2.6	6.91
2.8	4.61
3.0	4.48

It is clear from the data given in Table 3 that the rate of photodegradation increases on increasing the concentration of Fe^{3+} ions upto 4.0×10^{-5} M, while a reverse trend was observed beyond this limit.

This may be explained on the basis that on increasing Fe^{3+} ions in the reaction mixture, the concentration of Fe^{2+} ions also increases, which is accompanied by enhanced generation of the active species $^{\bullet}OH$ radicals and as a consequence, the rate of photodegradation also increases. However, on increasing the concentration of Fe^{3+} ions further, the rate of the reaction was found to decrease. This is because of the fact that Fe^{3+} ions imparts a yellow colour to the solution and at larger concentrations, it may also act as a filter for the incident light. As the concentration of Fe^{+3} was increased above its optimum concentration, the rates of the reactions (5) and (6) become very fast. Now in reaction (5) hydroperoxyl radicals ($^{\bullet}OOH$) are generated, which consumed more amounts of Fe^{3+} ions and hence, Fe^{3+} ions are less for reaction (4) and as a consequence less $^{\bullet}OH$ radicals are generated and the rate of photodegradation also decreases.

$$Fe^{3+}+H_2O+h\nu \rightarrow Fe^{+2}+^{\bullet}OH+H^+ \qquad (4)$$

$$Fe^{3+}+H_2O_2+h\nu \rightarrow Fe^{2+}+^{\bullet}O_2H + H^+ \qquad (5)$$

$$Fe^{3+}+^{\bullet}O_2H \rightarrow Fe^{2+}+O_2+H^+ \qquad (6)$$
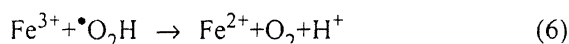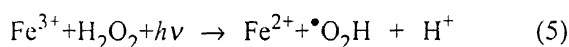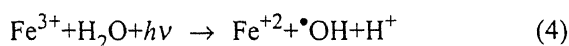
Effect of hydrogen peroxide : The effect of amount of hydrogen peroxide on the photodegradation of metanil yellow was also investigated. The results are tabulated in Table 4.

Table 4 – Effect of hydrogen peroxide.

[Metanil Yellow] = 2.4×10^{-5} M $[Fe^{3+}]$ = 4.0×10^{-5} M H_2O_2 (ml)	pH = 1.6 Light Intensity = 80.0 mWcm^{-2} $k \times 10^4$ (s^{-1})
0.5	7.85
1.0	8.72
1.5	9.60
2.0	8.53
2.5	8.40

It was observed that the rate of reaction increases on increasing the amount of H_2O_2 and it attained an optimum value at H_2O_2 = 1.5 ml. Thereafter, the rate of degradation decreases on increasing the amount of hydrogen peroxide above 1.5 ml. This can be explained on the basis that more H_2O_2 molecules are available for Fe^{2+} ions to react, which increases the number of $^{\bullet}OH$ radicals. On further increasing the amount of H_2O_2 more than 1.5 ml, the rate of reaction was found to decrease. It is because of the fact that as the amount of H_2O_2 was increased above its optimum value (1.5 ml) the rates of the reactions (7) and (8) become fast. From reaction (8) $^{\bullet}OH$ radicals are consumed rapidly due to more H_2O_2 molecules. From reactions (7) and (8) $^{\bullet}OOH$ radicals increase and are utilized in reaction (9) where H^+ ions are produced. The production of H^+ ions is confirmed by a slight decrease in pH of the reaction mixture at the end of reaction. As a consequence, the rate of photodegradation decreases.

$$Fe^{3+}+H_2O_2+h\nu \rightarrow Fe^{2+}+^{\bullet}O_2H+H^+ \qquad (7)$$

$$^{\bullet}OH+H_2O_2 \rightarrow ^{\bullet}O_2H+H_2O \qquad (8)$$

$$Fe^{3+}+^{\bullet}O_2H \rightarrow Fe^{2+}+O_2+H^+ \qquad (9)$$
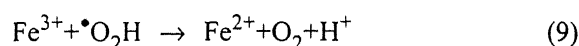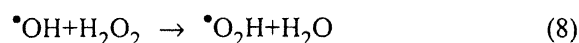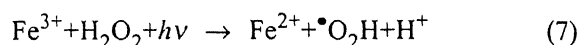
Effect of light intensity: The effect of light intensity on the photodegradation of metanil yellow was also observed. The results obtained are reported in Table 5.

Table 5 – Effect of light intensity.

[Metanil Yellow] = 2.4×10^{-5} M $[Fe^{3+}]$ = 4.0×10^{-5} M Light Intensity (mWcm^{-2})	pH = 1.6 H_2O_2 = 1.5 ml $k \times 10^4$ (s^{-1})
10.0	6.01
20.0	6.95
30.0	7.99
40.0	8.39
50.0	8.60
60.0	8.95
70.0	9.32
80.0	9.60

A linear plot was observed between the rate constant and light intensity, which indicates that an increase in the light intensity increases the rate of reaction. This may be attributed to the increased number of photons reacting with Fe^{3+} ions and as

a result, there is an increase in the number of active species, the hydroxyl radicals and corresponding increase in the rate of reaction.

Mechanism

On the basis of experimental observations and corroborating the existing literature, a tentative mechanism has been proposed for photodegradation of metanil yellow with photo-Fenton reagent.

$$Fe^{3+}+H_2O+h\nu \rightarrow Fe^{+2}+^{\bullet}OH+H^+ \quad (10)$$

$$Fe^{3+}+H_2O_2+h\nu \rightarrow Fe^{2+}+^{\bullet}O_2H+H^+ \quad (11)$$

$$Fe^{2+}+H_2O_2 \rightarrow Fe^{3+}+^{\bullet}OH+OH^- \quad (12)$$

$$^{\bullet}OH+H_2O_2 \rightarrow ^{\bullet}O_2H+H_2O \quad (13)$$

$$Fe^{2+}+^{\bullet}OH \rightarrow Fe^{3+}+OH^- \quad (14)$$

$$Fe^{3+}+^{\bullet}O_2H \rightarrow Fe^{2+}+O_2+H^+ \quad (15)$$

$$\cdot OH+^{\bullet}OH \rightarrow H_2O_2 \quad (16)$$

$$\text{Metanil yellow} + ^{\bullet}OH \rightarrow \text{Products} \quad (17)$$
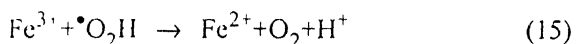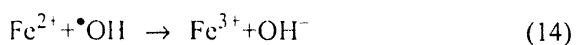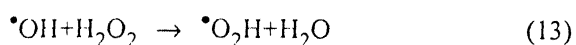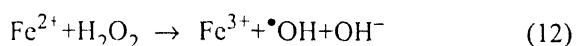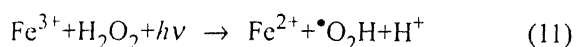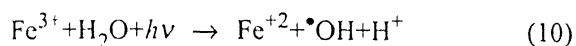
The aqueous solution of ferric ions on exposure to light dissociates water into a proton and $^{\bullet}OH$ radical and ferric ions are reduced to ferrous ions. These ferrous ions will decompose H_2O_2 into hydroxyl ion and hydroxyl radical, while ferrous ions undergo oxidation to ferric ions. The ferric ions generates $^{\bullet}OOH$ radical due to dissociation of H_2O_2 in presence of light. The incorporation of $^{\bullet}OH$ with H_2O_2 also produces $^{\bullet}OOH$ radicals. Ferrous ions will undergo oxidation to ferric ions by addition of $^{\bullet}OH$ radicals, while ferric ions get reduced to ferrous ions by incorporation of $^{\bullet}OOH$ radical and producing H^+ ions. $^{\bullet}OOH$ radicals are highly unstable in water and undergo facile disproportion rather than reacting slowly with dye molecules. The participation of hydroxyl radicals as an active oxidizing species was confirmed by using hydroxyl radical scavenger likes 2-propanol, where the rate of photodegradation was drastically reduced.

There are two possibilities for the consumption of $^{\bullet}OH$ radicals namely (a) hydroxyl radicals may dissociate H_2O_2 into $^{\bullet}OOH$ and water or combine together to form H_2O_2 molecules, (b) it may react with metanil yellow to give the colourless degradation products.

The main advantage of using photo-Fenton's reagent is the regeneration of the consumed Fe^{2+} ions on illumination. Every Fe^{2+} ion can produce many $^{\bullet}OH$ radicals in contrast with dark Fenton reaction and as this process is cyclic in nature, where only a single $^{\bullet}OH$ radical is formed by one ferrous ion. It means that the amount of ferrous salt required in photo-Fenton conditions is small as compared to Fenton condition, where one has to add ferrous ions at required intervals otherwise the reaction will stop after conversion of ferrous ions to ferric ions. It is important for industrial use as further separation of the ferric ions is not required after wastewater treatment[16-21].

Acknowledgements

One of the authors (Anil Kumar) wishes to thank the Council of Scientific and Industrial Research (CSIR) for the award of JRF.

References

1. Haag WR & Yao CCD. Rate constants for reaction of hydroxyl radicals with several drinking water contaminants. *Environ Sci Technol* 1992; **26** : 1005-1013.

2. Fenton HJH. Oxidation of tartaric acid in presence of iron. *J Chem Soc* 1894; **65** : 899-910.

3. Oh SY, Chiu PC, Kim BJ & Cha DK. Enhancing Feton oxidation of TNT and RDX through pretreatment with zero-valent iron. *Water Res* 2003; **37** : 4275-4283.

4. Lipczynska-Kochany E. Novel method for a photocatalytic degradation of 4-nitrophenol in homogeneous aqueous solution. *Environ Technol* 1991; **12** : 87-92.

5. Mogra D, Swarnkar H, Vardia J & Ameta SC. Photochemical degradation of p-chloroaniline by photo-Fenton's reagent. *Proc Nat Acad Sci India* 2005; **75A** : 79-84.

6. Liou MJ, Lu MC & Chen JN. Oxidation of TNT by photo-Fenton process. *Chemosphere* 2004; **57** : 1107-1114.

7. Daneshvar N & Khataee AR. Removal of azo dye D.I. acid red 14 from contaminated water using Fenton. UV/H_2O_2, $UV/H_2O_2/Fe(II)$, $UV/H_2O_2/Fe(III)$ and $UV/H_2O_2/Fe(II)$/oxalate process : a comparative study. *J Environ Sci Health A Tox Hazzard Subst Environ Eng* 2006; **41** : 315-328.

8. Ma J, Song W, Chen C, Ma W, Zhao J & Tang Y. Fenton degradation of organic compounds romoted by dyes under visible irradiation. *Environ Sci Technol* 2005; **39** : 5810-5815.

9. Dutta K, Mukhopadhyay S, Bhattacharjee S & Chaudhuri B. Chemical oxidation of methylene blue using a Fenton-like reaction. *J Hazard Mater* 2001; **84** : 57-61.

10. Prousek J, Ivanova E & Kocmanikova M. Utilization of Fenton reaction for the degradation of aqueous solutions of conventionally used dyes and coloured waste waters. *Chem Listy* 1997; **91** : 48-53.

11. Wu KG, Zang TY, Zhao JC & Hidaka H. Photodegradation of malachite green in the presence of Fe-3+/H_2O_2 under visible irradiation. *Chem Lett* 1998; **8** : 857-858.

12. Ruppert G, Baur R & Heisler G. The photo-Fenton reaction-an effective photochemical waste water treatment process. *J Photochem Photobiol* 1993; **73A** : 75-78.

13. Mogra D, Mehta M, Ameta R & Ameta SC. Photochemical degradation of p-dichlorobenzen by photo-Fenton's reagent. *J Indian Chem Soc* 2002; **79** : 593.

14. Mogra D, Agrawal R, Punjabi PB & Ameta SC. Photochemical degradation of o-chlorobenzole acid by photo-fenton's reagent. *Chem Environ Res* 2003; **12** : 227-235.

15. Walling C. Intermediates in the reactions of Fenton type reagents. *Acc Chem Res* 1998; **31** : 155-157.

16. Bozzi A, Yuranova T, Mielczarski J & Kiwi J. Evidence for immobilized photo-Fenton degradation of organic compounds on structured silica surfaces involving Fe-recycling. *New Journal of Chemistry* 2004; **28** : 519-526.

17. Tao X, Su J, Chen J & Zhao J. A novel route for waste water treatment : photo-assisted Fenton degradation of dye pollutants accumulated in natural polyelectrolyte microshells. *Chem Commun* 2005; **36** : 4607-4609.

18. Ma W, Huang Y, Li J, Cheng C, Song W & Zhao J. An efficient approach for the photodegradation of organic pollutants by immobilized iron ions at neutral pHs. *Chem Commun* 2003; 1582-1583.

19. Chen F, Ma W, He J & Zhao J. Fenton degradation of malachite green catalyzed by aromatic additives. *J Phys Chem A* 2002; **106** : 9485-9490.

20. Collins TJ. TAML oxidant activators : a new approach to the activation of hydrogen peroxide for environmentally significant problems. *Acc Chem Res* 2002; **35** : 782-790.

21. Zepp RG, Faust BC & Hoingne J. Hydroxyl radical formation in acqueous reactions (pH 3-8) of iron(II) with hydrogen peroxide : the photo-Fenton reaction. *Environ Sci Techno* 1992; **26** : 313-319.

Proc. Nat. Acad. Sci. India Sect. A, Vol. 78, Pt. II, 2008

Synthesis and biological significance of 2-amino-4-phenyl-1,3-thiazole derivatives

S.K. SONWANE and S.D. SRIVASTAVA*

Synthetic organic Chemistry Laboratory, Department of Chemistry, Dr. H.S. Gour University, Sagar (M.P.) 470 003, India.

Email : drsavitri@rediffmail.com

** for correspondence*

Received August 2, 2007; Revised November 6, 2007; Accepted November 7, 2007

Abstract

2-Amino-4-phenyl-1,3-thiazole on reaction with chloroacetyl chloride yielded 2-(2'-chloroacetyl)-amino-4-phenyl-1,3-thiazole, 1 which on amination with hydrazine hydrate afforded 2-(2'-hydrazinoacetyl)-amino-4-phenyl- 1,3-thiazole, 2 The compound 2 on condensation with various selected aromatic aldehydes yielded 2-(2'-arylidene-hydrazino-acetyl)-amino-4-phenyl-1,3-thiazole, 3a-n which on treatment with mercapto acetic acid underwent dehydrative annulation to afford 2-[2'-{2"-aryl-4-oxo-1,3-thiazolidene}-acetylamino]-4-phenyl-1,3-thiazoles 4a-n. The compounds 4a-n on the application of Knovenagel reaction with various substituted aromatic aldehydes gave 2-[2'-{2"-(aryl)-5"-arylidene-4-oxo-1,3-thiazolidene}-acetylamino]-4-phenyl-1,3-thiazoles, 5a-n. Their structures were confirmed by microanalytical and spectral data. The antimicrobial activity of the all synthesized compounds were screened against *Bacillus substilis, Eschericha coli, Streptococcus aureus* and *Klebsiella pneumoneae bacteria* and *Aspergillus niger, Aspergillus flavus, Fusarium oxisporium* and *Trichoderma viride* fungi respectively.

(**Keywords** : 2-amino-4-phenyl-1,3-thiazole derivatives/ arylidene/4-oxo-thiazolidene/antimicrobial activity)

Introduction

Heterocycles bearing nitrogen, sulphur and thiazole moieties constitute the core structure of a number of biologically interesting compounds[1]. The compounds containing thiazole nucleus have proved their efficiency in combating various diseases and found to have good antimicrobial activity[2]. It has been observed that the thiazole analogues incorporated with different nuclei have shown variety of pharmacological profile such as anticancer[3], analgesic[4], antiinflammatory[5], antitubercular[6], bacteriostatic[7,8], anaesthetic[9] and antifungal[10] activities. Based on the above reports we have synthesized various 4-oxo-1,3-thiazolidenes and their 5-arylidenes derivatives containing-4-phenyl-1,3-thiazole nuclei. The present paper reports the synthesis of 2-[2'-{2"(aryl)-4-oxo-1,3-thiazolidene}-acetylamino]-4-phenyl-1,3-thiazole, and 2-[2'-{2"-(aryl)-5"-(arylidene)-4-oxo-1,3-thiazolidene}-acetylamino]-4-phenyl-1,3-thiazoles, by appropriate methods. All the synthesized compounds have been screened for their antibacterial activity against *B. substilis, E. coli, S. aureus* and *K. pneumoneae* and antifungal activity against *A. niger, A. flavus, F. oxisporium* and *T. viride* respectively[11,12].

Materials and Methods

Experimental section

Melting points were taken in open capillaries. Purity of compounds was monitored on silica gel coated TLC plates. IR spectra were recorded on a Schimadzu 8201 PC spectrophotometer in KBr and ^{1}H NMR spectra on a Brucker DRX 300 spectrometer in $CDCl_3$ at 300 MHz using TMS as an internal standard. The reagent grade chemicals were purchased from the commercial sources and purified by either distillation or recrystallization before use.

Results and Discussion

2-Amino-4-phenyl-1,3-thiazole on reaction with chloroacetyl chloride yielded 2-(2'-chloroacetyl)-amino-4-phenyl-1,3-thiazole, 1, which on amination with hydrazine hydrate afforded 2-(2'-hydrazinoacetyl)-amino-4-phenyl -1,3-thiazole 2. The compound 2 on condensation with various selected aromatic aldehydes yielded 2-(2'-arylidene-hydrazino-acetyl)-amino-4-phenyl-1,3-thiazoles 3a-n. The compounds 3a-n on treatment with mercaptoacetic acid underwent dehydrative annulation in presence of anhydrous

$ZnCl_2$ to afford 2-[2'-{2"-(aryl)-4-oxo-1,3-thiazolidene}-acetylamino]-4-phenyl-1,3-thiazoles 4a-n. The compounds 4a-n which on application of Knovenagel reaction with various substituted aromatic aldehydes gave 2-[2'-{2"-(aryl)-5"-arylidene-4-oxo-1,3-thiazolidene}-acetylamino]-4-phenyl-1,3-thiazoles 5a-n (Scheme-1). Their structures have been elucidated on the basis of their spectral and microanalytical data.

2-(2'-Chloroacetyl)-amino-4-phenyl-1,3-thiazole (1) : A mixture of 2-amino-4-phenyl-1,3-thiazole (0.20 M, 35.20 g) dissolved in glacial acetic acid (100 ml) saturated with sodium acetate, chloroacetyl chloride (0.20 M, 15.94 g) was added drop wise in the ice bath (to avoid the vigorous reaction) followed by stirring for about 1 h. A light pale yellow coloured product was separated which was filtered, washed with water, purified over column chromatography and recrystallised from chloroform to give compound 1, see (Scheme 1). Yield 79%, m.p. 171-173°C. Anal. calcd. for $C_{11}H_9N_2OSCl$; C, 52.29, H 3.56, N 11.08%; found C 52.26, H 3.54 N 11.03%; IR : 3352 (-NH), 1665 (>C=O), 2963 ($-CH_2$), 2847 (-CH of thiazole), 1409 (-C=N), 1188, 1072, 686 (C-S-C), 3023, 1597, 742 (aromatic ring), 776 cm^{-1} (C-Cl); ^1H NMR δ6.89-7.78 (m, 5H, Ar-H), 6.58 (s, 1H, C-5 of thiazole), 8.15 (s, 1H, -NH), 4.35 (s, 2H, $-CH_2$).

2-(2'-Hydrazinoacetyl)-amino-4-phenyl-1,3-thiazole (2) : A mixture of compound 1 (0.10 M, 25.26 g) and hydrazine hydrate (0.10 M, 4.90 g) in methanol (100 ml) was refluxed on a water bath for about 10 h. It was filtered, cooled, purified over column chromatography and recrystallised from methanol to give compound 2 (Scheme 1). Yield 82%, m.p. 149-151°C. Anal. calcd. for $C_{11}H_{12}N_4OS$: C 53.22, H 4.84, N 22.58%; found C 53.19, H 4.82, N 22.56%; IR : 3356 (-NH), 3396, 3278 ($-NH_2$), 1669 (>C=O), 2967 ($-CH_2$), 2848 (-CH of thiazole), 1186, 1073, 688 (C-S-C), 1413 (-C=N), 3028, 1599, 738 cm^{-1} (aromatic ring); ^1H NMR δ6.90-7.76 (m, 5H, Ar-H), 6.55 (s, 1H, C-5 of thiazole), 8.15 (s, 1H, -NHCO), 4.79 (s, 2H, $-NH_2$), 7.88 (s, 1H, -NH), 4.34 (s, 2H, $-CH_2$).

2-(2'-Arylidene-hydrazino-acetyl)-amino-4-phenyl-1,3-thiazole (3a) : A mixture of compound 2 (0.007 M, 1.736 g) and benzaldehyde (0.007 M, 0.70 g) in methanol (40 ml) with 3-4 drops glacial acetic acid was refluxed on a water bath for about 3 h. The solvent was distilled off under reduced pressure and the solid thus obtained was purified over the column chromatography and recrystallised from ethanol to give compound 3a (Scheme 1). Yield 87%, m.p. 172-174°C. Anal. calcd. for $C_{18}H_{16}N_4OS$: C 64.29, H 4.75, N 16.65%; found C 64.26, H 4.73, N 16.62%; IR : 3349 (-NH), 1662 (>C=O), 1543 (-N=CH), 2963 ($-CH_2$), 2843 (-CH of thiazole), 1188, 1076, 691 (C-S-C), 1416 (C=N), 3025, 1596, 736 cm^{-1} (aromatic ring); ^1H NMR δ6.88-7.72 (m, 10H, Ar-H), 4.86 (s, 1H, -N=CH), 6.59 (s, 1H, C-5 of thiazole), 8.16 (s, 1H, -NHCO), 7.83 (s, 1H, -NH), 4.32 (s, 2H, $-CH_2$).

Scheme 1

NH_2

$ClCOCH_2Cl$

(1) $NHCOCH_2Cl$

$NH_2NH_2 \cdot H_2O$

(2) $NHCOCH_2NHNH_2$

Ar_1CHO

(3a-n) $NHCOCH_2NHN = CHAr_1$

$SHCH_2COOH/ZnCl_2$

(4a-n) $NHCOCH_2NHN-CHAr_1$

$Ar_2CHO/NaOC_2H_5$

(5a-n) $NHCOCH_2NHN-CHAr_1$

CH Ar_2
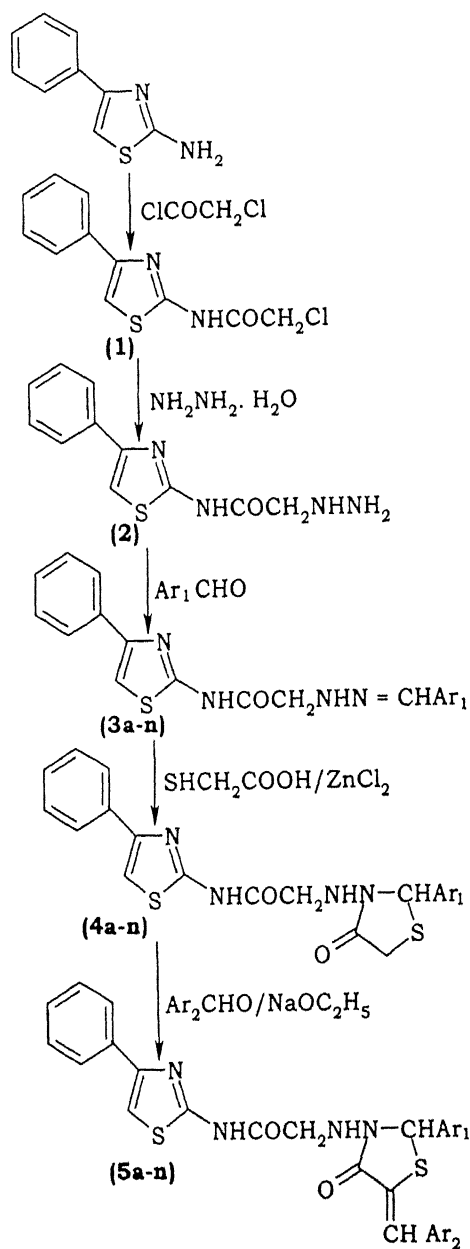
Table 1 - Characterization data of compounds 3b-n, 4b-n and 5b-n.

Comp.	Ar_1	Ar_2	Yield %	m.p. (°C)	Molecular formula	Found % (Calcd %)		
						C	H	N
3b	2-ClC_6H_4	–	90	195-197	$C_{18}H_{15}N_4OSCl$	57.96	3.98	14.94
						(58.00)	(4.02)	(15.02)
3c	3-ClC_6H_4	–	88	192-194	$C_{18}H_{15}N_4OSCl$	57.98	3.99	14.95
						(58.00)	(4.02)	(15.02)
3d	4-ClC_6H_4	–	91	199-201	$C_{18}H_{15}N_4OSCl$	57.95	3.96	14.96
						(58.00)	(4.02)	(15.02)
3e	2-BrC_6H_4	–	86	218-220	$C_{18}H_{15}N_4OSBr$	51.99	3.60	13.46
						(52.07)	(3.61)	(13.48)
3f	3-BrC_6H_4	–	84	222-224	$C_{18}H_{15}N_4OSBr$	51.96	3.57	13.48
						(52.07)	(3.61)	(13.48)
3g	4-BrC_6H_4	–	92	226-228	$C_{18}H_{15}N_4OSBr$	51.97	3.59	13.47
						(52.07)	(3.61)	(13.48)
3h	2-$OCH_3C_6H_4$	–	93	232-234	$C_{19}H_{18}N_4O_2S$	62.29	4.89	15.16
						(62.34)	(4.91)	(15.30)
3i	3-$OCH_3C_6H_4$	–	90	230-232	$C_{19}H_{18}N_4O_2S$	62.27	4.86	15.21
						(62.34)	(4.91)	(15.30)
3j	4-$OCH_3C_6H_4$	–	87	228-230	$C_{19}H_{18}N_4O_2S$	62.25	4.88	15.27
						(62.34)	(4.91)	(15.30)
3k	2-$NO_2C_6H_4$	–	86	167-169	$C_{18}H_{15}N_5O_3S$	56.68	3.91	18.32
						(56.70)	(3.93)	(18.36)
3l	3-$NO_2C_6H_4$	–	88	171-173	$C_{18}H_{15}N_5O_3S$	56.67	3.92	18.31
						(56.70)	(3.93)	(18.36)
3m	4-$NO_2C_6H_4$	–	85	178-180	$C_{18}H_{15}N_5O_3S$	56.69	3.87	18.29
						(56.70)	(3.93)	(18.36)
3n	4.4'-$(CH_3)_2NC_6H_4$	–	92	159-161	$C_{20}H_{21}N_5OS$	63.29	5.51	18.42
						(63.37)	(5.53)	(18.45)
4b	2-ClC_6H_4	–	79	133-135	$C_{20}H_{17}N_4O_2S_2Cl$	58.18	4.09	18.44
						(58.20)	(4.11)	(13.56)
4c	3-ClC_6H_4	–	82	139-141	$C_{20}H_{17}N_4O_2S_2Cl$	58.16	4.06	13.49
						(58.20)	(4.11)	(13.56)
4d	4-ClC_6H_4	–	78	133-135	$C_{20}H_{17}N_4O_2S_2Cl$	58.17	4.02	13.52
						(58.20)	(4.11)	(13.56)
4e	2-BrC_6H_4	–	74	141-143	$C_{20}H_{17}N_4O_2S_2Br$	49.02	3.39	11.41
						(49.09)	(3.47)	(11.44)
4f	3-BrC_6H_4	–	72	145-147	$C_{20}H_{17}N_4O_2S_2Br$	48.97	3.43	11.39
						(49.09)	(3.47)	(11.44)
4g	4-BrC_6H_4	–	75	142-144	$C_{20}H_{17}N_4O_2S_2Br$	48.99	3.45	11.42
						(49.09)	(3.47)	(11.44)

4h	2-$OCH_3C_6H_4$	–	81	212-214	$C_{21}H_{17}N_4O_3S_2$	51.52 (51.55)	3.42 (3.47)	14.25 (14.30)
4i	3-$OCH_3C_6H_4$	–	84	218-220	$C_{21}H_{17}N_4O_3S_2$	51.54 (51.55)	3.45 (3.47)	14.28 (14.30)
4j	4-$OCH_3C_6H_4$	–	86	206-208	$C_{21}H_{17}N_4O_3S_2$	51.53 (51.55)	3.46 (3.47)	14.26 (14.30)
4k	2-$NO_2C_6H_4$	–	95	170-172	$C_{20}H_{18}N_5O_4S_2$	52.59 (52.63)	3.91 (3.94)	15.30 (15.33)
4l	3-$NO_2C_6H_4$	–	94	174-176	$C_{20}H_{18}N_5O_4S_2$	52.61 (52.63)	3.89 (3.94)	15.32 (15.33)
4m	4-$NO_2C_6H_4$	–	93	168-170	$C_{20}H_{18}N_5O_4S_2$	52.60 (52.63)	3.92 (3.94)	15.29 (15.33)
4n	4,4'-$(CH_3)_2NC_6H_4$	–	74	162-164	$C_{22}H_{23}N_5O_2S_2$	58.34 (58.39)	4.91 (5.07)	15.39 (15.43)
5b	2-ClC_6H_4	2-ClC_6H_4	68	141-143	$C_{27}H_{20}N_4O_2S_2Cl_2$	57.14 (57.16)	3.51 (3.52)	9.86 (9.87)
5c	3-ClC_6H_4	3-ClC_6H_4	64	146-148	$C_{27}H_{20}N_4O_2S_2Cl_2$	57.12 (57.16)	3.50 (3.52)	9.86 (9.87)
5d	4-ClC_6H_4	4-ClC_6H_4	67	144-146	$C_{27}H_{20}N_4O_2S_2Cl_2$	57.11 (57.16)	3.49 (3.52)	9.84 (9.87)
5e	2-BrC_6H_4	2-BrC_6H_4	71	182-184	$C_{27}H_{20}N_4O_2S_2Br_2$	49.39 (49.41)	3.01 (3.04)	8.47 (8.53)
5f	3-BrC_6H_4	3-BrC_6H_4	73	189-191	$C_{27}H_{20}N_4O_2S_2Br_2$	49.38 (49.41)	2.99 (3.04)	8.51 (8.53)
5g	4-BrC_6H_4	4-BrC_6H_4	72	196-198	$C_{27}H_{20}N_4O_2S_2Br_2$	49.37 (49.41)	2.97 (3.04)	8.49 (8.53)
5h	2-$OCH_3C_6H_4$	2-$OCH_3C_6H_4$	77	204-206	$C_{29}H_{26}N_4O_4S_2$	62.33 (62.37)	4.61 (4.65)	9.96 (10.02)
5i	3-$OCH_3C_6H_4$	3-$OCH_3C_6H_4$	78	208-210	$C_{29}H_{26}N_4O_4S_2$	62.34 (62.37)	4.59 (4.65)	9.97 (10.02)
5j	4-$OCH_3C_6H_4$	4-$OCH_3C_6H_4$	75	214-216	$C_{29}H_{26}N_4O_4S_2$	62.35 (62.37)	4.62 (4.65)	9.99 (10.02)
5k	2-$NO_2C_6H_4$	2-$NO_2C_6H_4$	62	228-230	$C_{27}H_{20}N_6O_6S_2$	55.09 (55.11)	3.35 (3.39)	14.24 (14.27)
5l	3-$NO_2C_6H_4$	3-$NO_2C_6H_4$	65	217-219	$C_{27}H_{20}N_6O_6S_2$	55.07 (55.11)	3.37 (3.39)	14.23 (14.27)
5m	4-$NO_2C_6H_4$	4-$NO_2C_6H_4$	63	224-226	$C_{27}H_{20}N_6O_6S_2$	55.08 (55.11)	3.32 (3.39)	14.26 (14.27)
5n	4,4'-$(CH_3)_2NC_6H_4$	4,4'-$(CH_3)_2N C_6H_4$	69	183-185	$C_{31}H_{26}N_6O_2S_2$	64.11 (64.14)	4.79 (4.82)	14.44 (14.47)

Table 2 – Antibacterial activity of the compounds 1, 2, 3a-n, 4a-n and 5a-n against various bacteria at different concentrations (ppm).

Comp.	*B. substilis*		*E. coli*		*K. pneumoneae*		*S. aureus*	
	50	100	50	100	50	100	50	100
1	–	+	–	–	+	+	–	+
2	+	+	+	++	–	+	–	+
3a	–	–	–	+	–	+	–	–
3b	+	+	–	+	+	+	–	+
3c	–	+	+	+	–	+	+	++
3d	–	–	–	–	+	+	–	+
3e	+	++	+	+	+	++	+	++
3f	+	+	+	++	+	++	+	++
3g	+	+	–	+	–	+	+	+
3h	+	+	–	+	–	–	–	–
3i	+	+	+	+	+	+	–	+
3j	–	+	–	–	+	+	+	+
3k	–	–	+	+	–	+	-	+
3l	+	+	+	++	–	+	-	+
3m	+	+	–	+	–	+	+	+
3n	+	+	+	++	–	+	–	+
4a	+	++	+	+	+	+	+	++
4b	–	+	+	++	++	++	+	++
4c	+	++	+	+	–	+	++	++
4d	+	++	–	+	+	+	–	+
4e	++	++	+	++	+	++	+	+
4f	+	++	++	++	++	++	++	++
4g	++	++	+	+	++	++	++	++
4h	+	+	++	++	+	+	++	+++
4i	+	++	++	+++	–	+	++	+
4j	+	++	+++	+++	–	+	+	+
4k	+	++	++	++	+	++	–	–
4l	++	++	+	++	–	–	–	–
4m	++	++	+	+	+	++	+	+
4n	+	++	+	+	+	+	+	++
5a	–	+	–	–	–	–	–	–
5b	++	++	+	++	++	++	++	++
5c	+	+	++	++	+	++	++	++
5d	++	++	+	++	++	++	+++	+++
5e	++	++	+	+	++	++	++	++
5f	++	++	++	++	+++	+++	++	++
5g	+	+	++	++	+++	+++	++	++
5h	+	+	–	+	++	++	+	+
5i	+	+	+	++	++	++	+	++
5j	–	+	–	+	+	+	–	++
5k	+	+	+	++	+	+	–	–
5l	+	+	+	+	+	+	–	+
5m	+	+	–	+	+	+	+	+
5n	+	+	+	+	++	++	+	++
SM	+++	++++	+++	++++	+++	++++	+++	++++

SM = streptomycin, inhibition diameter in nm (-) <6, (+) 6-10, (++) 10-16, (+++) 16-25, (++++) 25-30.

Table 3 – Antifungal activity of the compounds 1, 2, 3a-n, 4a-n and 5a-n against various fungi at different concentrations (ppm).

Comp.	*A. niger*		*A. flavus*		*F. oxisporium*		*T. viride*	
	50	100	50	100	50	100	50	100
1	+	+	–	+	+	++	+	+
2	–	–	–	+	–	–	–	–
3a	+	+	–	+	–	+	–	+
3b	+	++	+	+	+	+	+	+
3c	–	+	+	++	+	+	+	++
3d	+	+	+	+	+	++	–	+
3e	+	++	+	+	+	++	–	+
3f	+	+	+	++	+	++	–	++
3g	+	+	+	++	+	+	+	+
3h	+	+	–	+	–	+	+	+
3i	+	+	+	+	+	++	+	+
3j	+	++	–	+	–	+	–	–
3k	+	+	–	+	–	+	–	+
3l	+	+	–	–	+	+	–	–
3m	+	+	–	–	–	+	–	+
3n	+	+	–	+	+	+	+	+
4a	–	+	+	++	–	+	+	+
4b	+	++	+	++	–	+	+	+
4c	+	++	–	+	+	++	+	++
4d	+	+	+	++	–	+	+	+
4e	+	+	+	+	+	+	+	+
4f	+	++	+	++	+	++	+	++
4g	+	++	+	++	+	++	+	++
4h	–	+	+	++	+	++	+	+
4i	+	+	+	+	–	+	–	+
4j	–	–	+	+	+	++	+	+
4k	+	+	+	++	+	+	+	+
4l	+	++	+	+	+	+	+	++
4m	+	++	+	+	+	++	–	+
4n	+	++	+	++	–	+	+	++
5a	+	++	–	+	+	++	+	+
5b	+	+	+	++	+	+	+	++
5c	+	++	++	+++	+	++	++	+++
5d	++	+++	++	++	++	+++	++	++
5e	++	+++	++	++	+	++	++	+++
5f	+++	++++	+	++	++	+++	++	++
5g	+++	++++	++	+++	+++	+++	++	++
5h	+	+	+	++	–	+	+	++
5i	–	+	+	+	+	++	+	++
5j	+	+	–	–	+	+	–	–
5k	+	+	–	+	–	++	–	+
5l	+	+	+	+	+	+	+	+
5m	–	+	+	+	+	+	+	++
5n	++	++	++	+++	++	++	++	+++
GF	+++	++++	+++	++++	+++	++++	+++	++++

GF = griseofulvin, inhibition diameter in mm, (-) <4, (+) 4-12, (++) 12-18, (+++) 18-26, (++++) 26-30.

Other compounds 3b-n were synthesized in the similar manner using compound 2 and various selected aromatic aldehydes. Characterization data are presented in Table 1.

2-[2'-{2''-(aryl)-4-oxo-1,3-thiazolidene}-acetylamino]-4-phenyl-1,3-thiazole (4a n) : A mixture of compound 3a (0.005 M, 1.681 g) and mercaptoacetic acid (0.005 M, 0.364 h) with a pinch of anhydrous $ZnCl_2$ was first stirred for about 2 h followed by refluxing on a water bath for about 14 h. The solvent was distilled off under reduced pressure and the solid thus obtained was purified over the column chromatography and recrystallised from ethanol to give compound 4a (Scheme 1). Yield 176-178°C. Anal. calcd. for $C_{20}H_{18}N_4O_2S_2$, C 58.54, H 4.38, N 13.64%; found C 58.51, H 4.36, N 13.62%; IR : 3353 (-NH), 1664 (>C=O), 2966 ($-CH_2$), 2992 (-N-CH-S), 1710 (cyclic >C=O), 2846 (-CH of thiazole), 1193, 1079, 689 (C-S-C), 1419 (-C=N-), 3021, 1598, 738 cm^{-1} (aromatic ring) : ^1H NMR, δ6.91-7.75 (m, 10H, Ar-H), 6.57 (s, 1H, C-5 of thiazole), 8.13 (s, 1H, -NHCO), 7.81 (s, 1H, NHN-), 4.83 (s, 1H, -N-CH), 4.36 (s, 2H, $-CH_2$), 3.68 (s, 2H, $-CH_2S$).

Similarly other compounds 4b-n were synthesized from 3b-n. Characterization data are presented in Table 1.

2-[2'-{2''-(aryl)-5''-(arylidene)-4-oxo-1,3-thiazolidene}-acetylamino]-4-phenyl-1,3-thiazole (5a n) : A mixture of compound 4a (0.004 M, 1.64 g), and benzaldehyde (0.005 M, 0.40 g) in benzene (30 ml) in the presence of sodium ethoxide were refluxed on a water bath for about 4 h. The solvent was distilled off under reduced pressure and the solid thus obtained was purified over the column chromatography and recrystallized from ethanol to give compound 5a (Scheme 1). Yield 79%, m.p. 177-179°C; Anal. calcd. for $C_{27}H_{22}N_4O_2S_2$, C 65.06, H 4.41, N 11.23%, found C 64.98, H 4.38, N 11.22%; IR : 3353 (-NH), 1668 (>C=O), 2963 ($-CH_2$), 2989 (N-C-S), 1632 (C=CH-Ar), 1196, 1076, 689 (C-S-C), 2843 (-CH of thiazole), 1416 (-C=N), 1713 (cyclic >C=O), 3027 1593, 734 cm^{-1} (aromatic ring); ^1H NMR δ6.93-7.78 (m, 15H, Ar-H), 6.62 (s, 1H, C-5 of thiazole), 8.12 (s, 1H, -NHCO-), 7.82 (s, 1H, -NHN), 4.81 (s, 1H, -N-CH), 4.35 (s, 2H, $-CH_2$), 5.26 (s, 1H, C=CH-Ar).

Other compounds 5b-n were synthesized in the similar manner using compounds 4b-n and various selected aromatic aldehydes. Characterization data are presented in Table 1.

Antimicrobial activity : All the synthesized compound 1, 2, 3a-n, 4a-n and 5a-n have been screened *in vitro* for their antimicrobial activity against *B. substilis, E. coli, S. aureus and K. pneumoneae* bacteria and antifungal activity against *A. niger, A. flavus, F. oxisporium* and *T. viride* fungi by filter paper disc diffusion method. Standard antibacterial streptomycin and antifungal griseofulvin were also screened under the similar conditions for comparison. Results are presented in Table 2 and 3 respectively.

Acknowledgement

The authors thank SAIF, CDRI Lucknow for providing spectral and analytical data of the compounds. We are also grateful to Dr. Mrs. Archana Tiwari, Department of Biotechnology, Dr. H.S. Gour University, Sagar (M.P.) for providing help in carrying out the antimicrobial screening. We thank Professor S.K. Srivastava, Department of Chemistry of this University for his cooperation and suggestions and to Head, Department of Chemistry for giving the facilities to carryout the work.

References

1. Asati KC, Srivastava SK & Srivastava SD. Synthesis of 5-arylidene-2-aryl-3-(benzotriazoloacetamidyl)- 1,3-thiazolidene-4-one as analgesic and antimicrobial agent. *Indian J Chem* 2006; **45B** : 526-531.
2. Yadav R, Srivastava SD & Srivastava SK. Synthesis, anti-microbial and anti-inflammatory activity of 4-oxothiazolidines and their 5-arylidens. *Indian J Chem* 2005; **44B** : 1262-1266.
3. Parikh AK, Oza PS & Bhatt SB. A synthesis of some new 2-azetidinones as potential antitubercular agents. *Indian J Chem* 2000; **39B** : 716-718.
4. Mistry KM & Desai KR. Microwave assisted rapid and efficient synthesis of nitrogen and sulphur containing heterocyclic compounds and their pharmacological evaluation. *Indian J Chem* 2006; **45B** : 1762-1766.
5. Pattan RS & Ali MS. Synthesis and microbiological evaluation of 2-acetamido-4-arylthiazole derivative. *Indian J Chem* 2006; **45B** : 1929-1932.
6. Altiantas H, Ates O & Otuk G. Synthesis, characterization and evaluation of antimicrobial activity of Mannich base of some 2-[(4-carbetoxymethylthiazole-2-yl) imino]-4-thiazolidines. *Indian J Chem* 2005; **44B** : 586-589.

7. Vashi BS, Mehta DS & Shah VH. Synthesis of new 2-(substituted-benzothiazolyl carbamoyl)-benzimidazole as potential CNS depressants. *Indian J Chem* 1995; **34B** : 802-805.

8. Pattan RS, Reddy VV & Desai BG. Synthesis of N-3[4-(4-chlorophenyl-thiazole-2-yl)-(2-amino-metyl)-quinazoline-4 (3H)-one] and their derivatives for antitubercular activity. *Indian J Chem* 2006; **45B** : 1778-1781.

9. Mehra SC, Zaman S & Khan AA. Synthesis of alkyl/arylaminopropionyl-2-amino-4-phenyl thiazole, 2-aminobenzothiazole and 2-amino(substituted) benzothiazole as potential local anaestetic. *Indian J Chem Soc* 1980; LVIII, 829-832.

10. Srivastava SK, Jain A, Srivastava S & Srivastava SD. Synthesis and biological evaluation of benzooxazolo-arylated-4-thiazolidinones and their 5-arylidines. *Proc Nat Acad Sci* 2007; **77A** : 101-108.

11. Desai KG & Desai KR. Synthesis of some novel pharmacologically active Schiff base using microwave method and their derivatives formazans by conventional method. *Indian J Chem* 2005; **44B** : 2097-2101.

12. Guru N & Srivastava SD. Synthesis of some new 1-5[5'-{2-benzothiazolyl thio) methyl}-1',3',4'-thiadiazole-2'-yl]-4-substituted-3-chloro-2-azetidinones : Antimicrobial agents. *J Sci Industrial Res* 2001; **60** : 601-605.

Proc. Nat. Acad. Sci. India Sect. A, Vol. 78, Pt. II, 2008

Recurrences with respect to a semi-symmetric metric connection on an almost Hermite manifold

P.N. PANDEY and B.B. CHATURVEDI*

Department of Mathematics, University of Allahabad, Allahabad-211 002, INDIA.

Email : pnpiaps@rediffmail.com; braj-bhushan25@rediffmail.com

Received November 9, 2006; Accepted May 15, 2007

Abstract

In the present paper recurrent almost Hermite manifolds with respect to a Riemannian connection and a semi-symmetric metric connection have been introduced and the necessary and sufficient condition for a recurrent almost Hermite manifold with respect to Riemannian connection to be recurrent almost Hermite manifold with respect to semi-symmetric metric connection has been obtained . The relation between the recurrences of Ricci tensor, H-projective tensor and projective tensor with respect to these connections have also been discussed.

(**Keywords** : almost Hermite manifold/semi-symmetric metric connection/Riemannian connection/Ricci-recurrent/H-projective recurrent/projective recurrent)

Introduction

Three dimensional spaces of recurrent curvature were studied by Ruse[1] for the first time. Rastogi[2] studied C^r-recurrent Riemannian spaces while Roter[3] studied second order recurrent spaces. The Riemannian manifold equipped with a semi-symmetric metric connection has been studied by Andonie[4], Chaki and Konar[5]. Pandey and Dubey[6] discussed an almost Grayan manifold equipped with semi-symmetric metric connection while Ray[7] studied a Kähler manifold equipped with semi-symmetric metric connection. The aim of the present paper is to discuss the relation between different types of recurrences with respect to a Riemannian connection and a semi-symmetric metric connection in an almost Hermite manifold.

An even dimensional differentiable manifold M_{2n} is said to be an almost Hermite manifold with structure $\{F,g\}$ if

$$\overline{\overline{X}} + X = 0, \tag{1}$$

and

$$g(\overline{X}, \overline{Y}) = g(X, Y) \tag{2}$$

where $\overline{X} \overset{def}{=} FX$, F is a tensor of type (1,1), g is the metric tensor and X,Y are arbitrary vector fields.

A linear connection ∇ on $\{F,g\}$ is said to be a semi-symmetric metric connection if the torsion tensor S of the connection ∇ and the metric g of the manifold satisfy the following conditions :

$$(\nabla_Z g)(X, Y) = 0, \tag{3}$$

$$S(X, Y) = \omega(Y) X - \omega(X) Y, \tag{4}$$

for arbitrary vector fields X and Y. The symbol ω stands for a 1–form associated with the torsion tensor of the connection ∇. The relation between the semi-symmetric metric connection ∇ and Riemannian connection D is given as[8,9]

$$\nabla_X Y = D_X Y + \omega(Y) X - g(X, Y)\rho \tag{5}$$

where

$$\omega(X) = g(X, \rho) \tag{6}$$

and ω also satisfies the equation

$$(\nabla_X \omega)(Y) = (D_X \omega) Y - \omega(X)\,\omega(Y) + \omega(\rho)\, g(X,Y). \tag{7}$$

Let us put

$$\omega(Y)X - g(X, Y) = H(X, Y), \tag{8}$$

equation (5) becomes

$$\nabla_X Y = D_X Y + H(X, Y). \quad (9)$$

Curvature Tensor on an almost Hermite Manifold with Condition $\nabla_X \omega = 0$

From equation (9), we have

$$\nabla_Y Z = D_Y Z + H(Y, Z). \quad (10)$$

On differentiating equation (10), we get

$$\nabla_X \nabla_Y Z = D_X D_Y Z + (D_X H)(Y, Z) + H(X, H(Y, Z))$$
$$+ H(D_X Y, Z) + H(Y, D_X Z) + H(X, D_Y Z). \quad (11)$$

Interchanging X, Y in equation (11), we have

$$\nabla_Y \nabla_X Z = D_Y D_X Z + (D_Y H)(X, Z) + H(Y, H(X, Z))$$
$$+ H(D_Y X, Z) + H(X, D_Y Z) + H(Y, D_X Z). \quad (12)$$

From equation (10), we can write

$$\nabla_{[X,Y]} Z = D_{[X,Y]} Z + H([X, Y], Z) \quad (13)$$

Subtracting equations (12) and (13) from equation (11), we get

$$K(X,Y,Z) = K(X,Y,Z) + (D_X H)(Y, Z) - (D_Y H)(X,Z)$$
$$+ H(X, H(Y,Z)) - H(Y, H(X, Z)). \quad (14)$$

Taking covariant derivative of equation (8) with respect to connection D, we have

$$(D_X H)(Y, Z) = (D_X \omega)(Z)\, Y - g(Y, Z)(D_X \rho). \quad (15)$$

If we suppose

$$\nabla_X \omega = 0, \quad (16)$$

then from equation (7), we can write

$$(D_X \omega) Z = \omega(X)\,\omega(Z) - \omega(\rho)\, g(X, Z). \quad (17)$$

From equation (17)

$$D_X \rho = \omega(X)\rho - \omega(\rho)X. \quad (18)$$

Using equations (17) and (18) in equation (15), we get

$$(\nabla_X H)(Y, Z) = \omega(X)\,\omega(Z)\, Y - g(X, Z)\,\omega(\rho) Y$$
$$- g(Y, Z)\, S(\rho, X). \quad (19)$$

Interchanging X and Y in equation (19), we have

$$(\nabla_Y H)(X, Z) = \omega(Y)\,\omega(Z)\, X - g(Y, Z)\,\omega(\rho) X$$
$$- g(X, Z)\, S(\rho, Y). \quad (20)$$

From (8), we get

$$H(X, H(Y, Z)) - H(Y, H(X, Z)) = \omega(Z)\, S(X, Y)$$
$$+ g(X, Z)\, S(Y, \rho) - g(Y, Z)\, S(X, \rho), \quad (21)$$

where S is the torsion tensor with respect to the connection ∇ and using equations (19), (20) and (21) in equation (14), we obtain

$$\tilde{K}(X,Y,Z) = K(X,Y,Z) + \omega(\rho)\{g(Y,Z)X - g(X,Z)Y\}. \quad (22)$$

Recurrent almost Hermite Manifold

An almost Hermite manifold M_{2n} is said to be recurrent with respect to Riemannian connection D if

$$(D_T K)(X,Y,Z) = T\, K(X,Y,Z) \quad (23)$$

where T is a recurrent vector field.

Now we propose :

Theorem 1 : If an almost Hermite manifold is a recurrent manifold with respect to Riemannian connection D, it is also recurrent with respect to semi-symmetric metric connection ∇ if and only if

$$g(T, X)\, K(\rho, Y, Z) + g(T, Y)\, K(X, \rho, Z) + g(T, Z)$$
$$K(X, Y, \rho) + {}'K(X, Y, Z, \rho)\, T = \omega(X) K(T, Y, Z)$$
$$+ \omega(Y)\, K(X, T, Z) + \omega(Z)\, K(X, Y, T) + {}'K(X, Y, Z, T)\rho$$
$$+ \omega(\rho)\, \{g(Y, Z)\, X - g(X, Z)\, Y\}. \quad (24)$$

Proof. Taking covariant derivative of equation (22) with respect to connection ∇, we have

$$(\nabla_T \tilde{K})(X,Y,Z) = (\nabla_T K)(X,Y,Z). \quad (25)$$

For vector field $K(X,Y,Z)$ equation (5) becomes

$$\nabla_T K(X,Y,Z) = D_T K(X,Y,Z) + \omega(K(X,Y,Z))T - g(K(X,Y,Z),T)\rho. \quad (26)$$

Equation (26) implies

$$(\nabla_T K)(X,Y,Z) + K(\nabla_T X,Y,Z) + K(X,\nabla_T Y,Z) + K(X,Y,\nabla_T Z) = (D_T K)(X,Y,Z) + K(D_T X,Y,Z) + K(X,D_T Y,Z) + K(X,Y,D_T Z) + \omega(K(X,Y,Z))T - g(K(X,Y,Z),T)\rho. \quad (27)$$

Using relation (5) in equation (27), we get

$$(\nabla_T K)(X,Y,Z) + \omega(X)K(T,Y,Z) - g(T,X)K(\rho,Y,Z) + \omega(Y)K(X,T,Z) - g(T,Y)K(X,\rho,Z) + \omega(Z)K(X,Y,T) - g(T,Z)K(X,Y,\rho) = (D_T K)(X,Y,Z) + {}'K(X,Y,Z,\rho)T - {}'K(X,Y,Z,T)\rho. \quad (28)$$

Using equations (23) and (25) in equation (28), we have

$$(\nabla_T \tilde{K})(X,Y,Z) = T\,K(X,Y,Z) + g(T,X)K(\rho,Y,Z) + g(T,Y)K(X,\rho,Z) + g(T,Z)K(X,Y,\rho) + {}'K(X,Y,Z,\rho)T - \omega(X)K(T,Y,Z) - \omega(Y)K(X,T,Z) - \omega(Z)K(X,Y,T) - {}'K(X,Y,Z,T)\rho. \quad (29)$$

Using equation (22) in equation (29), we get

$$(\nabla_T \tilde{K})(X,Y,Z) = T\,\tilde{K}(X,Y,Z) + [g(T,X)K(\rho,Y,Z) + g(T,Y)K(X,\rho,Z) + g(T,Z)K(X,Y,\rho) + {}'K(X,Y,Z,\rho)T] - [\omega(X)K(T,Y,Z) + \omega(Y)K(X,T,Z) + \omega(Z)K(X,Y,T) + {}'K(X,Y,Z,T)\rho] - T\,\omega(\rho)[g(Y,Z)X - g(X,Z)Y]T. \quad (30)$$

From equation (30) we observe that almost Hermite manifold is recurrent with respect to connection ∇ if and only if equation (24) holds.

Ricci recurrent almost Hermite Manifold

An almost Hermite Manifold is said to be Ricci recurrent with respect to Riemannian connection D if

$$(D_T Ric)(Y,Z) = T\,Ric(Y,Z) \quad (31)$$

where T is a recurrent vector field.

Contracting equation (22) with respect to X, we have

$$\widetilde{Ric}(Y,Z) = Ric(Y,Z) + (n-1)\omega(\rho)g(Y,Z). \quad (32)$$

$\widetilde{Ric}$ and Ric are the Ricci tensor with respect to semi-symmetric metric connection and Riemannian connection respectively.

Now, we propose :

Theorem 2 : If almost Hermite manifold is Ricci-recurrent with respect to connection D, it is Ricci recurrent with respect to connection ∇ if and only if

$$\omega(R)g(TY,Z) = g(T,R)g(\rho Y,Z) - (n-1)\omega(\rho)g(Y,Z)T. \quad (33)$$

Proof : Differentiating both sides of equation (32) covariantly with respect to the connection ∇, we get

$$(\nabla_T \widetilde{Ric})(Y,Z) = (\nabla_T Ric)(Y,Z). \quad (34)$$

By definition of Ricci tensor, we have

$$Ric\ (Y,\ Z) = g(RY,\ Z). \quad (35)$$

Differentiating equation (35) with respect to connection ∇, we get

$$(\nabla_T Ric)(Y,Z) + Ric(\nabla_T Y,Z) + Ric(Y,\nabla_T Z) = g(R\nabla_T Y,Z) + g(Y\nabla_T R,Z) + g(RY,\nabla_T Z). \quad (36)$$

Using equation (35) in equation (36), we get

$$(\nabla_T Ric)(Y,Z) = g(Y\nabla_T R,Z). \quad (37)$$

From equation (5) we may write

$$\nabla_T R = D_T R + \omega(R)T - g(T,R)\rho. \quad (38)$$

In view of equation (38), equation (37) gives

$$(\nabla_T Ric)(Y,Z) = g(YD_T R,Z) + \omega(R)g(TY,Z) - g(T,R)g(\rho Y,Z). \quad (39)$$

Differentiating equation (32) with respect to the connection D, we obtain

$$(D_T Ric)\ (Y, Z) = g(YD_T R, Z). \tag{40}$$

Using equation (40) in equation (39), we have

$$(\nabla_T \tilde{R}ic)(Y,Z) = (D_T Ric)(Y,Z) + \omega(R) g(TY,Z).$$
$$-g(T,R) g(\rho Y, Z). \tag{41}$$

Using equations (31) and (32) in equation (41), we get

$$(\nabla_T \tilde{R}ic)(Y,Z) = T\tilde{R}ic(Y,Z) + \omega(R) g(TY,Z)$$
$$-g(T,R) g(\rho Y,Z) - (n-1)\omega(\rho) g(Y,Z) T. \tag{42}$$

From equation (42) we observe that the almost Hermite manifold is Ricci-recurrent with respect to connection ∇ if and only if equation (33) holds.

H-projective Recurrent almost Hermite Manifold

An almost Hermite manifold is said to be H-projective recurrent with respect to Riemannian connection D if

$$(D_T P)\ (X,Y,Z) = T P(X,Y,Z), \tag{43}$$

where T is a recurrent vector field.

In an almost Hermite manifold, H-projective curvature tensor with respect to semi-symmetric metric connection ∇ is given by

$$2\tilde{P}(X,Y,Z) = 2\tilde{K}(X,Y,Z) - \frac{1}{n+1}\{\tilde{R}ic(Y,Z)X - \tilde{R}ic(X,Z)Y$$
$$-\tilde{R}ic(Y,\bar{Z})\bar{X} + \tilde{R}ic(X,\bar{Z})\bar{Y} + 2\,\tilde{R}ic(X,\bar{Y})\bar{Z}\}. \tag{44}$$

Differentiating equation (44) covariantly with respect to the connection ∇, we have

$$2(\nabla_T \tilde{P})(X,Y,Z) = 2(\nabla_T \tilde{K})(X,Y,Z) - \frac{1}{n+1}$$
$$\{(\nabla_T \tilde{R}ic)(Y,Z)X - (\nabla_T \tilde{R}ic)\ (X,Z)Y -$$
$$(\nabla_T \tilde{R}ic)\ (Y,\bar{Z})\bar{X} + (\nabla_T \tilde{R}ic)\ (X,\bar{Z})\bar{Y}$$
$$+2(\nabla_T \tilde{R}ic)\ (X,\bar{Y})\bar{Z}\}. \tag{45}$$

From equations (30), (42) and (45), we get

$$2(\nabla_T \tilde{P})\ (X,Y,Z) = 2T\tilde{K}(X,Y,Z) + g(T,X)K(\rho,Y,Z)$$
$$+g(T,Y)K(X,\rho,Z) + g(T,Z)K(X,Y,\rho) +' K(X,Y,Z,\rho)T$$
$$-\omega(X)K(T,Y,Z) - \omega(Y)K(X,T,Z) - \omega(Z)K(X,Y,T)$$
$$-'K(X,Y,Z,T)\rho - \omega(\rho)[g(Y,Z)X - g(X,Z)Y]T - \frac{1}{n+1}$$
$$[T\tilde{R}ic(Y,Z)X + \omega(R)g(TY,Z)X - g(T,R)g(\rho Y,Z)X$$
$$-(n-1)\omega(\rho)g(Y,Z)TX - T\tilde{R}ic(X,Z)Y - \omega(R)g(TX,Z)Y$$
$$+g(T,R)g(\rho X,Z)Y + (n-1)\omega(\rho)g(X,Z)TY$$
$$-T\tilde{R}ic(Y,\bar{Z})\bar{X} - \omega(R)g(TY,\bar{Z})\bar{X} + g(T,R)g(\rho Y,\bar{Z})\bar{X}$$
$$+(n-1)\omega(\rho)g(Y,\bar{Z})T\bar{X} + TRic(X,\bar{Z})\bar{Y} + \omega(R)g(TX,\bar{Z})\bar{Y}$$
$$-g(T,R)g(\rho X,\bar{Z})\bar{Y} - (n-1)\omega(\rho)g(X,\bar{Z})T\bar{Y}$$
$$+2TRic(X,\bar{Y})\bar{Z} + 2\omega(R)g(TX,\bar{Y})\bar{Z} - 2g(T,R)g(\rho X,\bar{Y})\bar{Z}$$
$$-2(n-1)\omega(\rho)g(X,\bar{Y})\bar{Z}]. \tag{46}$$

Equation (46) implies

$$2(\nabla_T \tilde{P})(X,Y,Z) = 2T\tilde{P}(X,Y,Z) + g(T,X)K(\rho,Y,Z)$$
$$+g(T,Y)K(X,\rho,Z) + g(T,Z)K(X,Y,\rho) +' K(X,Y,Z,\rho)T$$
$$-\omega(X)K(T,Y,Z) - \omega(Y)K(X,T,Z) - \omega(Z)K(X,Y,T)$$
$$-'K(X,Y,Z,T)\rho - \frac{n}{n+1}\omega(\rho)T[g(Y,Z)X - g(X,Z)Y]$$
$$-\frac{\omega(R)}{n+1}[g(TY,Z)X - g(TX,Z)Y - g(TY,\bar{Z})\bar{X}$$
$$+g(TX,\bar{Z})\bar{Y} + 2g(TX,\bar{Y})\bar{Z}] + \frac{g(T,R)}{n+1}[g(\rho Y,Z)X$$
$$-g(\rho X,Z)Y - g(\rho Y,\bar{Z})\bar{X} + g(\rho X,\bar{Z})\bar{Y} + 2g(\rho X,\bar{Y})\bar{Z}]$$
$$-\frac{(n-1)\omega(\rho)}{n+1}[g(Y,\bar{Z})\bar{X} - g(X,\bar{Z})\bar{Y} - 2g(X,\bar{Y})\bar{Z}]T. \tag{47}$$

From equation (47) it is clear that

$$g(T,X)K(\rho,Y,Z)+g(T,Y)K(X,\rho,Z)+g(T,Z)K(X,Y,\rho)$$

$$+'K(X,Y,Z,\rho)T-\omega(X)K(T,Y,Z)-\omega(Y)K(X,T,Z)$$

$$-\omega(Z)K(X,Y,T)-'K(X,Y,Z,T)\rho-\frac{n}{n+1}\omega(\rho)T[g(Y,Z)X$$

$$-g(X,Z)Y]-\frac{\omega(R)}{n+1}[g(TY,Z)X-g(TX,Z)Y-g(TY,\bar{Z})\bar{X}$$

$$+g(TX,\bar{Z})\bar{Y}+2g(TX,\bar{Y})\bar{Z}]+\frac{g(T,R)}{n+1}[g(\rho Y,Z)X$$

$$-g(\rho X,Z)Y-g(\rho Y,\bar{Z})\bar{X}+g(\rho X,\bar{Z})\bar{Y}+2g(\rho X,\bar{Y})\bar{Z}]$$

$$-\frac{(n-1)\omega(\rho)}{n+1}[g(Y,\bar{Z})\bar{X}-g(X,\bar{Z})\bar{Y}-2g(X,\bar{Y})\bar{Z}]T=0 \tag{48}$$

if and only if

$$(\nabla_T\tilde{P})(X,Y,Z)=T\tilde{P}(X,Y,Z). \tag{49}$$

Thus we conclude :

Theorem 3 : If an almost Hermite manifold is recurrent with respect to Riemannian connection then it is H-projective recurrent with respect to the semi symmetric connection ∇ if and only if equation (48) holds.

Theorem 4 : For an almost Hermite manifold, if any two of the following hold, third also holds:

(i) It is recurrent with respect to semi-symmetric metric connection.

(ii) It is Ricci-recurrent with respect to semi-symmetric metric connection.

(iii) It is H-projective recurrent with respect to semi symmetric metric connection.

Proof : Taking covariant derivatives of both sides of equation (44) with respect to connection ∇, we have

$$2(\nabla_T\tilde{P})(X,Y,Z)=2(\nabla_T\tilde{K})(X,Y,Z)-\frac{1}{(n+1)}$$

$$\{(\nabla_T\widetilde{Ric})(Y,Z)X-(\nabla_T\widetilde{Ric})(X,Z)Y-(\nabla_T\widetilde{Ric})(Y,\bar{Z})\bar{X}$$

$$+(\nabla_T\widetilde{Ric})(X,\bar{Z})\bar{Y}+2(\nabla_T\widetilde{Ric})(X,\bar{Y})\bar{Z}\}. \tag{50}$$

Suppose that the manifold is recurrent and Ricci recurrent then equation (44) becomes

$$(\nabla_T\tilde{P})(X,Y,Z)=T\Big[2\tilde{K}(X,Y,Z)-\frac{1}{n+1}\{\widetilde{Ric}(Y,Z)X$$

$$-\widetilde{Ric}(X,Z)Y-\widetilde{Ric}(Y,\bar{Z})\bar{X}+\widetilde{Ric}(X,\bar{Z})\bar{Y}\}\Big]. \tag{51}$$

Using equation (44) in equation (51), we get

$$(\nabla_T\tilde{P})(X,Y,Z)=T\tilde{P}(X,Y,Z).$$

This shows that the manifold is H-projective recurrent.

Now, suppose that the manifold is Ricci-recurrent and H-projective recurrent then equation (50) becomes

$$2(\nabla_T\tilde{K})(X,Y,Z)=2T\tilde{P}(X,Y,Z)+\frac{1}{n+1}\{T\widetilde{Ric}(Y,Z)X$$

$$-T\widetilde{Ric}(X,Z)Y-T\widetilde{Ric}(Y,\bar{Z})\bar{X}$$

$$+T\widetilde{Ric}(X,\bar{Z})\bar{Y}+2T\widetilde{Ric}(X,\bar{Y},)\bar{Z}\}, \tag{52}$$

and equations (52) and (44) imply

$$\nabla_T\tilde{K}(X,Y,Z)=T\tilde{K}(X,Y,Z).$$

This shows that manifold is recurrent manifold.

Again, suppose that the manifold is H-projective recurrent and recurrent then equation (50) can be written as

$$\frac{1}{n+1}\{(\nabla_T\widetilde{Ric})(Y,Z)X-(\nabla_T\widetilde{Ric})(X,Z)Y-(\nabla_T\widetilde{Ric})$$

$$(Y,\bar{Z})\bar{X}+(\nabla_T\widetilde{Ric})(X,\bar{Z})\bar{Y}+2(\nabla_T\widetilde{Ric})(X,\bar{Y})\bar{Z}\}=$$

$$=T(2\tilde{K}(X,Y,Z)-2\tilde{P}(X,Y,Z)). \tag{53}$$

Using equation (44) in equation (53), we get

$$(\nabla_T\widetilde{Ric})(Y,Z)X-(\nabla_T\widetilde{Ric})(X,Z)Y-(\nabla_T\widetilde{Ric})(Y,\bar{Z})\bar{X}$$

$$+(\nabla_T\widetilde{Ric})(X,\bar{Z})\bar{Y}+2(\nabla_T\widetilde{Ric})(X,\bar{Y})\bar{Z}$$

$$=T\{\widetilde{Ric}(Y,Z)X-\widetilde{Ric}(X,Z)Y-\widetilde{Ric}(Y,\bar{Z})\bar{X}+\widetilde{Ric}(X,\bar{Z})\bar{Y}$$

$$+2\widetilde{Ric}(X,\bar{Y})\bar{Z}\}.$$

This shows that the manifold is Ricci-recurrent.

Weyl Projective Recurrent almost Hermite Manifold

Weyl projective curvature with respect to semi symmetric metric connection is given by

$$\widetilde{W}(X,Y,Z)=\widetilde{K}(X,Y,Z)+\frac{1}{n-1}\{\widetilde{Ric}(X,Z)Y-\widetilde{Ric}(Y,Z)X\}. \tag{54}$$

Differentiating both sides of equation (54) covariantly with respect to connection ∇, we have

$$(\nabla_T\widetilde{W})(X,Y,Z)=(\nabla_T\widetilde{K})(X,Y,Z)+\frac{1}{n-1}\{(\nabla_T\widetilde{Ric})$$

$$(X,Z)Y-(\nabla_T\widetilde{Ric})(Y,Z)X\}. \tag{55}$$

Using equations (30) and (42) in equation (55) we get

$$(\nabla_T\widetilde{W})(X,Y,Z)=T\widetilde{K}(X,Y,Z)+g(T,X)K(\rho,Y,Z)$$

$$+g(T,Y)K(X,\rho,Z)+g(T,Z)K(X,Y,\rho)+'K(X,Y,Z,\rho)T$$

$$-\omega(X)K(T,Y,Z)-\omega(Y)K(X,T,Z)-\omega(Z)K(X,Y,T)$$

$$-'K(X,Y,Z,T)\rho-T\omega(\rho)[g(Y,Z)X-g(X,Z)Y]+\frac{1}{n-1}$$

$$[T\widetilde{Ric}(X,Z)Y+\omega(R)g(TX,Z)Y-g(T,R)g(\rho X,Z)Y$$

$$-(n-1)\omega(\rho)g(X,Z)TY-T\,Ric(Y,Z)X-\omega(R)g(TY,Z)X$$

$$-g(T,R)g(\rho Y,Z)X-(n-1)\omega(\rho)g(Y,Z)TX. \tag{56}$$

Using equation (54) in equation (56), we have

$$(\nabla_T\widetilde{W})(X,Y,Z)=T\,\widetilde{W}(X,Y,Z)+g(T,X)K(\rho,Y,Z)$$

$$+g(T,Y)K(X,\rho,Z)+g(T,Z)K(X,Y,\rho)+'K(X,Y,Z,\rho)T$$

$$-\omega(X)K(T,Y,Z)-\omega(Y)K(X,T,Z)-\omega(Z)K(X,Y,T)$$

$$-'K(X,Y,Z,T)\rho+\frac{1}{n-1}\{\omega(R)g(TX,Z)Y-\omega(R)g(TY,Z)X$$

$$-g(T,R)g(\rho X,Z)Y-g(T,R)g(\rho Y,Z)X\}. \tag{57}$$

From equation (57) it is clear that if

$$g(T,X)K(\rho,Y,Z)+g(T,Y)K(X,\rho,Z)+g(T,Z)$$

$$K(X,Y,\rho)+'K(X,Y,Z,\rho)T+\frac{1}{n-1}\{\omega(R)g(TX,Z)Y$$

$$-\omega(R)g(T,Y,Z)X-g(T,R)g(\rho X,Z)Y-g(T,R)g(\rho Y,Z)X\}=$$

$$\omega(X)K(T,Y,Z)+\omega(Y)K(X,T,Z)+\omega(Z)K(X,Y,T)$$

$$+'K(X,Y,Z,T)\rho. \tag{58}$$

Then equation (57) becomes

$$(\nabla_T\widetilde{W})(X,Y,Z)=T\widetilde{W}(X,Y,Z).$$

Thus, we conclude :

Theorem 5 : If an almost Hermite manifold is recurrent with respect to Riemannian connection then it is projective recurrent with respect to semi-symmetric metric connection ∇ if and only if equation (58) holds.

Theorem 6 : In an almost Hermite manifold, if any two of the following conditions hold, then third also holds:

(i) It is recurrent with respect to connection ∇.

(ii) It is Ricci-recurrent with respect to connection ∇.

(iii) It is projective recurrent with respect to connection ∇.

Proof . Suppose that the manifold is recurrent with respect to connection ∇, then equation (55) becomes

$$(\nabla_T \widetilde{W})(X,Y,Z) = T\left[\widetilde{K}(X,Y,Z) + \frac{1}{n-1}\left\{\widetilde{Ric}(X,Z)Y - \widetilde{Ric}(Y,Z)X\right\}\right]. \quad (59)$$

Using equation (54) in equation (59), we have

$$(\nabla_T \widetilde{W})(X,Y,Z) = T\widetilde{W}(X,Y,Z).$$

Hence the manifold is projective recurrent.

Now suppose that the manifold is Ricci-recurrent and projective recurrent then from equation (55), we have

$$(\nabla_T \widetilde{K})(X,Y,Z) = T\left[\widetilde{W}(X,Y,Z) - \frac{1}{n-1}\left\{\widetilde{Ric}(X,Z)Y - \widetilde{Ric}(Y,Z)X\right\}\right]. \quad (60)$$

Using equation (54) in equation (60), we get

$$(\nabla_T \widetilde{K})(X,Y,Z) = T\widetilde{K}(X,Y,Z).$$

Therefore manifold is recurrent.

Again suppose that the manifold is projective recurrent and recurrent with respect to ∇, then from equation (55), we have

$$\frac{1}{n-1}\left[(\nabla_T \widetilde{Ric})(X,Z)Y - (\nabla_T \widetilde{Ric})(Y,Z)X\right]$$

$$= T\left\{\widetilde{W}(X,Y,Z) - \widetilde{K}(X,Y,Z)\right\}. \quad (61)$$

Using equation (54) in equation (61), we get

$$(\nabla_T \widetilde{Ric})(X,Z)Y - (\nabla_T \widetilde{Ric})(Y,Z)X = T\,\widetilde{Ric}(X,Z)Y - T\,\widetilde{Ric}(Y,Z)X.$$

Hence the manifold is Ricci-recurrent.

Acknowledgement

One of the authors (BBC) thanks U.G.C., New Delhi for financial support.

References

1. Ruse HS. Three dimensional spaces of recurrent curvature. *Proc Lond Math Soc* 1949; **50** : 438-446.
2. Rastogi SC. CR-Recurrent Riemannian spaces. *Journ Tensor Soc India* 1995; **13** : 1-6.
3. Roter W. Some remarks on second order recurrent spaces. *Bull Acad Polon Sci Ser Sci Math, Astron Phys* 1964; **12** : 207-211.
4. Andonie OC. Sur Une connexion semi-symtrique qui laisse invariant la tenseur de Bochner. *Ann Fac Sc Kuishawa Zaire* 1976; **1** : 247-253.
5. Chaki MC & Konar A. On a type of semi-symmetric connection on a Riemannian manifold. *J Pure Math* 1981; **1** : 77-80.
6. Pandey PN & Dubey SK. Almost Grayan manifold admitting semi-symmetric metric connection. *Tensor NS* 2004; **65** : 144-152.
7. Pandey PN & Chaturvedi BB. Semi-symmetric metric connection on a Kähler manifold. *Bull Alld Math Soc* 2007; **22** : 51-57
8. Sharma R. On the curvature of contact metric manifolds. *Journal of Geometry* 1995; **53** : 179-190.
9. Yano K & Imai T. On-semi-symmetric metric -connection. *Tensor NS* 1975; **29** : 134-138.
10. Yano K. On semi-symmetric connection. *Revue Roumame de Math Pure et Appliquees* 1970; **15** : 1579-1586.

Proc. Nat. Acad. Sci. India Sect. A, Vol. 78, Pt. II, 2008

Effect of polluted soil on the growth dynamics of plant-herbivore system: a mathematical model

O.P. MISRA, P. SINHA* and S.K.S. RATHORE+

School of Mathematics and Allied Sciences, Jiwaji University, Gwalior (M.P.)-474011, India

**Shrimant Madhav Rao Scindia Govt. Model Science College, Gwalior (M.P.)-474001, India*

+Institute of Infromation Technology and Management, Jhansi Road, Gwalior (M.P.)-474001, India

Received August 24, 2005; Finally Revised January 11, 2007; Accepted May 25, 2007

Abstract

In this paper, a mathematical model is proposed to study the effect of soil pollution on the growth dynamics of plant-herbivore system. In the model the plant biomass is divided into two compartments consisting of leaves and roots. In the modeling process, it has been assumed that the pollution in the soil causes damage to the root compartment, thereby destroying the substrates in the soil that causes damage to the root compartment thereby destroying the substrates in this compartment. Also it is assumed in the model that the pollutant is being transferred from root compartment to the leaf compartment which in turn adversely affects the substrates in this compartment also. Since the growth of plant biomass in both the compartments depend on the substrate concentration, the weight of the leaf and root compartments of plant biomass will decrease on account of the polluted soil. In the model a separate equation has been considered to study the dynamics of herbivore population. The stability analysis of the two equilibrium points of the model has been conducted. From the stability of the positive equilibrium point it has been concluded that both the plant biomass and the herbivore population would co-exist but the equilibrium densities of these two population will be reduced due to the presence of pollutant in the soil.

(**Key words:** mathematical model/equilibrium point/stability/ plant biomass/herbivore population)

Introduction

Since long our environment is getting polluted by different types of chemicals, emitted due to various human activities, such as industrialization, use of pesticides and herbicides in agriculture, unplanned urbanization and technological advancement. The biological populations are regularly exposed to several natural and artificial chemicals which are toxic to them and their environment. It is well known that the biological population in terrestrial eco-systems are affected when their habitats are stressed by pollutants emitted in the environment. The effect of pollutants is to decrease the growth and productivity of the affected species as well as the carrying capacity of the environment. The pollutants in soil can adversely affect forest, agricultural crops and vegetation by destroying their characteristics and productivity. The direct influence of heavy metal ions on tree metabolism, specially root physiology, has the potential to reduce nutrient uptake[1]. Acid precipitation causes changes in the soil properties that influence root growth or function. The acidification of the soil raises the inorganic aluminum concentration at the root zone which, at sub-lethal concentration, reduces the cation uptake rate and at lethal concentration, increases the root mortality rate. Increased levels of acidity entering the soil system could result in the leaching of essential cations away from the rooted zone, decreasing plant-nutrient uptake, or could increase the mobilization of heavy metals in the root zone, causing root damage[2]. Over the last century hydrogen ion concentration in the soil has been growing, once the latent buffering potential of a soil has exceeded, an acidic layer is formed that damages root systems (principally through the leaching of essential nutrients, including potassium, magnesium and calcium, and the release of toxic metal ions such as aluminium, maganese and cadmium), leading to the death of trees (especially conifers, which have shallow rooting systems) and the inhibition of natural regeneration by acid-sensitive plants[3].

Growth in the plant, as in any organism, consist of an irreversible increase in size, which is commonly

but not necessarily, accompanied by an increase in solid or dry weight and in the protoplasm. Growth is, generally speaking, a quantitative matter and is concerned with the increasing amount of the organism. The quantitative study of the plant growth is important from the agricultural point of view and it is also equally important in the management and conservation of ecosystem. The herbivorous animals depend on plants for their growth and survival and if the plant populations are subjected to pollution stress then the growth and existence of herbivores will also be affected adversely.

In this paper, a mathematical model is suggested to study the effect of soil pollution on the growth dynamics of plant–herbivore system. In the proposed mathematical model the plant biomass is divided into two compartments consisting of leaves and roots. In the modelling process, it has been assumed that the pollution in the soil causes damage to the root compartment, thereby destroying the substrates in this compartment. Also it is assumed in the model that the pollutant is being transferred from root compartment to the leaf compartment which in turn adversely affects the substrates in this compartment. Since the growth of plant biomass in both the compartments depend on the substrate concentration, the weight of the leaf and root compartments of plant biomass will decrease on account of the polluted soil. In the model a separate equation for herbivore density is also considered. The mathematical modelling has proved quite useful in the study and analysis of the effects of toxicants on interacting populations. Some mathematical models have been developed in this direction by several workers[4-12].

Thus in view of the above, a mathematical model consisting of system of non-linear ordinary differential equations is proposed below.

Mathematical Model

The model has been formulated using the following system of non-linear ordinary differential equations :

$$\frac{dS_l}{dt} = Q_s - \frac{k_l S_l}{K_l + S_l} W_l - b_{lr} S_l - \beta_l S_l C_l - d_l S_l \quad (1)$$

$$\frac{dS_r}{dt} = b_{lr} S_l - \frac{k_r S_r}{K_r + S_r} W_r - d_r S_r - \beta_r S_r C_r \quad (2)$$

$$\frac{dT_2}{dt} = I_0 - \alpha_2 T_2 - b_{12} T_2 \quad (3)$$

$$\frac{dC_r}{dt} = b_{12} T_2 - \sigma_l C_r - h_r S_r C_r - a_{lr} C_r \quad (4)$$

$$\frac{dC_l}{dt} = a_{lr} C_r - \sigma_2 C_l - h_l S_l C_l \quad (5)$$

$$\frac{dW_l}{dt} = g_l \frac{k_l S_l}{K_l + S_l} W_l - C_{12} X W_l - d_l W_l \quad (6)$$

$$\frac{dW_r}{dt} = g_2 \frac{k_r S_r}{K_r + S_r} W_r - d_2 W_r \quad (7)$$

$$\frac{dX}{dt} = C_{21} X W_1 - d_4 X - u X^2 \quad (8)$$

with the initial conditions :

$T_2(0) = 0,\ C_l(0) = 0,\ C_r(0) = 0,\ W_r(0) > 0,\ W_l(0) > 0,$
$X(0) > 0,\ S_r(0) > 0,\ S_l(0) > 0,$

where, the definitions and dimensions of variables and parameters are given in Table 1.

Table 1 – Definitions and dimensions of variables and parameters.

Variables/ parameters	Definitions	Dimensions
S_l	Substrate density in leaf compartment	ML^{-2}
S_r	Substrate density in root compartment	ML^{-2}
T_2	Pollutant concentration in air (Atmospheric Compartment)	ML^{-2}
C_r	Pollutant concentration in root compartment	ML^{-2}
C_l	Pollutant concentration in leaf compartment	ML^{-2}
W_l	Weight of the leaf compartment of plant biomass	M

W_r	Weight of the root compartment of plant biomass	M
Y	Population density of herbivore	No.of individuals/ L^2
Q_s	Rate of formation of substrate in leaf due to photosynthesis	$ML^{-2}T^{-1}$
d_l	Natural decay rate of substrate in leaf compartment	T^{-1}
b_{lr}	Substrate transfer rate from leaf compartment to root compartment	T^{-1}
β_l	Depletion rate of substrate in leaf due to pollution	$T^{-1}C_l^{-1}$
β_r	Depletion rate of substrate in root due to pollution	$T^{-1}C_r^{-1}$
k_l	Positive constant	$L^{-2}T^{-1}$
k_r	Positive constant	$L^{-2}T^{-1}$
K_l	Positive constant	ML^{-2}
K_r	Positive constant	ML^{-2}
d_r	Natural decay rate of substrate in root compartment	T^{-1}
I_0	Input rate of pollutant	$ML^{-2}T^{-1}$
α_2	Decay rate of pollutant	T^{-1}
b_{12}	Transfer rate of pollutant in leaf compartment	T^{-1}
σ_1	Decay rate of C_r	T^{-1}
h_r	Interaction rate of S_r with C_r	$T^{-1}C_r^{-1}$
h_l	Interaction rate of S_l with C_l	$T^{-1}C_l^{-1}$
C_{12}	Consumption rate of leaves by herbivores	L^2T^{-1}
C_{21}	Growth rate of herbivores	$T^{-1}M^{-1}$
d_1	Natural decay rate of leaves of plant biomass	T^{-1}
d_2	Natural decay rate of roots of plant biomass,	T^{-1}
d_4	Death rate of herbivores	T^{-1}
u	Intraspecific interaction rate	L^2T^{-1}
g_1	Conversion coefficients	L^2
g_2	Conversion coefficients	L^2
σ_2	Decay rate of C_l	T^{-1}
a_{lr}	Transfer rate of C_l to leaf compartment.	T^{-1}

Note – Since the model is of predictive nature, the time scale for variables will be taken either in months or in years depending upon the type of plant species, type of herbivore population and type of source of pollutant.

Here, Q_s, d_l, b_{lr}, β_l, d_r, β_r, I_0, α_2, b_{12}, σ_1, a_{lr}, h_r, σ_2, h_l, C_{12}, d_1, d_2, C_{21}, d_4, u, k_l, K_l, k_r, K_r, g_1, g_2 are all real and positive constants.

Equilibrium Points

Following two equilibrium points are obtained from the mathematical model :

(i) $E_1\left(S_l^*, S_r^*, T_2^*, C_l^*, C_r^*, W_l^*, W_r^*, X^*\right)$

where,

$$T_2^* = \frac{I_0}{\alpha_2 + b_{12}}, \quad S_r^* = \frac{d_2 K_r}{g_2 k_r - d_2}, \quad S_r^* > 0 \text{ if } g_2 k_r > d_2$$

$$C_l^* = \frac{a_{rl} C_r^*}{\sigma_2 + h_l S_l^*},$$

$$C_r^* = \frac{b_{12} I_0 (g_2 k_r - d_2)}{(\alpha_2 + b_{12})[(\sigma_l + \alpha_{rl})(g_2 k_r - d_2) + h_r d_2 K_r]},$$

$$C_r^* > 0 \text{ if } g_2 k_r > d_2$$

$$W_l^* = \frac{(K_l + S_l^*)}{k_l S_l^*}\left[Q_s - (d_l + b_{lr}) S_l^* - \frac{\beta_l a_{rl} S_l^* C_r^*}{\sigma_2 + h_l S_l^*}\right],$$

$$W_l^* > 0 \text{ if } Q_s(\sigma_2 + h_l S_l^*) > (\sigma_2 + h_l S_l^*)$$
$$(d_l + b_{lr}) S_l^* + \beta_l a_{rl} S_l^* C_r^*$$

$$W_r^* = \frac{\left(K_r + S_r^*\right)}{k_r S_r^*}\left[b_{lr} S_l^* - d_r S_r^* - \beta_r S_r^* C_r^*\right],$$

$$W_l^* > 0 \text{ if } b_{lr} S_l^* > d_r S_r^* + \beta_r S_r^* C_r^*$$

$$X^* = \frac{1}{C_{12}}\left(\frac{g_l k_l S_l^*}{K_l + S_l^*} - d_1\right),$$

$$X^* > 0 \text{ if } g_l k_l S_l^* > d_1 (K_l + S_l^*),$$

S_l^* is given by the equation,

$$B_4 S_l^{*4} + B_3 S_l^{*3} + B_2 S_l^{*2} + B_l S_l^* - B_0 = 0$$

where,

$$B_0 = \sigma_2 K_1^2 Q_s$$

$$B_1 = Q_s h_l K_1^2 + 2K_l \sigma_2 Q_s + \sigma_2 K_l k_l \left(\frac{ud_1}{C_{12}C_{21}} - \frac{d_4}{C_{21}} \right)$$

$$-\sigma_2 K_1^2 (d_l + b_{lr}) - K_1^2 \beta_l a_{rl} C_r^*$$

$$B_2 = \sigma_2 Q_s + 2K_l h_l Q_s - \frac{\sigma_2 k_l^2 u g_l}{C_{12}C_{21}} + k_l$$

$$\left(\frac{ud_1}{C_{12}C_{21}} - \frac{d_4}{C_{21}} \right) (\sigma_2 + K_l h_l) - (d_l + b_{lr})$$

$$(2\sigma_2 + K_l h_l) K_l - 2K_l \beta_l a_{rl} C_r^*$$

$$B_3 = h_l Q_s + h_l k_l \left(\frac{ud_1}{C_{12}C_{21}} - \frac{d_4}{C_{21}} \right) - \frac{h_l k_l^2 u g_l}{C_{12}C_{21}}$$

$$-\beta_l a_{rl} C_r^* - (d_l + b_{lr})(\sigma_2 + 2h_l K_l)$$

$$B_4 = h_l (d_l + b_{lr})$$

$$S_l^* = \frac{a_{rl} C_r^* - \sigma_2 C_l^*}{h_l C_l^*}$$

Above equation in S_l^* will have only one positive root provided, $B_1>0$, $B_2>0$ and $B_3>0$.

Therefore, for the uniqueness of the equilibrium point E_1 the above conditions should be strictly followed and hence the study of bifurcation is not needed at present.

Linear Stability Analysis

Theorem 1 : The equilibrium state E_1 is linearly asymptotically stable provided the following inequalities hold :

$$y_1 y_5 D_5 > (\beta_l S_l^* + D_5 h_l C_l^*)^2 \tag{9}$$

$$2D_2 D_4 y_2 y_4 > 3(D_2 \beta_r S_r^* + D_4 h_r C_r^*)^2 \tag{10}$$

Proof of Theorem 1 : Taking the perturbatiions from the equilibrium points E_1 as

$$S_1 = S_1^* + m_1,\ S_r = S_r^* + m_2,\ T_2 = T_2^* + m_3,$$
$$C_r = C_r^* + m_4,\ C_l = C_l^* + m_5,\ W_l = W_l^* + m_6,$$
$$W_r = W_r^* + m_7,\ X = X^* + m_8 \tag{11}$$

The linearised system of differential equations (1) to (8) about E_1 is given by

$$\left.\begin{aligned}
\frac{dm_1}{dt} &= -y_1 m_1 - \frac{k_l S_l^*}{K_l + S_l^*} m_6 - \beta_l S_l^* m_5 \\
\frac{dm_2}{dt} &= b_{lr} m_1 - y_2 m_2 - \beta_r S_r^* m_4 - \frac{k_r S_r^*}{K_r + S_r^*} m_7 \\
\frac{dm_3}{dt} &= -y_3 m_3 \\
\frac{dm_4}{dt} &= -h_r C_r^* m_2 + b_{12} m_3 - y_4 m_4 \\
\frac{dm_5}{dt} &= -h_l C_l^* m_1 + a_{rl} m_4 - y_5 m_5 \\
\frac{dm_6}{dt} &= \frac{g_1 k_l K_l W_l^*}{\left(K_l + S_l^*\right)^2} m_l - C_{12} W_l^* m_8 \\
\frac{dm_7}{dt} &= \frac{g_2 k_r K_r W_r^*}{\left(K_r + S_r^*\right)^2} m_2 \\
\frac{dm_8}{dt} &= C_{21} X^* m_6 - u X^* m_8
\end{aligned}\right\} \tag{12}$$

where,

$$y_1 = \frac{k_l K_l W_l^*}{\left(K_l + S_l^*\right)^2} + d_l + b_{lr} + \beta_l C_l^*,$$

$$y_2 = \frac{k_r K_r W_r^*}{\left(K_r + S_r^*\right)^2} + d_r + \beta_r C_r^*,$$

$$y_3 = \alpha_2 + b_{12},$$

$$y_4 = \sigma_1 + h_r S_r^* + a_{rl},$$

$$y_5 = \sigma_2 + h_l S_l^*.$$

Now consider the positive definite function $G(t)$ as

$$G(t) = \frac{1}{2}\left(m_1^2 + \sum_{i=2}^{8} D_i m_i^2 \right) \tag{13}$$

where,

$D_i (i = 2, 3...8)$ are arbitrary positive constants.

The time derivative of $G(t)$ is given by

$$\frac{dG}{dt} = m_1 \frac{dm_1}{dt} + \sum_{i=2}^{8} D_i m_i \frac{dm_i}{dt} \tag{14}$$

which on using the system (12) becomes,

$$\frac{dG}{dt} = -\left[\left\{ \frac{1}{2} y_1 m_1^2 - D_2 b_{lr} m_1 m_2 + \frac{1}{2} D_2 y_2 m_2^2 \right\} \right.$$

$$+ \left\{ \frac{1}{2} y_1 m_1^2 + \left(\beta_l S_l^* + D_5 h_l C_l^* \right) m_1 m_5 + \frac{1}{2} D_5 y_5 m_5^2 \right\}$$

$$+ \left\{ \frac{1}{2} D_2 y_2 m_2^2 + \left(D_2 \beta_r S_r^* + D_4 h_r C_r^* \right) m_2 m_4 \right.$$

$$\left. + \frac{1}{3} D_4 y_4 m_4^2 \right\} + \left\{ D_3 y_3 m_3^2 - D_4 b_{12} m_3 m_4 \right.$$

$$\left. + \frac{1}{3} D_4 y_4 m_4^2 \right\} + \left\{ \frac{1}{3} D_4 y_4 m_4^2 - D_5 a_{rl} m_4 m_5 \right.$$

$$\left. \left. + \frac{1}{2} D_5 y_5 m_5^2 \right\} + D_8 u X^* m_8^2 \right]$$

Using the Sylvester's criteria in the above expression and then choosing D_2, D_4, D_5, D_6, D_7 as follows :

$$D_2 < \frac{y_1 y_2}{b_{lr}^2}, \quad D_4 < \frac{4 y_3 y_4}{3 b_{12}^2} D_3, \quad D_5 < \frac{2 y_4 y_5}{3 a_{rl}^2} D_4,$$

$$D_6 = \frac{S_l^* (K_l + S_l^*)}{g_1 K_l W_l^*}, \quad D_7 = \frac{S_r^* (K_r + S_r^*)}{g_2 K_r W_r^*} D_2,$$

$$D_8 = \frac{C_{12} W_l^*}{C_{12} X^*} D_6.$$

it can be shown that dG/dt is negative definite if the conditions (9) to (10) are being satisfied. Thus it is proved that the equilibrium point E_1 is linearly asymptotically stable.

Non-Linear stability analysis about non-trivial positive equilibrium state E_1

Now we shall establish the existence of region of attraction for non-linear stability of E_1

Lemma 1 : The region

$R_1 = \{(S_l, S_r, T_2, C_l, C_r, W_l, W_r, X) : 0 < S_{ll} \leq S_l \leq S_{lu}, \; 0 < S_{rl} \leq S_r \leq S_{ru}, \; 0 < T_2, \; 0 < C_r, \; 0 < C_l, \; 0 < W_l, 0 < W_r, \; 0 < X\}$ is a region of attraction

where,

$$\left.\begin{aligned} S_{ll} &= \frac{Q_s}{k_l W_{lu} + d_l + b_{lr} + \beta_l C_{lu}}, \quad S_{lu} = \frac{Q_s}{d_l + b_{lr}}, \\ S_{rl} &= \frac{b_{lr} S_{ll}}{k_r W_{ru} + d_r + \beta_r C_{ru}}, \\ S_{ru} &= \frac{b_{lr}}{d_r} \frac{Q_s}{(d_l + b_{lr})}, \\ W_{lu} &= \frac{Q_s}{\theta}, \end{aligned}\right\} \tag{15}$$

here $\theta = \min \{(d_l + b_{lr}), (d_l - g_1 k_l S_{lu})\}$
also $d_l > g_1 k_l S_{lu}$

$$C_{ru} = \frac{b_{12} T_{2u}}{\sigma_1 + a_{rl}}, \quad C_{ll} = \frac{a_{rl} C_{rl}}{\sigma_2 + h_l S_{lu}},$$

$$C_{lu} = \frac{a_{rl} C_{ru}}{\sigma_2}, \quad C_{rl} = \frac{b_{12} T_2^*}{\sigma_1 + a_{rl} + h_r S_{ru}},$$

$$W_{ru} = \frac{b_{lr} S_{lu}}{\phi},$$

and $\phi = \min (d_r, d_2 - g_2 k_r S_{lu})$
also $d_2 > g_2 k_r S_{lu}$

Proof of Lemma 1 : We have $\dfrac{dS_l}{dt} \leq Q_s - (d_l + b_{lr}) S_l$

Hence,

$$\lim_{t\to\infty} S_l \le \frac{Q_s}{d_l + b_{lr}}.$$

Now

$$\frac{dS_r}{dt} \le b_{lr} S_{lu} - d_r S_r.$$

So

$$\lim_{t\to\infty} S_r \le \frac{b_{lr} S_{lu}}{d_r}.$$

or

$$\lim_{t\to\infty} S_r \le \frac{b_{lr} \; Q_s}{d_r (d_l + b_{lr})}.$$

Now,

$$\frac{dS_r}{dt} \ge b_{lr} S_{ll} - (k_r W_{ru} + d_r - \beta_r C_{ru}) S_r.$$

so

$$\lim_{t\to\infty} S_r \ge \frac{b_{lr} S_{ll}}{(k_r W_{ru} + d_r + \beta_r C_{ru})}.$$

Again,

$$\frac{d}{dt}(S_l + W_l) \le Q_s - (d_l + b_{lr}) S_l$$
$$+(d_l - g_l k_l S_{lu}) W_l \le Q_s - \theta(S_l + W_{lr}),$$

where $\theta = \min \{(d_l + b_{lr}), (d_l - g_1 k_l S_{lu})\}$ and $d_l > g_1 k_l S_{lu}$.

so

$$\lim_{t\to\infty} (S_l + W_l) \le \frac{Q_s}{\theta}.$$

Hence,

$$\lim_{t\to\infty} W_l \le \frac{Q_s}{\theta}.$$

Now,

$$\frac{dC_r}{dt} \le b_{12} T_{2u} - (\sigma_1 + a_{rl}) C_r,$$

$$\lim_{t\to\infty} C_r \le \frac{b_{12} T_{2u}}{\sigma_l + a_{rl}}.$$

Also,

$$\frac{dC_l}{dt} \le a_{rl} C_{ru} - \sigma_{ru} C_l,$$

so

$$\lim_{t\to\infty} C_l \le \frac{a_{rl} C_{ru}}{\sigma_2}.$$

Now,

$$\frac{dS_l}{dt} \ge Q_s - k_l S_l W_{lu} - d_l S_l - b_{lr} S_l - \beta_l S_l C_{lu},$$

$$\frac{dS_l}{dt} \ge Q_s - (k_l W_{lu} + d_l + b_{lr} + \beta_l C_{lu}) S_l,$$

so

$$\lim_{t\to\infty} S_l \ge \frac{Q_s}{k_l W_{lu} + d_l + b_{lr} + \beta_l C_{lu}}.$$

Also,

$$\frac{dC_r}{dt} \ge b_{12} T_2^* - (\sigma_l + a_{rl} + h_r S_{ru}) C_r,$$

so

$$\lim_{t\to\infty} C_r \ge \frac{b_{12} T_2^*}{\sigma_1 + a_{rl} + h_r S_{ru}}.$$

Now,

$$\frac{dC_l}{dt} \ge a_{rl} C_{rl} - (\sigma_2 + h_l S_{lu}) C_l,$$

so

$$\lim_{t\to\infty} C_l \ge \frac{a_{rl} C_{rl}}{\sigma_2 + h_l S_{lu}}.$$

Also,

$$\frac{dT_2}{dt} \le I_0 - \alpha_2 T_2,$$

Hence, .

$$\lim_{t\to\infty} T_2 \le \frac{I_0}{\alpha_2}.$$

Now,

$$\frac{d}{dt}(S_r + W_r) \le b_{lr}S_{lu} - d_rS_r - (d_2 - g_2k_rS_{ru})W_r$$
$$\le b_{lr}S_{lu} - \phi(S_r + W_r).$$

where $\phi = \min(d_r, d_2 - g_2k_rS_{ru})$ and $d_2 > g_2k_rS_{ru}$,

so

$$\lim_{t\to\infty}(S_r + W_r) \le \frac{b_{lr}S_{lu}}{\phi},$$

Hence,

$$\lim_{t\to\infty} W_r \le \frac{b_{lr}S_{lu}}{\phi},$$

Theorem 2 : The equilibrium point E_1 is non linearly asymptotically stable with respect to solution initiating in the interior of R_1 if the following inequalities hold :

$$\left.\begin{aligned}
&A_3\left\{\frac{k_lK_lW_l^*}{(K_l + S_l^*)(K_l + S_{lu})S_{lu}} + \frac{(d_l + b_{lr})}{S_{lu}} + \frac{\beta_lC_l^*}{S_{lu}} - \frac{A_1b_{lr}}{2S_{rl}}\right\}(\sigma_2 + h_lS_{ll}) > \frac{1}{2}(\beta_l + A_3h_lC_l^*)\\
&A_1A_4\left\{\frac{k_rK_rW_r^*}{(K_r + S_r^*)(K_r + S_{ru})S_{ru}} + \frac{(d_r + \beta_rC_r^*)}{S_{ru}} - \frac{b_{lr}}{2S_{rl}}\right\}(\sigma_1 + a_{rl} + h_rS_{rl}) > \frac{3}{4}\\
&(A_1\beta_r + A_4h_rC_r^*)^2 A_4(\alpha_2 + h_lS_{ll})\\
&(\sigma_l + a_{rl} + h_rS_{rl}) > \frac{3}{2}A_3a_{rl}^2\\
&A_2(\sigma_2 + b_{12})(\sigma_1 + a_{rl} + h_rS_{rl}) > \frac{3}{4}A_4b_{12}^2 \text{ and}\\
&\frac{d_r + \beta_rC_r^*}{S_{ru}} + \frac{k_rK_rW_r^*}{(K_r + S_r^*)(K_r + S_{ru})S_{ru}} > \frac{1}{2}\frac{b_{lr}}{S_{rl}}.
\end{aligned}\right\} \quad (16)$$

Proof : Taking the perturbations from the equilibrium points E_1 as

$$S_l = S_l^* + n_1,\ S_r = S_r^* + n_2,\ T_2 = T_2^* + n_3,$$
$$C_l = C_l^* + n_4,\ C_r = C_r^* + n_5,\ W_l = W_l^* + n_6,$$
$$W_r = W_r^* + n_7,\ X = X^* + n_8.$$

the non-linear system of differential equations (1) to (8) about E_1 is given by

$$\frac{dn_l}{dt} = -\frac{k_lK_lW_l^*n_1}{(K_l + S_l^*)(K_l + S_l^* + n_1)} - \frac{k_l(S_l^* + n_1)n_6}{(K_l + S_l^* + n_1)} - (d_l + b_{lr})n_1 - \beta_lS_l^*n_4 - \beta_l(C_l^* + n_4)n_1$$

$$\frac{dn_2}{dt} = b_{lr}n_1 - \frac{k_rK_rW_r^*n_2}{(K_r + S_r^*)(K_r + S_r^* + n_2)} - \frac{k_r(S_r^* + n_2)n_7}{(K_r + S_r^* + n_2)} - (d_r + \beta_rC_r^*)n_2 - \beta_r(S_r^* + n_2)n_5$$

$$\left.\begin{aligned}
&\frac{dn_3}{dt} = -(\alpha_2 + b_{12})n_3\\
&\frac{dn_4}{dt} = a_{rl}n_5 - h_lC_l^*n_1 - (\sigma_2 + h_lS_l^* + h_ln_1)n_4\\
&\frac{dn_5}{dt} = b_{12}n_3 - (\sigma_1 + a_{rl} + h_rS_r^* + h_rn_2)n_5 - h_rC_r^*n_2\\
&\frac{dn_6}{dt} = (W_r^* + n_6)\left[\frac{g_lk_lK_ln_1}{(K_l + S_l^*)(K_l + S_l^* + n_1)} - C_{12}n_8\right]\\
&\frac{dn_7}{dt} = (W_r^* + n_7)\left[\frac{K_rg_2k_rn_2}{(K_r + S_r^*)(K_r + S_r^* + n_2)}\right]\\
&\frac{dn_8}{dt} = (X^* + n_8)(-un_8 + C_{12}n_6).
\end{aligned}\right\} \quad (17)$$

Now consider the positive definite function $V(t)$ as

$$V(t)=\left\{n_1 - S_l^* \log\left(1+\frac{n_1}{S_l^*}\right)\right\} + A_1\left\{n_2 - S_r^* \log\left(1+\frac{n_2}{S_r^*}\right)\right\}$$

$$+\frac{1}{2}A_2 n_3^2 + \frac{1}{2}A_3 n_4^2 + \frac{1}{2}A_4 n_5^2$$

$$+A_5\left\{n_6 - W_l^* \log\left(1+\frac{n_6}{W_l^*}\right)\right\} + A_6\left\{n_7 - W_r^*\right.$$

$$\left.\log\left(1+\frac{n_7}{W_r^*}\right)\right\} + A_7\left\{n_8 - X^* \log\left(1+\frac{n_8}{X^*}\right)\right\}$$

where, A_i $(i = 1, 2 \ldots 7)$ are arbitrary positive constants.

The time derivative of $V(t)$ is given by

$$\frac{dV}{dt} = \frac{n_1}{S_l^* + n_1}\frac{dn_1}{dt} + A_1\frac{n_2}{S_r^* + n_2}\frac{dn_2}{dt}$$

$$+A_2 n_3 \frac{dn_3}{dt} + A_3 n_4 \frac{dn_4}{dt} + A_4 n_5 \frac{dn_5}{dt}$$

$$+A_5 \frac{n_6}{W_l^* + n_6}\frac{dn_6}{dt} + A_6 \frac{n_7}{W_r^* + n_7}\frac{dn_7}{dt}$$

$$+A_7 \frac{n_8}{X^* + n_8}\frac{dn_8}{dt}$$

which on using the system (17) becomes,

$$\frac{dV}{dt} = -\frac{k_l K_l W_l^* n_1^2}{(S_l^* + n_1)(K_l + S_l^*)(K_l + S_l^* + n_1)}$$

$$-\frac{k_l(S_l^* + n_1)n_1 n_6}{(S_l^* + n_1)(K_l + S_l^* + n_1)}$$

$$-\frac{(d_l + b_{lr})n_1^2 + \beta_l(S_l^* + n_1)n_1 n_4 + \beta_1 C_l^* n_1^2}{(S_l^* + n_1)}$$

$$+A_1\frac{b_{lr} n_1 n_2}{(S_r^* + n_2)}$$

$$-\frac{A_1 k_r K_r W_r^* n_2^2}{(S_r^* + n_2)(K_r + S_r^*)(K_r + S_r^* + n_2)}$$

$$-\frac{A_1 k_r n_2 n_7}{(K_r + S_r^* + n_2)}$$

$$-\frac{A_1(d_r + \beta_r C_r^*)n_2^2 + \beta_r A_1(S_r^* + n_2)n_2 n_5}{(S_r^* + n_2)}$$

$$-A_2(\alpha_2 + b_{12})n_3^2 + A_3 a_{rl} n_4 n_5 - A_3\sigma_2 n_4^2$$

$$-A_3 h_l C_l^* n_1 n_4 - A_3 h_l(S_l^* + n_1)n_4^2 + A_4 b_{12} n_3 n_5$$

$$-A_4(\sigma_1 + a_{rl})n_5^2 - A_4 h_r C_r^* n_2 n_5$$

$$-A_4 h_r(S_l^* + n_2)n_5^2 - A_5 C_{12} n_6 n_8$$

$$+\frac{A_5 g_1 k_l K_l n_1 n_6}{(K_l + S_l^*)(K_l + S_l^* + n_1)}$$

$$+\frac{A_6 K_r g_2 k_r n_2 n_7}{(K_r + S_r^*)(K_r + S_r^* + n_2)}$$

$$- A_7 u n_8^2 + A_7 C_{21} n_6 n_8.$$

Now choosing,

$$A_5 = \frac{K_l + S_l^*}{g_1 K_l},\ A_6 = \frac{A_1(K_r + S_r^*)}{g_2 K_r},\ A_7 = \frac{A_5 C_{12}}{C_{21}}$$

we have

$$\frac{dV}{dt} = -\frac{k_l K_l W_l^* n_1^2}{(S_l^* + n_1)(K_l + S_l^*)(K_l + S_l^* + n_1)}$$

$$-\frac{d_l + b_{lr}}{S_l^* + n_1}n_1^2 - \beta_1 n_1 n_4 - \frac{\beta_1 C_l^* n_1^2}{S_l^* + n_1}$$

$$+\frac{A_1 b_{lr}}{S_l^* + n_2} n_1 n_2 - \frac{A_1\left(d_r + \beta_r C_r^*\right) n_2^2}{S_l^* + n_2}$$

$$-\frac{A_1 k_r K_r W_r^* n_2^2}{\left(S_r^* + n_2\right)\left(K_r + S_r^*\right)\left(K_r + S_r^* + n_2\right)}$$

$$-A_1 \beta_r n_2 n_5 - A_2(\alpha_2 + b_{12}) n_3^2 + A_3 a_{rl} n_4 n_5$$

$$-A_3 \sigma_2 n_4^2 - A_3 h_l C_l^* n_1 n_4 - A_3 h_l \left(S_l^* + n_1\right) n_4^2$$

$$+A_4 b_{12} n_3 n_5 - A_4(\sigma_1 + a_{rl}) n_5^2 - A_4 h_r C_r^* n_2 n_5$$

$$-A_4 b_r \left(S_l^* + n_2\right) n_5^2 - A_7 u n_8^2 .$$

Now using the region of attraction R_1, dV/dt becomes,

$$\frac{dV}{dt} \le -\left[\left(B_1 n_1^2 + D_l n_1 n_4 + \frac{1}{2} B_2 n_4^2\right) + \right.$$

$$\left(B_3 n_2^2 + D_2 n_2 n_5 + \frac{1}{3} B_4 n_5^2\right)$$

$$+\left(\frac{1}{2} B_2 n_4^2 + D_3 n_4 n_5 + \frac{1}{3} B_4 n_5^2\right)$$

$$\left. + B_5 n_3^2 \left(D_4 n_3 n_5 + \frac{1}{3} B_4 n_5^2\right) + A_7 u n_8^2 \right]. \qquad (18)$$

where,

$$B_1 = \frac{k_l K_l W_l^*}{\left(K_l + S_l^*\right) S_{lu}\left(K_l + S_{lu}\right)} + \frac{d_l + b_{lr}}{S_{lu}}$$

$$+\frac{\beta_l C_l^*}{S_{lu}} - \frac{1}{2}\frac{A_1 b_{lr}}{S_{rl}}$$

$$B_2 = A_3 \sigma_2 + A_3 h_l S_{ll}$$

$$B_3 = \frac{A_1\left(d_r + \beta_r C_r^*\right)}{S_{ru}} + \frac{A_1 k_r K_r W_r^*}{\left(K_r + S_r^*\right) S_{ru}\left(K_r + S_{ru}\right)}$$

$$-\frac{1}{2}\frac{A_l b_{lr}}{S_{rl}}$$

$$B_4 = A_4(\sigma_1 + a_{rl}) + A_4 h_r S_{rl}$$

$$B_5 = A_2(\alpha_2 + b_{12})$$

$$D_1 = \beta_1 + A_3 h_l C_l^*$$

$$D_2 = A_1 \beta_r + A_4 h_r C_r^*$$

$$D_3 = -A_3 a_{rl}$$

$$D_4 = -A_4 b_{12} .$$

Using the Sylvester's criteria and choosing A_1 as

$$0 < A_1 < \frac{2 S_{rl}}{b_{lr} S_{lu}}\left[\frac{k_l K_l W_l^*}{\left(K_l + S_l^*\right)\left(K_l + S_{lu}\right)} + \left(d_l + b_{lr} + \beta_l C_l^*\right)\right]$$

we derive that dV/dt is negative definite if

$$B_1 B_2 > \frac{D_1^2}{2},\ B_3 B_4 > \frac{3}{4} D_2^2,\ B_2 B_4 > \frac{3}{2} D_3^2,\ B_3 > 0,$$

$$B_4 B_5 > \frac{3}{4} D_4^2 \text{ hold good.} \qquad (19)$$

Under the conditions (19) the non-trivial positive equilibrium point is asymptotically globally (non-linearly) stable in the region R_1.

Conclusion

The non-trivial positive equilibrium point E_1 is found to be both locally and non-linearly asymptotically stable and from the stability of this equilibrium point it may be derived that both the plant biomass and the herbivore population would co-exist.

Further it may be noted from the equilibrium values that the equilibrium densities of plant biomass and the herbivore population are reduced due to the presence of pollutant in leaf and root compartments.

References

1. Barker Jerry R & Tingey David T. Air Pollution Effect on Biodiversity, Van Nostrand Reinhold, 1992; New York.

2. Robart K Dixon, Ralpha S Meldahl, Gregory A Ruark & William G. Warren Process modeling of forest growth responces to environmental stress Timber Press, Portland Oregon, Hongkong, 1990.

3. Kari Heliovaara & Rauno Vaisanen. Insect and Pollution CRC, Londan Tokyo, 1992.

4. De Luna JT & Hallam TG. Effect of toxicant on population : A qualitative approach IV. Resource-consumer-toxicant model :*Ecolog Model* 1987; **35** : 249-273.

5. Hallam TG & Clark CE. Non-autonomous logistic equations as models of populations in a deteriorating environment. *J Theor Biol* 1982; **93** : 303-311.

6. Hallam TG, Clark CE & Jordan GS. Effect of toxicant on populations : Aqualitative approach II. First order kinetics *J Math Biol* 1983; **18** : 25-37.

7. Hallam TG & De Luna JT. Effect of toxicant on populations : Aqualitative approach III. Environmental and food chain pathways. *J Theor Biol* 1984; **109** : 411-429.

8. Hallam TG, Clark CE & Lassister RR. Effect of toxicant on populations : Aqualitative approach I. Equilibrium environmental exposure. *Ecology Model* 1983; **18** : 291-304.

9. Misra OP & Saxena VP. Effects of environmental pollution on the growth and existence of biological populations, modeling and stability analysis. *Indian J Pure & Appl Math* 1991; **22(10)** : 805-819.

10. Freedman HI & Shukla JB. Models for the effect of toxicant in single species and predator prey system. *J Math Biol* 1991; **30** : 15-30.

11. Miller NL. Stability analysis of toxic substances within aquatic ecosystem and their effect on aquatic populations : *Ecology Model* 1992; **60**: 151-165.

12. Misra OP, Jadon BPS & Saxena AK. Mathematical study of the effects of chemical transformation of toxicants on single species population : A qualitative approach : *Proc Nat Acad Sci India* 2000; **70** A : 259-280.

13. Monod J. The growth of bacterial cultures *Ann Rev Microbial* 1949; **3** : 371-394.

Proc. Nat. Acad. Sci. India Sect. A, Vol. 78, Pt. II, 2008

Infraexponential decay of wavelets

R.S. PATHAK and S.K. SINGH

Department of Mathematics, Banaras Hindu University, Varanasi-221 005, India

Email : ramshankarpathak@yahoo.co.in, sks_math@yahoo.com.

Received January 10, 2007; Revised June 26, 2007; Accepted August 26, 2007

Abstract:

Using the theory of ultradifferentiable functions it is shown that there exist band-limited wavelets of infraexponential decay.

(**Keywords** : infraexponential decay/ultradifferentiable functions/ultradistributions/wavelets)

Introduction

It is well known that there is no C^∞ orthonormal wavelet on $\Re$ with exponential decay such that all its derivatives are bounded. But there are band-limited wavelets belonging to the Schwartz space $S(\Re)$. Using the theory of functions of Gevrey class, Dziubański and Hernández[1] constructed band-limited wavelts of subexponential decay.

In this paper using the theory of ultradifferentiable functions[2–5] and following the techniques used by Dziubański and Hernández[1] a construction of band-limited wavelets of infraexponential decay (more general than sub-exponential decay) is presented. This paper extends some of the results given by these authors[1] and Wojtaszezyk[6]. We have also obtained certain results on Fourier transform of composition of ultradifferentiable functions.

Ultradifferentiable Functions

In this section we recall some definitions and properties of ultradifferentiable functions used in the present investigation.

Let $\{M_p\}$, $p = 0, 1, 2.....$ be an increasing sequence of positive numbers. An infinitely differentiable function ϕ on an open interval I in $\Re$ will be called an ultradifferentiable function of class M_p (of Roumieu type) if on each compact set K in I its derivatives are estimated in the form

$$\sup_K \left| D^p \phi(x) \right| \le C A^p M_p, \ p = 0, 1, \ldots.$$

for some positive numbers C and A depending on ϕ. The following conditions are imposed on M_p[4,5]:

(M.1) $M_p^2 \le M_{p-1} M_{p+1}, \ p \in N_0$

(M.2) there exist some constants $R>0$, $H>0$ such that

$$M_p \le R H^p \min_q M_q M_{p-q}, \ p,q \in N_0,$$

(M.3) $\sum_{j=0}^{\infty} M_j / M_{j+1} < \infty.$

Definition 1 : For each increasing sequence $\{M_p\}$ of positive numbers we define its associated function $M(\rho)$ on $[0, \infty)$ with $M(0) = 0$, $M(\infty) = \infty$ by

$$M(\rho) = \sup_p \ \log(\rho^p M_0 / M_p). \tag{1}$$

The following Lemma contains some important properties[7] of the function $M(\rho)$.

Lemma 1 : If the sequence $\{M_p\}$ satisfies (M.1), then

$$M(\rho + \delta) \le M(2\rho) + M(2\delta), \ \rho>0, \ \delta>0. \tag{2}$$

Let the sequence $\{M_p\}$ satisfy (M.1) and (M.2), then we have

$$2M(\rho) \le M(H\rho) + \log(RM_0), \ \rho>0, \tag{3}$$

where R and H are the constants used in (M.2). If $L \geq 1$, there is a constant C_1 such that

$$M(L\rho) \leq \frac{3}{2} LM(\rho) + C_1, \quad \rho > 0. \tag{4}$$

If $L \geq 1$, there is a constant $H > 1$ and a constant E_L depending on L such that

$$LM(\rho) \leq M(H^{L-1}\rho) + E_L, \quad \rho > 0. \tag{5}$$

For $M_p = p^{p\alpha}$, $\alpha > 1$, $M(\rho) = -\frac{\alpha}{e}\rho^{\frac{1}{\alpha}}$.

Definition 2 : Let $\omega(\xi) = \omega(|\xi|)$ be a real valued, continuous, increasing and concave function on $\Re$ such that

$$0 \leq \omega(\xi + \eta) \leq \omega(\xi) + \omega(\eta), \tag{6}$$

$$\int_0^\infty \frac{\omega(t)}{1+t^2} dt < \infty, \tag{7}$$

$$\omega(\xi) \geq a + b \log(1 + |\xi|) \tag{8}$$

for some real number a and positive number b. The set[3] of all such functions ω is denoted by m.

Some typical examples of the above function are

$\omega(t) = \log(1 + t)$,

$\omega(t) = t^{1/\alpha}$,

$\omega(t) = t^{1/\alpha} (\log(1 + t))^\beta$,

where $t > 0$, $\alpha > 1$ and $\beta \in \Re$.

Notice that the functions $M(\rho)$ and $\omega(\rho)$ possess similar, but not identical properties. However, Petzsche[7] on p. 17 of his paper proved that there are certain positive constants λ_1, λ_2, C_1 and C_2 such that $M(\rho) \leq \lambda_1\omega(\rho) + C_1$ and $\omega(\rho) \leq M(\lambda_2\rho) + C_2$.

Definition 3 : Let $M(\rho)$ be the associated function defined by relation (1) corresponding to any increasing sequance $\{M_p\}$ satisfying (M.1), (M.2) and (M.3). A function on $\Re$ decaying faster than $e^{-\delta M(|x|)}$ (or $e^{-\delta\omega(x)}$), $\delta > 0$, is said to be of infraexponential decay.

Decay of Fourier Coefficients

In what follows we show that infraexponential decay of Fourier coefficients depends on the infraexponential decay of the function and conversely.

Theorem 1 : Suppose that $|g(x)| \leq C\, e^{-\lambda M(|x|)}$ for some constant C and $\lambda > 1$,

then

$$\left| \int_{-\infty}^{\infty} g(x-k)\overline{g(x)}dx \right| \leq C_\beta e^{-\beta M(|k|)}$$

for each $0 < \beta \leq \frac{1}{3}(\lambda - 1)$ and conversely, if a sequence $\{a_k\}$; $k \in Z$ satisfies $|a_k| \leq C\, e^{-aM(|k|)}$ then also

$$\left| \sum_{k\in Z} a_k g(x-k) \right| \leq C_\beta e^{-\frac{(\beta-1)}{3}M(|x|)}$$

for each $\beta < \min(\alpha, \lambda)$.

Proof : Assume that $k \geq 0$ then using equation (2) we have

$$|I| = \left| \int_{-\infty}^{\infty} g(x-k)\overline{g(x)}dx \right| \leq C^2 \int_{-\infty}^{\infty} e^{-\lambda M(|x|)} e^{-\lambda M(|x-k|)} dx$$

$$= C^2 \int_{-\infty}^{0} e^{-\lambda M(|x|)} e^{-\lambda M(|x-k|)} dx$$

$$+ C^2 \int_0^\infty e^{-\lambda M(|x|)} e^{-\lambda M(|x-k|)} dx$$

$$= C^2 \int_0^\infty e^{-\lambda M(|x|)} e^{-\lambda M(|x+k|)} dx$$

$$+ C^2 \int_0^k e^{-\lambda M(|x|)} e^{-\lambda M(|x-k|)} dx$$

$$+ C^2 \int_k^\infty e^{-\lambda M(|x|)} e^{-\lambda M(|x-k|)} dx.$$

Since $M(\rho)$ is increasing and satisfies relation (2), therefore we have

$$|I| \le C^2 e^{-\lambda M(|k|)} \int_0^\infty e^{-\lambda M(|x|)} dx + C^2 \int_0^k e^{-\lambda M\left(\frac{|x|+|x-k|}{2}\right)} dx$$

$$+C^2 e^{-\lambda M(|k|)} \int_k^\infty e^{-\lambda M(|x-k|)} dx$$

$$\le C^2 e^{-\lambda M(|k|)} C_\lambda + C^2 \int_0^k e^{-\lambda M\left(\frac{(|k|)}{2}\right)} dx$$

$$+C^2 e^{-\lambda M(|k|)} \int_0^\infty e^{-\lambda M(|y|)} dy$$

$$\le 2C^2 e^{-\lambda M(|k|)} C_\lambda + 2C^2 \frac{k}{2} e^{-\lambda M\left(\frac{|k|}{2}\right)}$$

$$\le 2C^2 e^{-\lambda M(|k|)} C_\lambda + 2C^2 \frac{M_1}{M_0} e^{M\left(\frac{|k|}{2}\right)} e^{-\lambda M\left(\frac{|k|}{2}\right)}$$

$$\le 2C^2 e^{-(\lambda-1) M(|k|)} + \frac{2C^2 M_1}{M_0} e^{-(\lambda-1) M\left(\frac{|k|}{2}\right)}$$

$$\le \left(2C^2 C_\lambda + \frac{2C^2 M_1}{M_0}\right) e^{-(\lambda-1) M\left(\frac{k}{2}\right)}$$

$$\le 2C^2 \left(C_\lambda + \frac{M_1}{M_0}\right) e^{-(\lambda-1)\left[\frac{1}{3} M(k) - \frac{c_1}{3}\right]}$$

by relation (4)

$$= 2C^2 \left(C_\lambda + \frac{M_1}{M_0}\right) e^{+(\lambda-1)\frac{c_1}{3}} e^{-\left(\frac{\lambda-1}{3}\right) M(k)}$$

We may note that in the above

$$C_\lambda = \int_0^\infty e^{-\lambda M(|x|)} dx$$

Thus

$$|I| \le C_\beta e^{-\beta M(k)}, \qquad 0 < \beta < \frac{1}{3}(\lambda - 1).$$

This shows the first part.

To show the other statement we observe that

$$\left|\sum_{k\in Z} a_k g(x-k)\right| \le C^2 \sum_{k\in Z} e^{-\alpha M(k)} e^{-\lambda M(|x-k|)}.$$

Now, if we assume that $x \ge 0$, then

$$\left|\sum_{k\in Z} a_k g(x-k)\right| \le C^2 \sum_{k\in Z} e^{-\beta M(|k|)} e^{-\beta M(|x-k|)};$$

$$\beta \le \min(\alpha, \lambda)$$

$$\left|\sum_{k\in Z} a_k g(x-k)\right|$$

$$\le C^2 \sum_{k=-\infty}^{0} e^{-\beta M(|k|) - \beta M(|x-k|)}$$

$$+C^2 \sum_{k=0}^{[x]} e^{-\beta M(|k|) - \beta M(|x-k|)}$$

$$+C^2 \sum_{k=[x]+1}^{\infty} e^{-\beta M(|k|) - \beta M(|x-k|)}$$

$$\le C^2 \sum_{k=0}^{\infty} e^{-\beta M(|k|) - \beta M(|x+k|)} + C^2 \sum_{k=0}^{[x]} e^{-\beta M\left(\frac{|k|+|x-k|}{2}\right)}$$

$$+C^2 \sum_{k=[x]+1}^{\infty} e^{-\frac{\beta}{2} M(|k|) - \frac{\beta}{2} M(|k|)}$$

$$\le C^2 e^{-\beta M(|x|)} \sum_{k=0}^{\infty} e^{-\beta M(|k|)} + C^2 e^{-\beta M\left(\frac{|x|}{2}\right)} \sum_{k=0}^{[x]} 1$$

$$+C^2 e^{-\frac{\beta}{2} M(|[x]+1|)} \sum_{k=0}^{\infty} e^{-\frac{\beta}{2} M(|k|)}$$

$$\le C^2 e^{-\beta M(|x|)} C'_\beta + C^2 e^{-\beta M\left(\frac{|x|}{2}\right)} [x]$$

$$+C^2 e^{-\frac{\beta}{2} M(|x|)} \sum_{k=0}^{\infty} e^{-\frac{\beta}{2} M(|k|)}$$

$$\leq C^2 e^{-\beta M(|x|)} C'_\beta + C^2 e^{-\beta M\left(\frac{|x|}{2}\right)} x + C^2 e^{-\frac{\beta}{2}M(|x|)} C'_\beta$$

$$\leq 2C^2 C'_\beta e^{-\frac{\beta}{2}M(|x|)} + 2C^2 \frac{M_1}{M_0} e^{M\left(\frac{|x|}{2}\right)} e^{-\beta M\left(\frac{|x|}{2}\right)}$$

by relation (1)

$$\leq 2C^2 C'_\beta e^{-\frac{\beta}{2}M(|x|)} + 2C^2 \frac{M_1}{M_0} e^{-(\beta-1)\left\{\frac{1}{3}M(|x|)-C_1/3\right\}}$$

$$\leq 2C^2 C'_\beta e^{-\frac{(\beta-1)}{3}M(|x|)}$$

$$+ 2C^2 \frac{M_1}{M_0} e^{\frac{(\beta-1)c_1}{3}} e^{-\frac{(\beta-1)}{3}M(|x|)}$$

$$\leq C_\beta e^{-\frac{(\beta-1)}{3}M(|x|)},$$

where

$$C_\beta = 2C^2 C'_\beta + 2C^2 \frac{M_1}{M_0} e^{-\frac{(\beta-1)c_1}{3}}.$$

If $x < 0$, then for $-x = y > 0$, proceeding as in the above we can show that

$$\left|\sum_{k\in Z} a_k g(x-k)\right| \leq C^2 \sum_{k\in Z} e^{-\beta M(|k|)} e^{-\beta M(|x-k|)}.$$

$$\leq C_\beta e^{-\frac{(\beta-1)}{3}M(|y|)}.$$

Theorem 2 : Suppose that property (8) of ω holds for $b \geq 1$, and $|g(x)| \leq C\ e^{-\lambda\omega(x)}$ for some constant C and $\lambda > 0$ then

$$\left|\int_{-\infty}^{\infty} g(x-k)\overline{g(x)}dx\right| \leq C_\beta e^{-\beta\omega(k)},\ 0<\beta\leq 1-\lambda/b;$$

and conversely, if a sequence $\{a_k\}_{k\in Z}$ satisfies : $|a_k| \leq Ce^{-\alpha\omega(k)}$ then we have

$$\left|\sum_{k\in z} a_k g(x-k)\right| \leq C_\beta e^{-\left(\frac{\beta}{2}-\frac{1}{b}\right)\omega(x)}$$

for each β, $0 < \beta \leq \min(\alpha, \lambda)$.

Proof : The proof is similar to the proof of Theorem 1, where properties (6)-(8) of the function ω are to be applied.

Remark 1 : Theorem 1 and 2 extend Lemma 3.16 of Wojtaszczyk[6].

Proposition 1 : Let g be a function of $\Re$ satisfying $|g(x)| \leq C\ e^{-\lambda M(x)}$ (or, $|g(x)| \leq C\ e^{-\lambda\omega(x)}$) for some constants C and $\lambda > 0$. Then there exists a 2π-periodic function G analytic in $|\mathrm{Im}\ z| \leq \lambda$ such that for all $\xi \in \Re$,

$$G(\xi) = \sum_{\ell=-\infty}^{\infty} \left|\hat{g}(\xi + 2\pi\ell)\right|^2.$$

Proof : Since $g \in L_2(\Re)$, we have

$$\int_0^{2\pi}\left(\sum_\ell \left|\hat{g}(\xi - 2\pi\ell)\right|^2\right) e^{-ik\xi} d\xi = \int_{-\infty}^{\infty} |\hat{g}(\xi)|^2$$

$$e^{-ik\xi}\ d\xi = \int_{-\infty}^{\infty} g(x-k)\ \overline{g(x)}\ dx;$$

so that by Theorem 1,

$$\sum_{\ell=-\infty}^{\infty} \left|\hat{g}(\xi - 2\pi\ell)\right|^2 = \frac{1}{2\pi}\sum_k \int_{-\infty}^{\infty} g(x-k)\overline{g(x)}dx\ e^{-ik\xi}$$

$$= \sum_k a_k e^{-ik\xi}$$

where $|a_k| \leq C_\beta e^{-\beta M(k)}$; $0 < \beta \leq 1-\lambda/b$

$\cdot$ (resp. $|a_k| \leq C_\beta e^{-\beta\omega(k)}$; $0 < \beta \leq 1-\lambda/b$).

Let us set

$$G(z) = \sum_{n=-\infty}^{\infty} a_n e^{inz} = \sum_{n=0}^{\infty} a_n e^{inz} + \sum_{n=1}^{\infty} a_{-n} \overline{e}^{inz}.$$

Since $|a_n e^{\pm inz}| \leq C_\beta e^{-\beta M(n)+n|\mathrm{Im}(z)|}$, the series is convergent, if

$|\mathrm{Im}(z)| < \beta \frac{M(n)}{n} \to 0$ as $n \to \infty$. Similar result is true for the ω-case.

Remark 2 : Note that for $\lambda > 0$, $e^{-\lambda M(x)}$ and $e^{-\lambda\omega(x)}$, possess the following properties of the function $W : [0, \infty) \to \Re^+$ exploited by Hernández and Weiss[8].

(a) $W \in L_1([0, \infty))$, (b) W is decreasing and (c) $W(0)<\infty$.

Therefore there exist wavelet ψ and scaling function ϕ associated with MRA satisfying

$$|\psi(x)| < C_1 e^{-\lambda M(x)} \text{ (or } < C_1 e^{-\lambda\omega(x)}),$$

and $|\phi(x)| < C_2 e^{-\mu M(x)}$(resp. $< C_2 e^{-\mu\omega(x)}$), $\mu > 0$, in terms of which expansion[8] of any $f \in L_p(\Re)$, $1 \le p \le \infty$ can be given.

The Space $\mathcal{E}(M_p : \Re)$

We denote $\mathcal{E}(M_p : \Re)$ the set of all those C^∞–functions ϕ on $\Re$ such that for every compact set $K \subset \Re$, $|D^\alpha\phi(x)| \le C A^\alpha M_\alpha$ for some constants $C>0$ and $A>0$. We show that the space $\mathcal{E}(M_p : \Re)$ contains "cutoff" functions. With $\chi = \chi_{[0,1]}$ set $\chi_a = \frac{1}{a}\chi\left(\frac{x}{a}\right)$. Then by Theorem 1.3.5 of Hörmander[9] for any sequence $a_1 \ge a_2 \ge \ldots >0$ such that $a = \sum_{j=1}^{\infty} a_j < \infty$ the function $\phi_k = \chi_{a1} * \chi_{a2} * \chi_{a3} * \ldots * \chi_{ak}$ belongs to $C^{k-1}(\Re)$, has support in $[0, a]$, and converges as $k \to \infty$ to a function $\phi \in C^\infty(\Re)$, with support in $[0, a]$, such that

$$\int_R \phi(x)dx = 1 \text{ and } \left|D^n\phi(x)\right| \le \frac{2^n}{a_1 a_2 \ldots a_n}. \tag{9}$$

By taking $a_n = \frac{M_{n-1}}{M_n}$ in the above construction we have

$$\sum_{n=1}^{\infty} a_n = \sum_{n=1}^{\infty} \frac{M_{n-1}}{M_n} < \infty,$$

and

$$\left|D^n\phi(x)\right| \le \frac{2^n}{\frac{M_0}{M_1} \cdot \frac{M_1}{M_2} \cdots \frac{M_{n-1}}{M_n}} = \frac{2^n}{\frac{M_0}{M_n}} = 2^n M_0^{-1} M_n.$$

Thus $\phi \in \mathcal{E}(M_p : \Re)$. The subspace of $\mathcal{E}(M_p : \Re)$ consisting of functions of compact support is denoted by $\mathcal{D}(M_p : \Re)$.

Theorem 3 : For every $a > 0$ there exists $\phi_a \in \mathcal{E}(M_p : \Re)$. Moreover, $\phi_a \ge 0$, supp $\phi_a \subset [-a, a]$ and $\int_{-\infty}^{\infty} \phi_a(x)dx = \frac{\pi}{2}$.

Proof : Since $\mathcal{E}(M_p : \Re)$ is invariant under dilations and multiplication by constants, it is enough to show the result for $a = 1$ and show that $\int_{-\infty}^{\infty} \phi_a(x)dx < \infty$.

Let h be an even function of compact support containing $[-1, 1]$, such that $h \in C^\infty([-1, 1])$, $h > 0$, and $\int_{-1}^{1} h(x)dx = 1$. Let N_m be an increasing sequence of positive integers such that

$$\sum_{n \ge N_m} \frac{M_{m+n-1}}{M_{m+n}} < \frac{1}{2^m}.$$

Choose $a_n = \frac{M_{m+n-1}}{M_{m+n}}$ when $N_m \le n \le N_{m+1}$. Notice that

$$\sum_{n \ge N_1} a_n = \sum_{n \ge N_1} \frac{M_{m+n-1}}{M_{m+n}} \le \sum_{m=1}^{\infty} \frac{1}{2^m} = 1.$$

Define $\phi_n = h_{a_{N_1}} * h_{a_{N1+1}} * h_{a_{N1+2}} * \ldots * h_{a_n}$, where $h_a(x) = \frac{1}{a} h\left(\frac{x}{a}\right)$; so that $\int_{\Re} h_a(x)dx = 1$ and supp $\phi_n \subset [-1, 1]$.

For $N = 1, 2, 3\ldots$ choose m and n so large that $N_m + N < n$. Then

$$D^N\phi_n = h_{a_{N_1}} * h_{a_{N_2}} * \ldots * h_{a_{N_m}} * Dh_{a_{N_{m+1}}} * \ldots * Dh_{a_{N_{m+N}}} * h_{a_{N_{m+n+1}}} * \ldots * h_{a_n}.$$

We have for some $C > 0$,

$$\left\|Dh_{a_n}\right\|_1 = \frac{1}{a_n}\int_{\Re}\left|Dh\left(\frac{x}{a_n}\right)\right| dx \le \frac{C}{a_n} \le C\frac{M_{m+n}}{M_{m+n-1}},$$

if $n \ge N_m$.

Then using $\int(u*v)dx=\left(\int udx\right)\left(\int vdx\right)$, $\int_R h_a dx=1$ and (M.2), we deduce that

$$\left|D^N\phi_n\right|\le C^N\frac{M_{m+N_m+1}}{M_{m+N_m}}\frac{M_{m+N_m+2}}{M_{m+N_m+1}}\cdots\frac{M_{m+N_m+N}}{M_{m+N_m+N-1}}$$

$$\le C^N\frac{M_{m+N_m+N}}{M_{m+N_m}}\le\frac{C^N R^{m+N_m+N}M_{m+N}M_{N_m}}{M_{N_m}}$$

$$\le RC^N H^{m+N_m+N}M_{m+N}$$

$$\le RH^{m+N_m+N}C^N RH^{m+N}M_m M_N$$

$$\le R^2H^{m+n}C^N RH^{m+n}M_m M_N$$

$$=R^2H^{2m+2n}M_m C^N M_N.$$

Therefore, for $Q_n=R^2H^{2m+2n}M_m$, we have

$$\left|D^N\phi_n\right|\le Q_n C^N M_N.$$

Hence, ϕ_n is in $\mathcal{E}(M_p:\Re)$ and supp $\phi_n\subset[-1,1]$. Let $\{\phi_n\}\to\phi$ in $\mathcal{E}(M_p:\Re)$. Then $\phi\in\mathcal{E}(M_p:\Re)$ with supp $\phi\subset[-1,1]$.

We shall need the following result in investigating properties of wavelets in next section.

Lemma 2 : Suppose that M_p satisfies (M.1) and K is a compact convex set in $\Re^n$. An entire function $\hat{\phi}(\xi)$ on C^n is the Fourier-Laplace transform of an ultradifferentiable function $\phi(x)$ in $\mathcal{D}(M_p:K)$, viz.,

$$\hat{\phi}(\xi)=(F(\phi))(\xi)=\int_{R^n}\phi(x)\exp\,(i(x,\xi))dx,$$

if and only if there are positive constants A and C such that

$$\left|\hat{\phi}(\xi)\right|\le C\exp\left(-M\left(\frac{|\xi|}{A}\right)+H_K(\xi)\right),$$

where $H_K(\xi)=\sup_{x\in K}(-\operatorname{Im}(x,\xi))$ is the support function of K and

$$M(\rho)=\sup_p\log\left(\rho^p M_0/M_p\right).$$

Proof : See Pathak[5].

Theorem 4 : Suppose F is an entire function and $f\in\mathcal{E}(M_p:\Re)$.

Then $g(x)=F(f(x))\in\mathcal{E}(M_p:\Re)$.

Proof : We have to show that for every compact set $K\subset\Re$ there exist constants C_1 and A_1 such that $|D^N g(x_0)|\le C_1A_1^N M_N$. For arbitrary $x_0\in K$ and all $N=1,2,3....$ using the Taylor expansion we can write

$$f(x)=\sum_{n=0}^{N}\frac{1}{n!}D^n f(x_0)(x-x_0)^n+R_N(x)$$

$$=f_N(x)+R_N(x).$$

Set $D^N g(x_0):=D^N[F(f_N)](x_0)$. By the assumption $F(f_N(z)), z\in C$, is analytic and by the Cauchy formula we can write

$$D^N g(x_0)=\frac{N!}{2\pi i}\int_{\omega_N}\frac{F(f_N(z))}{(z-x_0)^{N+1}}dz,$$

where $\omega_N=\left\{z\in C:\ |z-x_0|=\frac{N}{2eCAM_N^{1/N}}\right\}$.

Now

$$|f_N(z)|\le\sum_{n=0}^{N}\frac{1}{n!}CA^nM_n\left(\frac{N}{2eCAM_N^{1/N}}\right)^n$$

$$\le\sum_{n=0}^{N}\frac{e^n}{n^n}CA^nM_n\frac{N^n}{2^ne^nC^nA^nM_N^{n/N}}$$

$$\le\sum_{n=0}^{N}\frac{1}{C^{n-1}}\left(\frac{NM_n^{1/n}}{nM_N^{1/N}}\right)^n\frac{1}{2^n}$$

$$\le C'\sum_{n=0}^{N}\frac{1}{2^n}=2C'\quad\text{as}\quad\frac{NM_n^{1/n}}{nM_N^{1/N}}<1.$$

Since F is analytic we have

$|F(F_N(z))| \leq C''$ on ω_N.

Therefore

$$\left|D^N g(x_0)\right| \leq \frac{N!}{2\pi} C'' \frac{2\pi N}{2eCAM_N^{1/N}} \left(\frac{N}{2eCAM_N^{1/N}}\right)^{-N-1}$$

$$= N! C''\left(2eCAM_N^{1/N}\right)^N N^{-N}$$

$$\leq N^N N^{-N} C''(2eCA)^N M_N.$$

Thus $\left|D^N g(x_0)\right| \leq C_1 A_1^N M_N$;

so that $g(x) = F(f(x)) \in \mathcal{E}(M_p : \Re)$.

Construction of Wavelets

For fixed $a > 0$ choose a "cutoff" function $\phi_a \in \mathcal{E}(M_p : \Re)$, as in Theorem 3. Set

$$\theta_a(x) = \int_{-\infty}^{x} \phi_a(t)\, dt, \tag{10}$$

then $\theta_a(x) \in \mathcal{E}(M_p : \Re)$.

Now, set $S_a(x) = \sin(\theta_a(x))$ and $C_a(x) = \cos(\theta_a(x))$. Then by Dziubański and Hernández[1] we have

$$b_a(x) = S_a(x-\pi)\, C_{2a}(x-2\pi), \quad a \leq \pi/3 \tag{11}$$

is a bell function associated with the interval $[\pi, 2\pi]$. Using Theorem 4 it can be shown that $b_a(x) \in \mathcal{E}(M_p : \Re)$.

Then the function ψ defined by

$$\hat{\psi}_a(\xi) = e^{i\xi/2}\, b_a(\xi) \tag{12}$$

is an orthonormal wavelet[8] in $L_2(\Re)$.

Theorem 5 : There exist band-limited C^∞– orthonormal wavelets in $L_2(\Re)$ with infra-exponential decay. Moreover all of their derivatives have also infraexponential decay.

Proof : The function b_a defined by relation (11) as well as its even extension to $(-\infty, 0]$ belongs to $\mathcal{E}(M_p : \Re)$, by theorem 4. By Lemma 2 the orthonormal wavelet ψ_a given by relation (12) satisfies

$$|\hat{\psi}_a(x)| = \left|\frac{1}{2\pi}\hat{b}_a\left(-x - \frac{1}{2}\right)\right|$$

$$= C \exp\left(-M \frac{x + \frac{1}{2}}{A}\right).$$

$$\leq C\, e^{-\frac{2}{3A} M\left(\left|x+\frac{1}{2}\right|\right) + \frac{2C_1}{3A}}$$

by relation (4)

$$= C\, e^{\frac{2C_1}{3A}}\, e^{-\frac{2}{3A} M\left(\left|x+\frac{1}{2}\right|\right)}.$$

Now in view of relation (2) we can write

$$M\left(\frac{|x|}{2}\right) = M\left(\left|\frac{x}{2} + \frac{1}{4} - \frac{1}{4}\right|\right) \leq M\left(\left|\frac{x}{2} + \frac{1}{4}\right| + \frac{1}{4}\right)$$

$$\leq M\left(\left|x + \frac{1}{2}\right|\right) + M\left(\frac{1}{2}\right);$$

so that

$$|\psi_a(x)| \leq C e^{\frac{2C_1}{3A}}\, e^{-\frac{2}{3A}\left\{M\left(\frac{|x|}{2}\right) - M\left(\frac{1}{2}\right)\right\}},$$

$$= C e^{\frac{2C_1}{A}}\, e^{\frac{2M\left(\frac{1}{2}\right)}{3A}}\, e^{-\frac{2}{3A} M\left(\frac{|x|}{2}\right)}.$$

Now from relation (4) for $L = 2$, we have

$$\frac{1}{3} M(2\rho) - \frac{1}{3} C_1 \leq M(\rho).$$

Hence

$$|\psi_a(x)| \leq C\, e^{\frac{2C_1}{A}}\, e^{\frac{2M\left(\frac{1}{2}\right)}{3A}}\, e^{-\frac{2}{3A}\left\{\frac{1}{3} M(|x|) - \frac{C_1}{3}\right\}}$$

$$\leq C_2\, e^{-\frac{2}{9A} M(|x|)}$$

$$= C_2\, e^{-\lambda M(|x|)}$$

where $\lambda = \dfrac{2}{9A}$.

The fact that all of its derivatives have also infraexponential decay follows from Lemma 2. Indeed,

$$\left|D^n \psi_a(x)\right| = C\left|\left(\xi^n e^{i\xi/2} b_a(\xi)\right)^{\wedge}(x)\right|$$

and $$\xi^n e^{i\xi/2} b_a(\xi) \in \mathcal{D}(Mp : K).$$

Acknowledgement

One of the authors, (SK) is grateful to University Grants Commision (UGC), New Delhi, for the award of Junior Research Fellowship.

References

1. Dziubański J & Hernández E. Band-limited wavelets with sub-exponential decay. *Canad Math Bull* 1998; **41** : 398-403.
2. Roumieu C. Sur quelques extensions de la notion de distribution. *Ann Sci Ecole Norm Sup* 1960; **77** : 41-121.
3. Bjorck G. Linear partial differential operators and generalized distributions. *Ark Mat* 1966; **6** : 351-407.
4. Komatsu H. Ultradistributions, I : Structure theorems and a characterization. *J Fac Sci Univ Tokyo Sect IA Math*. 1973; **20** : 25-105.
5. Pathak RS. Integral Transforms of Generalized Functions and their Applications. Gordon and Breach Science Publishers : Amsterdam 1997; pp. 82-83.
6. Wojtaszczyk P. A Mathematical Introduction to Wavelets. Cambridge University Press : London, 1997; pp. 58-61.
7. Petzsche HJ. Die Nuklearitat der ultradistributionsraume und der satz vom kern I. *Manuscripta math* 1978; **24** : 133-171.
8. Hernandez E & Weiss G. A First Course on Wavelets. CRC Press : Boca Raton, Florida, 1996; pp. 218, 222-228.
9. Hörmander L. The Analysis of Linear Partial Differential Operators I. Springer-Verlag : Berlin Heiedelberg New York, Tokyo, 1983; pp. 19-20.

Proc. Nat. Acad. Sci. India Sect. A, Vol. 78, Pt. II, 2008

Thermoluminescence and nonstoichiometry in optical crystals

SANGEETA* and S.C. SABHARWAL

Crystal Technology Laboratory, Technical Physics and Prototype Engineering Division, Bhabha Atomic Research Centre, Trombay, Mumbai-400085 INDIA.

**Corresponding author, FAX : +91 022 5505151; e-mail : sangita@barc.gov.in*

Received November 25, 2005; Revised February 13, 2006; Accepted August 8, 2007

Abstract

Thermally stimulated luminescence (TSL) from well synthesized crystals W_5 of $PbWO_4$, $CdWO_4$, $Y_3Al_5O_{12}$, $Bi_4Ge_3O_{12}$ and LiB_3O_5 characterized by XRD and DTA has been studied by TSL is found to be useful in detecting minute nonstoichiometry in these oxide crystals.

(**Keywords** : thermoluminescence/optical crystal/nonstoichiometry/oxides)

Introduction

The phenomenon giving rise to emission of light from a medium under the influence of an external excitation is known as luminescence. The emission process may or may not involve an intermediate state. The emission in the former case is known as phosphorescence and in the latter as fluorescence. In fluorescence, the emission occurs within a very short duration (= ns) of excitation while the emission in phosphorescence can be delayed for long period depending upon the lifetime of the intermediate state. If the life time of intermediate state is too large and at ambient temperature the trapped charges can not be emptied, the emission may be observed by heating the solid to a higher temperature. The emission observed in such a case is known as thermally stimulated luminescence (TSL) or thermoluminescence.

A plot of the light emitted versus temperature for an irradiated sample is known as the glow curve and spectral distribution of light emitted as the emission spectra. A glow curve contains information about the number of traps, thermal activation energy of the traps and the kinetics of recombination of trapped charges. On the other hand, the emission spectra contains details of the emitting center. The TSL measurement is far more sensitive (by about four orders of magnitude) than the optical absorption. In order to have an appreciable change in the optical absorption, about 10^{14} active centers are required to contribute and in contrast about 10^{10} TSL active centers are sufficient to produce a measurable signal. Thus, a study of the TSL glow curve and emission spectra provides a very sensitive tool to investigate the defect structure of materials that have the presence of optically active centers.

Consequent to its highly sensitive nature, TSL has been widely used in different investigations like geological activity, in dating of ancient pottery, lunar materials and radiation dosimetry[1]. We have also exploited the phenomena to study (i) the role of certain impurities in starting material used for the growth of NaI scintillation crystals[2], (ii) the defect equilibrium of CaF_2 crystals[3], (iii) the effect of shock in quartz phase Geo_2[4] (iv) to defect the presence of flux inclusion in BaB_2O_4 crystals grown from Na_2O flux[5], (v) energy transfer process in $YLiF_4$ (U^{4+}) crystals[6] and (vi) effect of lattice oxygen in BaF_2 crystal[7].

Single crystals of many binary oxides find applications as scintillators, solid state lasers, non linear optical devices, acoustooptic modulators and pyroelectric detectors[8]. A major problem faced with the growth of good quality and large size oxide crystals is the detection and control of stoichiometry. Stoichiometric deviations can result if the constituent oxides of a crystal have different vapor pressures at the operating temperatures. The intrinsic nonstoichiometry has been observed in several oxide crystals[9-12]. The nonstoichiometry may occur via

a vacancy formation on sublattice of the deficit cations. Alternately, the cation that is left in excess may combine with some impurity ions present in the lattice to form impurity phases. These impurity phases may alloy with the oxide material under consideration in which case their removal during crystal growth becomes difficult. Aliovalent impurities,

is significant to note that the detection of minor fraction in a material may be reliably done down to parts per million (ppm) or parts per billions (ppb) levels with the help of a wide variety of analytical techniques[13]. On the contrary, stoichiometric deviations of the order of ~ 0.1% are even quite difficult to detect by conventional material characterization techniques. The same is the case with the incorporation of minute amount of secondary phases present in the phase diagram into the crystal lattice owing to the fact that the atoms involved are essentially the same. For many oxide crystals, the measurement of certain crystal properties like refractive indices, phase transition temperatures, absorption edges and accurate lattice spacing etc which are sensitive to compositional changes is found useful to detect small stoichiometric variations[14,15].

In this communication, we present results of our comprehensive investigations on TSL from $PbWO_4$, $CdWO_4$, $Y_3Al_5O_{12}$, $Bi_4Ge_3O_{12}$ and LiB_3O_5 and establish application of TSL in the detection of

for $PbWO_4$ to 2000°C for $Y_3Al_5O_{12}$ [illegible]. The other crystal growth details are summarized in Table 1. The growth of LiB_3O_5 was effected by top seeded solution growth using B_2O_3 as a flux[20]. The crystals were characterized by X-ray diffraction and differential thermal analysis (DTA). The optical absorption spectra of the crystals were recorded over the wavelength range 200 – 1100 nm. TSL glow curves for the samples were recorded using a PC based recorder[21]. For studying TSL, samples were irradiated in a ^{60}Co gamma chamber and the glow curves were recorded employing a linear heating rate of 50°C/min. The spectral characteristics of TSL emission were studied by employing selectively transmitting filters in different spectral ranges.

Table 1 – Relevant details of single crystal growth of different materials employed in the present study.

Material	Growth technique	Growth ambient	Growth axis	Thermal setup	Growth rate
$PbWO_4$	CZ	Normal	Random	RF, Moderate axial gradient	1 – 2 mmh^{-1}
$CdWO_4$	CZ	Normal	<100>	RF, Moderate axial gradient	2 – 3 mmh^{-1}
$Y_3Al_5O_{12}$	CZ	N_2 + Ar+O_2	<001>	RF and well shielded	1 mmh^{-1}
$Bi_4Ge_3O_{12}$	CZ	Normal	Random	Resistance, High Insulation	1 mmh^{-1}
Li B_3O_5	TSSG Flux : B_2O_3	Normal	Random	Resistance heating	<1 mm day, cooling rate 0.1°Ch^{-1}

CZ : Czochralski pulling (melt growth), TSSG : Top seeded solution growth

Results and Discussion

$PbWO_4$

The crystals grown using charges prepared by solid state sintering of the constituent oxides showed pale yellow coloration. This coloration increased when a left over charge from the previous run was used for the growth, indicating the occurrence of stoichiometric deviations in the charge on holding at growth temperatures. However, application of the material purified through re-crystallization and mixed with a certain amount of lead oxide powder was found to be suitable for the growth of colorless crystals. This result suggests that the crystal coloration is arising due to the selective loss of a crystal constituent from the starting powder material used for growth during initial heating. This point was further confirmed by the results of crystal stability studied at the elevated temperatures. For this, the colorless crystals were heated to 1000°C and this treatment was found to have no detectable effect on their optical transmission spectra. The result shows that colorless crystals are quite stable at high temperatures. The optical transmission spectra recorded for different crystals are shown in Fig. 1. In the case of colored crystals, the transmission on gamma irradiation was observed to become uniformly poorer at all wavelengths. On the other hand, the transmission characteristics of the colorless crystals remained unaffected on gamma irradiation. The former result shows that the transmission is affected due to changes in the crystal lattice as a whole and not on account of the change in the charge state of any particular ion. The absence of any radiation damage in colorless crystals shows that non stoichiometry is responsible for coloration. In both cases, only one glow peak is observed over the temperature range 30 – 325°C as shown in Fig. 2. However, a slight shift in the glow peak temperature for the two types of samples was noted. In case of the colorless samples, the peak temperature occurs at 170°C and for the colored crystals it gets shifted to 155°C. It is important to note that for colorless crystals while TSL was observed, no changes in the transmission spectra could be seen on gamma irradiation. The TSL output observed for both types of crystals was weak with emission from colorless samples being comparatively higher. The TSL emission spectrum was found to peak around 480 nm. The colored samples have enhanced absorption in this region and hence the observed TSL output is smaller than that from colorless crystals essentially due to self absorption. The order of kinetics of the glow peak was studied by peak shape method[22] and it was determined to be of first order.

Fig. 1 – Plots of optical transmission for $PbWO_4$ crystals grown from; (a) fresh charge, (b) left out charge from previous crystal growth run and (c) re-crystallized charge.

$CdWO_4$

The single crystal growth has been effected by melt method. A major concern here was the preferentially high loss of CdO at the growth temperature. This gives rise to large compositional changes, which are indeed reflected in the optical transmission characteristics of the crystal. A starting charge that is rich in CdO by a controlled amount enabled to grow good quality crystals. The optical transmission spectra recorded for crystals grown from charges containing 50 and 53.5 mole percent of CdO are shown in Fig. 3. The deviation from stoichiometry is observed to affect the crystal transmission. Typical glow curves recorded for different crystals are shown in Fig. 4. For stoichiometric crystal composition one glow peak around 148°C is observed. The normalized TSL output is found to be very weak. For the crystal having imperfect transmission a single glow peak is observed but its peak temperature is shifted towards higher temperature side by about 10°C and also the normalized output is enhanced considerably. These results show that the glow peak temperature and the intensity are both sensitive to stoichiometric deviations. The order of kinetics was determined to be of first order. The TSL emission was observed to peak at 490 nm.
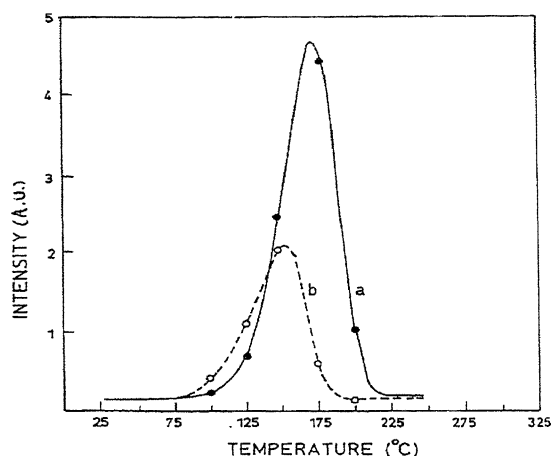
Fig. 2 - TSL glow curves of $PbWO_4$ crystals; (a) colorless and (b) colored. Emission peaking around 490 nm.
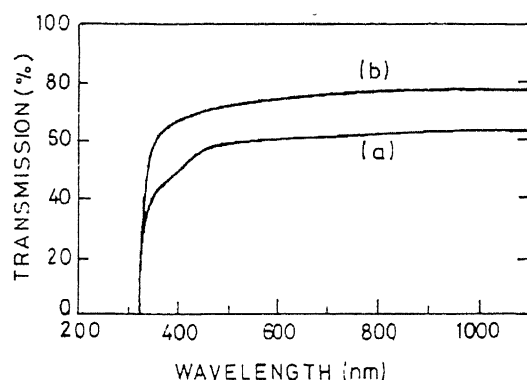
Fig. 3 - Optical transmission spectra recorded for $CdWO_4$ crystals grown from charges containing 50 and 53.5 mole percent of CdO.
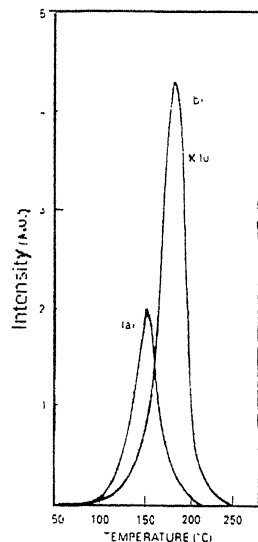
Fig. 4 - TSL glow curves of $CdWO_4$ crystals of, (a) stoichiometric and (b) off-stoichiometric compositions. Emission is peaking at 490 nm.

$Y_3Al_5O_{12}$

TSL glow curves for single crystal and sintered powder material samples recorded are shown in Fig. 5. Two isolated peaks at 120°C and 260°C were observed for the single crystal sample (plot-a). For the polycrystalline material synthesized by sintering of the constituent oxides, two peaks were again observed but they showed some fine structure. This result indicates the existence of some overlapping peaks which implies the presence of impurity phase(s). The XRD analysis revealed it to be a multiphase[19]. Clearly these results show that TSL is sensitive to deviations from stoichiometry. The TSL emission was found to peak around 525 nm.

$Bi_4Ge_3O_{12}$

Typical TSL glow curve recorded for a transparent and colorless crystal and shown in Fig. 6a contains a single glow peak at 112°C. For crystals grown from the starting materials having Bi_2O_3 deficiency of 0.12% by weight, a typical glow curve obtained is shown in Fig. 6b. While, a single peak is seen, the peak temperature is, however, lowered to ~ 96°C. The powder XRD pattern recorded in this case matched very well with the pattern reported in the literature and hence it gave no indication of the presence of any foreign phase[19]. In some of the crystal growth experiments where not so well synthesized starting charge was used, large deposition on the cooler walls of the growth chamber was observed. The X-ray fluorescence analysis of the deposit revealed it to be rich in germanium. The crystal composition in such cases was expected to be different from that of the initial charge. In the recorded glow curves (Fig. 6c), besides the peak ~ 96°C, an additional peak around 140°C is also seen. The XRD powder pattern recorded for this sample did not show the presence of any foreign phase. The order of kinetics of the glow peaks recorded in various cases was found to be of first order. The TSL emission spectra here peaked at 480 nm.

LiB_3O_5

In the phase diagram of $Li_2O - B_2O_3$ system, lithium triborate (LiB_3O_5 – 135) is the composition which crystallizes in orthorhombic form and contains

B_2O_7 as the structural units. Its transparency range extends from 160 nm to 2.6 μm, however, the crystals from different sources are found to exhibit poorer transmission in the UV region. The 135 is known to decompose into $Li_2B_4O_7$ (247) and $Li_2B_8O_{13}$ (2813) phases when raised to a few degrees above the melting point of 836°C. Consequently, the single crystal growth has been effected by top seeded solution growth (TSSG) technique using boron rich charges[23]. The impurity phases under reference have the same atomic constituents and hence their detection as minor fraction by conventional material characterization techniques is not easy[13].
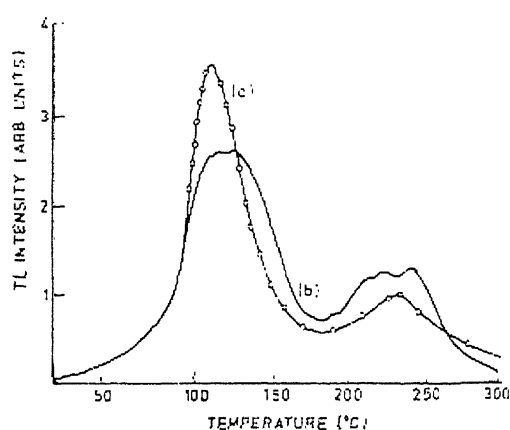
Fig. 5 – TSL glow curves for $Y_3Al_5O_{12}$; (a) single crystal sample and (b) mixed phase polycrystalline material synthesized by solid state sintering method. Emission is peaking around 525 nm.
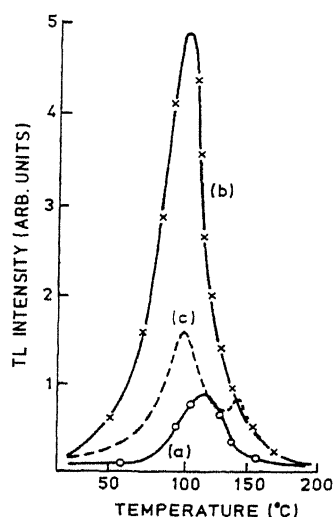
Fig. 6 – TSL glow curves recorded for $Bi_4Ge_3O_{12}$ crystals grown; (a) using re-crystallized material, (b) charge deficient in Bi_2O_3 by 0.12% by weight and (c) grown from not a well prepared charge. Emission is peaking at 480 nm.

When the growth of 135 crystal is seeded with a platinum wire, the grown crystals have opaque central region and transparent outer portion, as shown in Fig. 7. The powder XRD pattern recorded for transparent crystal portion was found to match with that of 135 phase[24]. For opaque portion, while majority of the reflections matched with those of 135 phase, the presence of some additional reflections corresponding to 2813 phase was also observed. These results showed that the central opaque portion of the crystal contains detectable amount of 2813 phase. The optical transmission spectra for different regions of the transparent portion were studied for a number of samples and the plots obtained are shown in Fig. 8. The samples belonging to outermost portion of the clear region showed good transmission throughout the wavelength range of 200 to 1100 nm.
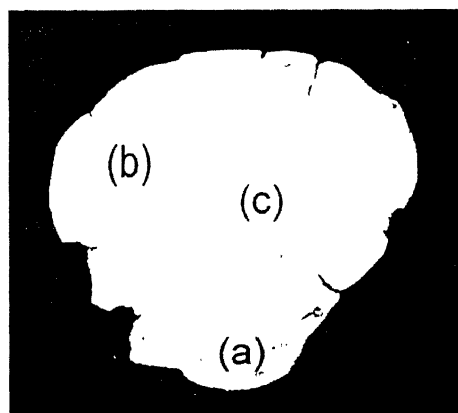
Fig. 7 – The photograph of LiB_3O_5 crystal ingot showing; (a) transparent, (b) translucent and (c) opaque regions.
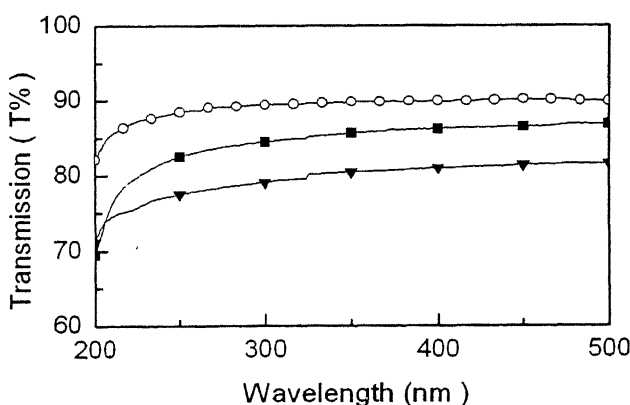
Fig. 8 – Transmission spectra of the samples representing three regions in clear portion of a LiB_3O_5 ingot; the three plots represent samples taken from (O) outermost region, (■) middle and (▼) region in the proximately of translucent portion.

However, the increased absorption at lower wavelength region was observed for samples taken from the transparent part closer to the translucent region of the ingot.

The TSL glow curves recorded for the well synthesized 135, 247 and 2813 polycrystalline materials are shown in Fig. 9 (a to c). For 135 sample only one peak around 140°C was obtained (plot-a). In case of 2813 material, two peaks around 130°C and 190°C were obtained (plot-b). For 247 material two peaks around 87°C and 210°C were observed (plot-c). The normalized TSL outputs for both 135 and 2813 phases were found to be of almost equal magnitudes, while for 247 it was about 50% less intense. These results showed that TSL glow curves are characteristic of the particular phase. It may be noted that the most prominent glow peaks of 135 and 2813 are separated only by about 10°C
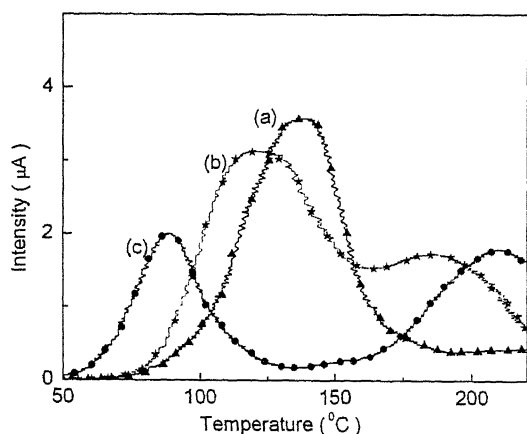
Fig. 9 – TSL glow curves of different phases of lithium borate; (a) LiB_3O_5, (b) $Li_2B_8O_{13}$ and (c) $Li_2B_4O_7$. Emission broad band is peaking around 420 nm.

For TSL studies on single crystals, the samples representing different portions of an ingot viz. (a) transparent, (b) translucent and (c) opaque as marked in Fig. 7 were selected. The glow curves recorded for the three types of samples are shown in Fig. 10. A well resolved glow peak around 136°C was observed in all the three cases. For the transparent sample, a small peak around 115°C was also observed. The normalized TSL output was the lowest for transparent portion and the highest for opaque portion. The glow curves for 247 crystals were also recorded and the results obtained were essentially the same as reported for the polycrystalline material as shown in Fig. 9(c). The TSL emission was found to spread over a broad band peaking around 420 nm.
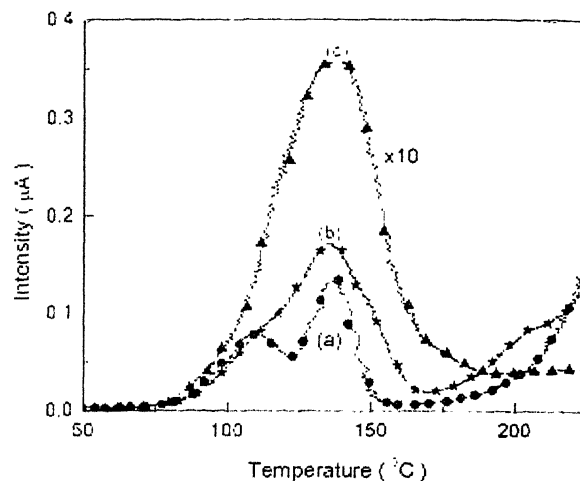
Fig. 10 – TSL glow curves recorded for samples selected from specific regions of LiB_3O_5 crystal ingot shown in the Fig.7 as marked (a), (b) and (c).

Prominent changes in UV edge are observed for samples obtained from the transparent region at the proximity of translucent portion. The increased UV absorption is due to defect structure of the lattice which may be arising from (a) stoichiometric deviations and/or (b) impurity phase. Indeed, the stoichiometric deviations are known to affect the absorption edge. However, this defect is most probable in case of melt growth, where preferentially high loss of one component over the other causes compositional changes. Thus, in the present case the second possibility viz. impurity phase appears to be the most probable one. The results of reported powder XRD support this view.

The following inferences could be drawn from the above results :

1. The TSL is sensitive to minute deviations from stoichiometry.

2. Both the TSL intensity and glow peak temperatures are affected by the changes in stoichiometry.

3. The TSL output observed from good quality crystal samples is quite weak and hence a high gamma exposure was required to observe the effect. This result implies that the number of

intrinsic centers responsible for TSL emission should be very small. The observed increase in the TSL intensity for supposedly poorer quality crystal samples shows that the TSL active centers are related to stoichiometric deviations, and if sufficiently large are also revealed by the XRD measurements.

4. The stoichiometric crystals were subjected to thermal treatment at two third of their melting temperatures. This was found to have no appreciable effect on the TSL intensity, indicating that the centers involved here did not arise as a result of the thermal considerations like in the case of alkali and alkaline earth halide crystals[25].

5. Another factor that supports the conclusion of a relationship between the observed TSL and stoichiometry is that the TSL spectral characteristics match with those of the intrinsic scintillation observed from $PbWO_4$, $CdWO_4$ and $Bi_4Ge_3O_{12}$ crystals. Here the kinetics of the TSL emission was found to be of first order which means that the trapping and the emitting centers are essentially the same. These facts rule out the possibility of impurity assisted TSL in the present case and the observed changes in glow curve are due to stoichiometric deviations.

Conclusion

Minute amount of stoichiometric deviations that are inherently present in oxide crystals can be effectively detected by TSL. This is a novel application of TSL in the field of materials science. Indeed, a larger data base on TSL from different oxide crystals synthesized under careful conditions needs to be developed for a large scale exploitation of this application.

References

1. McDeugall DJ, *Thermoluminescence of Geological Materials*, 1968; Academy Press, New York.
2. Sabharwal SC, Kathuria SP & Ghosh B. Effect of impurities on scintillation, optical and thermo luminescent properties of NaI(TI). *Nucl Instr. Methods* 1987; **A255** : 501-506.
3. Sangeeta, Sabharwal SC, Ghosh B & Gupta MK. Thermo luminescence from europium doped calcium fluoride crystals. *Phys Status Solidi(a)* 1990; **121** : 657-665.
4. Suresh N, Jyoti G, Gupta SC, Sikka SK, Sangeeta & Sabharwal SC. Shock induced amorphisation of q-GeO_2. *J Appl Phys* 1994; **76** : 1530-1534.
5. Sabharwal SC & Sangeeta. Effect of sodium doping on thermo luminescence and optical properties of barium borate single crystals. *J Crystal Growth* 1998; **187** : 253-258.
6. Sangeeta, Sabharwal SC. & Gesland JY. Thermally stimulated luminescence from single crystals of $LiYF_4$ and its constituent fluorides. *J Luminescence* 2001; **93** : 167-172.
7. Sabharwal SC, Sangeeta & Chauhan AK. Effect of oxygen on optical absorption, radiation hardness and thermally stimulated luminescnece of BaF_2 crystal. *J Crystal Growth* 2002; **240** : 473-478.
8. Sabharwal SC & Deshpande RY. Solid State Infrared Materials. Proceedings of DAE Symposium on Infrared Technology and Instrumentation, 1980; 5-7 March, Mumbai, India.
9. Baumard JF & Abelard P. An approach to the defect chemistry in barium titanate. *Solid State Ionics* 1984; **12** : 47-51.
10. Abrahams SC & Marsh P. Defect structure dependence on composition in lithium niobate. *Acta Cryst* 1986; **B42** : 61-64.
11. Morris PA, Optical Materials. In : Poker DB, Ortiz C, editors. Processing and Science : Pittsburg PA, Materiak Research Society 1989
12. Sangeeta, Sabharwal SC, Non-stoichiometry factor in crystal growth. In Jayavel R, Kitamura K, editors Advanced Materials for Optoelectronics: Vijay Nicole, Chennai, 2004 pp. 134-139.
13. Millett EJ. Progress in analysis of crystalline solids. *J Crystal Growth* 1980; **48** : 666-682.
14. Bergman JG, Ashkin A, Ballman AA, Dziedzic JM, Levinstein HJ & Smith RG. Curie temperature, birefringence and phase matching temperature variation in $LiNbO_3$ as function of melt stoichiometry. *Appl Phys Lett* 1968; **12**: 92-94.
15. Allibert M, Chatillon C, Mareshal J, Lissalde F. du diagramme de phase dans le systeme Gd_2O_3-Ga_2O_3.*J. Crystal Growth* 1974; **23** : 289-294.
16. Sabharwal SC, Sangeeta, Desai DG, Karandikar SC, Chauhan AK, Sangiri AK, Keshwani KS&Ahuja MN, Preparation and characterization of radiation hard $PbWO_4$ crystal Scintillator. *J Crystal Growth* 1996; **169**: 304-308.
17. Sabharwal SC&Sangeeta. Study of growth imperfections, optical absorption, thermoluminescene and radiation hadness of $CdWO_4$ crystals. *J Crystal Growth* 1999; **200**: 191-198.

18. Sangeeta, Sabharwal SC & Gupta MK. On the growth of single crystal $Y_3Al5_3O_{12}$. *Proc Indian Natn Sci Acad* 1991; **57**: 153-157.

19 Sangeeta, Prasad H&Sabharwal SC.Crystal stoichiometry and thermo luminescence of BGO and YAG. *J Crystal Growth* 1992; **118**: 396-400.

20. Sabharwal SC, Tiwari B & Sangeeta. Effect of highest temperature invoked on the crystallization of LiB_3O_5 from boron-rich solution. *J Crystal Growth* 2003; **249**: 502-506.

21. Sangeeta, Chaudhary S, Ved N. Rao MKV & Sabharwal SC. Development of a PC based system for thermally stimulated luminescence studies. *Proc Solid State Phys Symp* 2002; **45**: 131-132.

22. Chen R. On the calculation of activation energy and frequency factor from glow curves. *J Appl Phys* 1969; **40**: 570-585.

23. Bruck E, Raymakers RJ, Route RK & Feigelson RS. Crystal growth of compounds in $MgO-Nb_2O_5$ system. *J Crystal Growth* 1993; **128**: 842-845.

24. Sabharwal SC, Tiwari B & Sangeeta. Investigations on the growth of LiB_3O_5 crystal by top seeded solution growth technique. *J Crystal Growth* 2004; **263**: 327-331.

25. Schulman JH & Compton WD. Color Centers in Solids. London : Pergamon Press, 1963.

Proc. Nat. Acad. Sci. India Sect. A, Vol. 78, Pt. II, 2008

Vibrational studies of pharmaceutically important carboxylic acid's monomers and dimers in ground electronic states

Y.P.SINGH*, RATNESH DAS# and R.A.SINGH+

*Department of Physics, Govt. Women's Polytechnic College, Sagar (MP),470 001

#Department of Chemistry, Dr H.S. Gaur University, Sagar (MP)-470 003

+Department of Physics, Dr. H.S. Gour University , Sagar (MP),470 003

Email . Y_P_S_2k@yahoo.com, ratnesh_das@Yahoo.com.

Received Aughust 3, 2006; Accepted October 18, 2007

Abstract

Absorption spectra of formic, acetic and benzoic acid's monomers and dimers are recorded by FTIR spectrometer. Assuming C_s point symmetry, vibrational assignments for the observed frequencies have been proposed. The spectra exhibit distinct features originating from low frequency vibrational modes caused by intra-molecular motion. Experimental frequencies are compared with those calculated by GF matrix and AM1 methods.

(**Keywords** : benzoic acid/acetic acid/formic acid/FTIR spectra/MOPAC/vibrational spectra)

Introduction

Molecular structures and inter/intra molecular interactions have a direct influence on the type of structural framework that biomolecules can adopt. Understanding of fundamental processes, dynamics, molecular-orbital studies and force constants calculations are, thus, main objectives of spectroscopists. Intramolecular force field helps us to identify fundamental frequencies, assign fundamental frequencies to correct mode of vibrations, determine reliable force constants and design the drug as input parameters and to predict vibrational frequencies of related molecules.

Benzoic acid is the simplest aromatic carboxylic acid containing carboxyl group bonded directly to benzene ring[1]. It naturally occurs in many plants and resins. It is also detected in animals.

Benzoic acid is used externally as an antiseptic and is employed in lotions, ointments and mouthwashes. When used as preservative in foods and in pharmaceutical products, benzoic acid and its salts are more effective as the pH is lowered[2]. Semi-empirical molecular orbital theory was used to predict the FTIR and Raman spectra of molecules in their ground electronic states[3].

Carboxylic monomers and dimmers are the simplest models for studying hydrogen bonded systems[4,5] and they are important as doubly bonded hydrogen atoms are abundant in nucleic acid base pairs holding together the double stranded helices in DNA[6].

Many workers have studied vibrational spectra of carboxylic acids. Ito and Bernstein[7] made vibrational assignment of acetate ions. Salto and Hirata[8] investigated the electronic structure of acetic acid by self consisted field study. Neikabayashi *et al.*[9] used Raman and *ab initio* calculation for studying liquid structure of acetic acid. Ibrahim and Koglin[10] used density functional theory(DFT) to investigate structure and vibrational frequencies of acetate group. Experimental and theoretical studies have also been done by many workers[11-16] on steady state O-H stretching bonds of carboxylic group. In depth study of low frequency vibrational coherence in cyclic dimmers of acetic acid was done by Heyne *et al.*[17] . The infrared absorption spectra of benzoic acid and some of its mono substituted derivatives have been done by many workers[18-19]. In recent study of benzoic acid monomer and dimmer, mid frequency spectrum has been carried out[20]. Trout *et al.*[21] compared experimental results with calculated

frequencies using *ab initio* and molecular orbital calculations. Marechal[23] reanalysed the IR spectra of carboxylic acid dimers in the gas phase. Ito and Nakanaga[24,25] studied formic acid dimers by jet cooled infrared spectra. Florio *et al.*[16] made theoretical modeling of OH stretch infrared spectrum of carboxylic acid dimers on first principles anharmonic couplings.

In present paper we have made studies on formic acid (FA), acetic acid (AA) and benzoic acid(BA) monomers and dimers. These molecules are of considerable interest from the point of understanding fundamental molecular properties, benchmarking GF matrix and MOPAC calculations. Also, experimental results were compared with calculated frequencies of acids using force matrix method and MOPAC method. This method was able to account extent of spectrum as well as description of vibrational modes to encourage the application of a similar procedure to a larger and more complex groups.

Formic Acid Monomer   Acetic Acid Monomer   Benzoic Acid Monomer

Formic Acid Dimer   Acetic Acid Dimer   Benzoic Acid Dimer
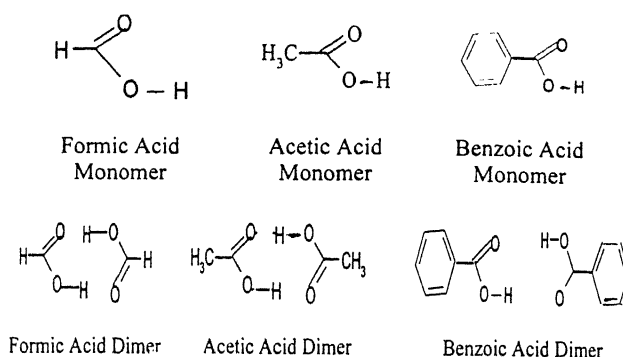
Probably this is the first time, when we had compared experimental frequencies with theoretical frequencies calculated by G F matrix and AM1 method.

Table 1 – Experimental and calculated frequencies and potential distribution in acetic acid monomer

Assignment	Experimental frequencies (cm^{-1})	G F matrix		AM1calculation
		Frequencies (cm^{-1})	Potential energy distribution and mode	Frequencies (cm^{-1})
		Species a′		
1	3567	3529.2	OH str	3328.69
2	3010	2905.7	CH_3 d-str	3069.34
3	2842	2811.3	CH_3 s-str	2614.90
4	1801	1819.6	C=O str	1896.74
5	1465	1513.2	CH_3 d-deform	1512.42
6	1457	1449.4	CH_3 s-deform	1388.75
7	1298	1273.5	OH bend	1298.27
8	1235	1215.8	C-O str	1114.03
9	1006	983.6	CH_3 rock	915.73
10	801	810.7	CC str	843.61
11	657	662.5	OCO deform	528.20
12	568	561.9	CCO deform	375.99
		Species a″		
13	2996	2945.3	CH_3 d-str	1973.32
14	1430	1419.6	CH_3 d-deform	1107.59
15	1048	1037.2	CH_3 rock	797.55
16	642	638.1	C=O op-bend	531.88
17	534	541.8	C-O torsion	510.25
18	–	139.5	CH_3 torsion	134.93

Table 2 – Experimental and calculated frequencies and potential distribution in formic acid monomer.

Assignment	Experimental frequencies (cm^{-1})	G F matrix		AM1calculation
		Frequencies (cm^{-1})	Potential energy distribution and mode	Frequencies (cm^{-1})
		Species a′		
1	3557	3511.3	OH str	3429.97
2	2911	2926.4	CH str	3187.76
3	1815	1806.2	C=O str	2049.86
4	1409	1421.7	CH bend	1489.68
5	1313	1326.8	OH bend	1437.70
6	1206	1219.9	C-O str	1231.94
7	613	601.5	OCO deform	603.89
		Species a″		
8	1008	992.6	CH bend	988.24
9	619	610.6	Torsion	603.95

Materials and Methods

Spectroscopic measurements were recorded using Perkin-Elmer spectrometer Model 397 using neat liquid films between KBr windows. A small amount of finally grounded solid sample was intimately mixed with about 100 times or more than its weight of potassium bromide powder. The finally grounded mixture was then pressed under vacuum at high pressure to obtain a transparent disc (about 1-2 mm thick and 1 cm in diameter).

Results and Discussion

Results of FTIR measurements and the calculated frequencies for all symmetry species are summarized in Table 1,2 and 3. Values in Table 4 and 5 has been taken from references 6, 26, 27 and 18. . The values of bond lengths and bond angles are presented in Table 6.

The results are compared with calculated values using GF Matrix and AM1. Table 6 presents bond lengths in Å determined experimentally. Experimental and DFT results are used for comparison with AM1 results.

Monomer

Results for carboxylic acids monomer are summarized in Table 1, 2 and 3.

OH stretch : Experimental OH stretch band frequencies for AA, FA and BA are 3567 cm^{-1}, 3557 cm^{-1} and 3507 cm^{-1} respectively.. Ibrahim *et al*[10] observed it for acetic acid at 3583 cm^{-1} and Florio *et al.*[16] got this for formic acid at 3569 cm^{-1}. Antony *et al.*[6] observed this frequency for benzoic acid at 3602 cm^{-1} which is higher than those observed by others. Theoretically calculated frequencies by GF Matrix method and AM1 methods are (3529.2 cm^{-1} and 3328.7 cm^{-1}), (3511.3 cm^{-1} and 3429.9 cm^{-1}) and (3532.2 cm^{-1} and 3427.3 cm^{-1}) for AA, FA and BA respectively.

CH_3 s-stretch : Experimental CH_3 s-stretch frequencies for AA, FA and BA are 2842 cm^{-1}, 2911 cm^{-1} and 2987 cm^{-1} respectively. Ibrahim *et al.*[10] observed it for acetic acid at 3186 cm^{-1} and Florio *et al.*[16] got this for formic acid at 2943 cm^{-1}. Antony *et al.*[6] observed this frequency for benzoic acid at 2943 cm^{-1}. Thus these frequencies observed by us are lower than other's observations. Theoretically calculated frequencies by GF Matrix method and

Table 3 – Experimental and calculated frequencies and potential distribution in benzoic acid monomer.

Assignment	Experimental frequencies (cm^{-1})	G F matrix		AM1
		Frequencies (cm^{-1})	Potential energy distribution and mode	Frequencies (cm^{-1})
		Species a′		
1	3507	3532.2	OH str	3427.3
2	3217	3210.6	CH str	3198.2
3	3130	3118.8	CH str	3190.2
4	3100	3111.5	CH str	3182.2
5	3087	3072.4	CH str	3175.7
6	2987	3012.9	CH str	3172.0
7	1823	1716.5	C=O str	2076.2
8	1696	1818.1	CC ring deformation	1821.9
9	1585	1561.4	C-C str	1765.5
10	1499	1518.7	COH bnding	1638.6
11	1456	1443.8	CCH bending	1572.6
12	1328	1341.5	OH bending	1541.9
13	1228	1211.8	C-O str	1435.7
14	1292	1312.3	CCh bending	1378.9
15	1280	1277.3	O-H bend	1359.0
16	1186	1171.4	CH ib	1314.7
17	1179	1192.5	COH bending	1229.4
18	1129	1134.6	Ring id+C-O str	1198.3
19	1074	1063.1	Ring CCH bending	1177.5
20	1029	1011.1	Ring id + CC str	1168.0
21	1000	1013.9	CH od	1089.4
22	808	801.3	CH od	796.5
23	668	652.7	OCO deform	646.3
24	600	587.3	Ring CCC bending	536.8
25	548	525.6	COH bending	509.9
26	420	412.1	C-O bending	409.
27		310.5	C=O bending	200.0
		Species a″		
28	980	971.6	CC wagging	1013.2
29	970	967.3	CC wagging	995.6
30	935	929.5	rocking	971.8
31	935	937.6	CC wagging	894.5
32	850	844.1	Ring CCH	886.3
33	812	801.9	Ring CCH bend	825.9
34	709	719.8	C=O o.p.bend	723.6
35	664	657.1	Ring CCH bend	610.2
36	613	609.3	torsion	411.9
37	591	593.4	torsion	371.9
38		199.4	wagging	150.6
39		57.6	twisting	44.0

Table 4 – Calculated and experimental frequencies of formic acid dimer.

S.N.	Symmetries	Experimental frequencies (cm^{-1})	GF matrix calculated frequencies (cm^{-1})	Mode
		Dimer		
1	B_u	3110	3113.2	OH str
2	A_g	2949	3009.4	CH str
3	B_u	2957	2957.6	CH str
4	A_g	–	2949.8	OH str
5	B_u	1754	1749.6	C=O str
6	A_g	1670	1683.1	C=O str
7	A_g	1415	1411.5	OH bend
8	B_u	–	1421.6	OH bend
9	A_g	1375	1351.4	CH bend
10	B_u	1362	1347.9	CH bend
11	B_u	1218	1229.5	C-O str
12	A_g	1214	1221.9	C-O str
13	A_u	1060	1043.2	CH o.p. bend
14	B_g	1050	909.5	CH o.p. bend
15	A_u	917	901.7	OH torsion
16	B_g	–	857.3	OH torsion
17	B_u	699	710.6	CO_2 bend
18	A_g	677	651.9	CO_2 bend
19	B_u	248	270.3	i.p. rock (dimmer)
20	B_g	230	256.4	o.p. wag (dimmer)
21	A_g	190	211.6	i.p. rock (dimmer)
22	A_u	163	189.7	o.p. wag (dimmer)
23	A_g	137	173.4	stretch (dimmer)
24	A_u	68	79.5	wist (dimmer)

Note : experimental frequencies from Ref 26 and 27.

AM1 methods are (2811.3 cm^{-1} and 2614.9 cm^{-1}), (2926.4 cm^{-1} and 3187.7 cm^{-1}) and (3111.5 cm^{-1} and 3182.2 cm^{-1}) for AA, FA and BA respectively.

C=O stretch : Experimental observed frequencies for this bands are 1801 cm^{-1}, 1815 cm^{-1} and 1823 cm^{-1} for for AA, FA and BA. Ibrahim *et al.*[10] observed it for acetic acid at 1788 cm^{-1} and Florio *et al.*[16] got this for formic acid at 1804 cm^{-1}. Antony *et al.*[6] observed this frequency for benzoic acid at 1752 cm^{-1}. For AA, FA and BA theoretically calculated frequencies by GF Matrix method and AM1 methods are (1819.6 cm^{-1} and 1896.74 cm^{-1}), (1806.2 cm^{-1} and 2049.8 cm^{-1}) and (1818.1 cm^{-1} and 1821.9 cm^{-1}).

O-H bend : Observations for this bending mode are at 1298, 1313 and 1328 cm^{-1} for AA, FA and BA. Ibrahim *et al.*[10] observed it for AA at 1355 cm^{-1} and Florio *et al.*[16] got this for FA at 1223 cm^{-1}. Antony *et al.*[6] observed this frequency for benzoic acid at 1381 cm^{-1}. Theoretically calculated frequencies by GF Mat-rix method and AM1 methods are (1273.5 cm^{-1} and 1298.3 cm^{-1}), (1326.8 cm^{-1} and 1437.7 cm^{-1}) and (1277.3 cm^{-1} and 1359.0 cm^{-1}) for AA, FA and BA respectively.

C-O stretch : Experimental frequencies for AA, FA and BA are 1235 cm^{-1}, 1206 cm^{-1} and 1228 cm^{-1} respectively. Ibrahim *et al.*[10] observed it for AA at 1182 cm^{-1} and Florio *et al.*[16] got this for FA at 1105 cm^{-1}. Antony *et al.*[6] did not observe this frequency for benzoic acid. Thus frequencies observed by us are in good agreement with each othsr and are higher than observed by others. By GF Matrix method and AM1 methods we get frequencies as (1215.8 cm^{-1} and 1114.0 cm^{-1}), (1219.9 cm^{-1} and 1231.9 cm^{-1}) and (1341.5 cm^{-1} and 1541.9 cm^{-1}) for AA, FA and BA respectively.

O-C-O deformation : Frequencies at 657 cm^{-1}, 613 cm^{-1} and 668 cm^{-1} for AA, FA and BA respectively are comparative to those observed by others[6,10]. Theoretically calculated frequencies by GF Matrix method and AM1 methods are (662.5 cm^{-1} and 528.2 cm^{-1}), (601.5 cm^{-1} and 603.8 cm^{-1}) and (652.7 cm^{-1} and 646.3 cm^{-1}) for AA, FA and BA respectively.

Table 5 – Calculated and experimental frequencies of benzoic acid dimer

S.N.	Symmetries	Experimental frequencies (cm^{-1})	G.F.matrix calculated frequencies (cm^{-1})	Mode
11	A_g	3350	3307.3	O-H str
12	B_u		2974.6	O-H str
13	A_g	1693	1750.9	C=O str
14	B_u	1649	1655.8	C-C str ring deform
15	A_g	1521	15.7.3	C-O-H bending
16	B_u	1471	1481.1	C-O-H o.p. bending
17	B_u		1336.4	C=O str
29	A_g	1328	1330.4	C-O str
30	B_u		1521.8	C-O str
21	A_g	1424	1486.7	OH bend
22	B_u		1010.9	OH bend
41	A_u	936	972.6	OH ocking
48	B_g		920.1	OH ocking
51		815	801.4	scissoring
69	A_g		393.8	$C0_2$ bendiing
72	B_u		296.3	$C0_2$ bendiing
73	A_g		262.5	rocking
74	B_u		189.3	rocking
75	A_u		169.3	wagging
76	B_g		70.1	wagging
79	A_u		68.3	twisting
80	B_g		115.3	twisting
77	A_g		113.2	H-H str (inter molecular
78	A_g		62.8	H-H shearing (inter-molecular
81	B_g		59.8	tilting
82	B_u		53.6	cogwheel
83	A_u	32	33.2	torsion
84	A_u		25.9	butterfly

Note : experimental frequencies from Ref 28 and 6.

Torsion : Experimental observed frequency for the torsion mode for AA, FA and BA are 534 cm^{-1}, 619 cm^{-1} and 591 cm^{-1} respectively. Ibrahim *et al.*[10] observed it for AA at 542 cm^{-1} and Florio *et al.*[16] got this for FA at 642 cm^{-1}. Antony *et al.*[6] observed this frequency for benzoic acid at 444 cm^{-1}. FA has got more value because here torsion is of OH. For AA, FA and BA theoretically calculated frequencies by GF Matrix method and AM1 methods are (541.8 cm^{-1} and 510.2 cm^{-1}), (610.6 cm^{-1} and 603.9 cm^{-1}) and (593.4 cm^{-1} and 371.9 cm^{-1}).

Table 6 – Bond lengths and bond angles in acetic acid.

	Bond length (A°)		Bond Angle (°)		
Bond	Experimental[10]	By AM1 Calculation	Bond Angle	Experimental[10]	By AM1 Calculation
H_5-C_1	1.102	0.888	H_5-C_1-H_6		50.1
H_6-C_1	1.102	0.922	H_6-C_1-H_7		49.8
H_7-C_1	1.102	0.887	H_5-C_1-C_2		135.6
C_1-C_2	1.520	1.070	H_7-C_1-C_2		124.5
O_4-C_2	1.214	0.968	O_4-C_2-C_1	107.0	126.2
O_3-C_2	1.364	0.993	O_3-C_2-C_1	126.6	130.1
O_3-H_8	0.970	0.982	O_4-C_2-O_3	128.0	103.8
			H_8-O_3-C_2	122.0	129.5

Table 7 – Bond lengths and bond angles in formic acid.

	Bond length (A°)		Bond Angle (°)		
Bond	Experimental[10]	By AM1 Calculation	Bond Angle	Experimental[10]	By AM1 Calculation
O_3-C_2	1.364	0.993	O_3-C_2-C_1	126.6	130.1
H_5–C_1	1.30	1.448	H_5–C1–O_3	139.6	135.3
C1–O_2	1.13	1.163	H_5–C1–O_2	138.9	135.3
C1–O_3	1.10	1.127	O_3–C1–O_2	92.6	89.3
O_2–H_4	1.98	1.284	C1–O_2–H_4	131.8	136.2

Dimer

The intramolecular vibrational modes are doubled in dimers. A' modes of monomers correlate with A_g and B_u modes of the dimers and A'' modes correlate with A_u and B_g. In most cases, the dimer modes are best described as either symmetric (gerade) or anti-symmetric (ungerade) combinations of two monomeric vibrations where only the latter ones are infrared active[6] .

Experimentally obtained frequencies for formic acid dimer (FAD) compare with those obtained by GF matrix method. Theoretical calculations of vibrational spectrum by ab inito method and density functional theory for FAD are possible but we have used GF matrix method. Experimentally OH stretch frequency obtained at 3110 (B_u), but for A_g it had not been observed. By GF matrix method we got them at 3009.4 (B_u) and 2956.4 (A_g). Harmony[27] observed CH stretch at 2949 cm^{-1} and Ito and Nakanaga[25] observed it at 2937.7 cm^{-1}. Theoretically, it has been observed at 3009.4 cm^{-1}. Here one observes intense peak because of mixing of CH and OH stretch local modes.

B_u frequency for OH stretch is 3110 cm^{-1} and A_g frequency had not been observed by Harmony[27]. Theoretically, we get them at 3113.2 cm^{-1} and 2949.8 cm^{-1}, difference between these two is 163.4 cm^{-1}. Bertie and Michadian[29,30] observed B_u OH bend at 1450 cm^{-1} and A_g OH at 1475 cm^{-1}. B_u OH bend vibration was rejected by Qian and Krimm[31], they got it at 1450 cm^{-1}. Our theoretical results are in agreement with Harmony[27].

In benzoic acid dimer (BAD) almost all the frequencies are shifted by 15%.due to Fermi resonance interactions and they are very broad. Normal mode OH bending of BAD is contributed by CH bends, hence many interactions are possible here. In case of benzoic acid monomer (BAM) OH stretching is at 3507 cm^{-1}, but in BAD it is at 3350 cm^{-1}.

C=O stretch in BAM is at 1823 cm^{-1} and it is 1693 in BAD, C-C stretching is higher(1649 cm^{-1}) for BAD than Bam (1585 cm^{-1}), similar case is for OH bending. In BAM C-O stretch is at 1585 cm^{-1} whereas it is 1328 cm^{-1} for BAD. Our theoretical calculations agree with the experimental values.

References

1. w w w.Chemicalland21.com. November 2005.
2. Wilson WA & Gisvolds O. Textbook of Organic, Medicinal and Pharmaceutical Chemistry. Lippincott Williams & Wilkins; 10th edition, 2004; p. 113-114.
3. Wong MW. Vibrational frequency prediction using density functional theory. *Chem Phys Letters* 1996; **256** : 391-399.
4. Madeja F & Haveniyh M. High resolution spectroscopy of carboxylic acid in the gas phase, *J Chem Physics* 2002; **117** : 7162-7168.
5. Markwick PRL, Doltsinis NL & Marx D. Elucidating double proton transfer in formic acid dimer. *J Chem Phys* 2005; **122** : 054112-054119.

6. Antony J, Helden G, Meijer G & Schmidt B. Anharmonic mid IR vibrational spectra of benzoic acid monomer and dimer. *J Chem Phys* 2005; **123** : 014305-014316.

7 Ito K & Bernstein HJ. The vibrational spectra of the fomate, acetate and oxalate ions. *Canadian Journal Chemistry* 1956; **24** : 170-178.

8 Salto H & Hirata F. The anti conformational equilibrium of acetic acid in water. *J Mol Structure* 1999; **113** : 401-462.

9. Nakabayashi T, Koscigi K & Nishi N. Liquid structure of acetic acid studied by Raman spectroscopy and ab initio molecular orbital calculations. *J Phys Chem* 1999; **103** : 8595-8603.

10. Ibrahim M & Koglin E. Vibrational Spectroscopic Study of Acetate Group. *Acta Chim* 2004; **51** : 453-460.

11. Marechal Y & Witkowski A. IR Spepctra of H-Bonded System. *J Chem Phys* 1968; **48** : 3697-3705.

12 Marechal Y. IR spectra of carboxylic acids in the gas phase : A quantitative reinvestigation. *J Chem Phys* 1987; **87** : 6344-6353

13 Fuji Y, Yamada H & Mitzuta M. Self-association of acetic acid in some organic soovents *J Phys Chem* 1988; **92** : 6768-6774.

14. Chamma D & Henri-Rousseau D. IR theory of weak H-bonds : Davydov coupling, Fenmi resonances and direct relxation. I. Bassis equation within the linear response theory. *Chem Phys* 1999; **248** : 53-70.

15. Chamma D & Henri-Rousseau D. IR theory of weak H-bonds : Davydov coupling, Fermi resonances and direct relaxations. II. General trends, from numerical experiments, *Chem Phys* 1999; **248** : 71-89.

16. Florio GM, Zwier TS, Myshakin EM, Jordan KD & Sibert III E L. Theoretical modeling of the OH stretch infrared spectrum of carboxylic acid dimers, *J Chem Phys* 2003; **118** : 1735-1746.

17. Heyne K, Huse N, Dreyer N, Nibbering ETJ, Elsaesser T & Mukanand S. Coherent low frequency motions of hydrogen bonded acetic acid, *J Chem Phys* 2004; **121** : 2-9.

18. Llett M & St J. IR spectrum of Benzoic acid, *J Chem Soc* 1955; **11** : 962-969.

19. Green JHS. Vibrational spectra of Benzene Derivatives, *Spectrochim Acta* 1970; **26A** : 1523-1536.

20. Bakker JM, Alease LM, .Helden GV & Meyer G. The IR absorption spectrum of the gas phase neutral benzoic acid monomer and dimer, *J Chem Phys* 2003; **119** : 11180-1185.

21. Trout CC, Tambach YJ & Kubicki JD. Correlation of observed and model vibrational frequencies for aqueous organic acids, 2005, www.engr.psu.edu.

22. Wilson EB. The mormal modes and frequencies of vibration of the regular plane hexagon model of Benzene, Molecular Vibrations, *Phys Rev* 1934; **45** : 706-712.

23. Marechal Y. IR spectra of carboxylic acids in the gas phase, *J Chem Phys* 1987; **87** : 6344-6353.

24. Ito F & Nakanaga T. A jet-cooled IR spectrum of the formic acid dimer by cavity ring-down spectroscopy, *Chem Phys Lett* 2000; **318** : 571-577.

25. Ito F & Nakanaga T. Micro salvation of aniline clusters cation studied by IR depletion spectroscopy, *Chem Phys* 2002; **277** : 171-178.

26. Almenningen A, Bastiansen O & Motzfeld T. A gas phase electron diffraction and ab-initio molecular orbital investigation, *Actachim* 1969; **23** : 1848.

27. Harmony MD. Molecular structures of gas-phase polyatomic molecules determined by spectroscopic methods, *J Chem Phys* 1979; **8** : 619-721.

28. Blanca ES de la, Nunez JL & Martinez P. *An Quim Ser A* 1986; **82** : 480-487.

29. Bertie JE & Michaelian KH. The Raman spectra of gaseous formic acid-h_2 and -d_2, *J Chem Phys* 1982; **76** : 886-894.

30. Bertie JE, Michaelian KH, Eysel HH & Hager D. The Raman-active O-H and O-D stretching vibrations and Raman spectra of gaseous formic acid, *J Chem Phys* 1986; **85** : 4779-4789.

31. Quian W & Krimm S. Vibrational spectroscopy of hydrogen bonding, *J Phys Chem A* 1998; **102** : 659-667.

THE NATIONAL ACADEMY OF SCIENCES, INDIA

5, Lajpatrai Road, New Katra, Allahabad - 211002

Guidelines for the Authors/Contributors for submitting papers

in Proceedings of the National Academy of Sciences, India

(Section A - Physical Sciences)

[A] WHAT TO SUBMIT

(1) **Scope of the Journal - Chemical Sciences** (Analytical, Inorganic, Organic, Physical, Theoretical Chemistry, Applied Chemistry), **Earth Sciences** (Atmospheric Sciences, Geo-Sciences, Oceanography Geography-Scientific aspects), **Engineering Sciences including Engineering Technology** (Engineering and Engineering Science, Chemical and Material Technology, Electronics & Telecommunication, Information Technology, Instrumentation), **Mathematical Sciences** (Pure Mathematics, Applied Mathematics, Statistics, Computer/Information Science), **Physical Sciences** including (Astronomy, Astrophysics, Experimental and Theoretical Physics, Applied Physics).

The following three categories of papers are published in the Proceedings of the National Academy of Sciences, India (Section A - Physical Sciences) :

Review articles: This should be a critical review on any relevant subject of topical interest and should bring the status of the research work done. This should be written in a manner to help either in initiating the work in that area or in increasing the comprehension of the current challenges. The review article should not be a compilation of literature survey. If such an article is accepted by the Academy for publication, then *Rupees Two Thousand only* would be given to the 'corresponding author' after the publication of the paper in the Proceedings to meet the contingency expenses. Ordinarily, the Review article should not exceed 25 printed pages.

Full length articles: The articles discussing complete investigation on a research problem will be published under this category. The publication of a research problem into fragments will not be encouraged. Ordinarily, such articles should not be more than 12 printed pages.

Short Notes : The articles on a topic of research with sufficient details on experimental or theoretical part will be published under this category. Normally, Short Notes will not be longer than 6 printed pages.

(2) **Special Issues for Conference Proceedings :** Proceedings of National and International Conferences, as a special issue of the journal, can also be brought out with organizers as Guest Editors. At least, one of the Guest Editors should be Fellow of the Academy. Guest Editors shall be responsible for proper refereeing of the papers and for ensuring their high quality.

It is presumed that the articles submitted for publication have not been submitted to any other journal by the authors. Authors shall be liable themselves for such an act.

[B] WHO CAN SUBMIT

(1) All scientists (Indian or Foreign) can directly send their article for publication. If there are more than one author, each author should certify that he/she agrees to the submission of the review/research paper.

(2) In addition to above, all the Fellows of the National Academy of Sciences, India are also authorized to forward quality papers in their research field for publication in the journals of the Academy. The name of the communicating Fellow would be printed in the paper as "Communicated by......................FNASc".

The communicating Fellow should certify that : (i) The forwarded paper is in his/her field of specialization. (ii) He/she has read the paper and reviewed it carefully.

However, if the Editorial Board finds it necessary, it may get the paper reviewed again.

[C] WHOM TO SUBMIT

The papers, on line, on CD and 3-hard copies should be sent to the Managing Editor, Proceedings of the National Academy of Sciences, India (Section A - Physical Sciences); 5 Lajpatrai Road, New Katra, Allahabad - 211 002 (E-mail : sahai.nasi@gmail.com).

[D] HOW TO SUBMIT

The authors may submit the papers directly or forwarded through a Fellow of the Academy as prescribed above. It is mandatory to submit "An Electronic Version on CD" as well as "three hard-copies". The text of the manuscript as per format of the journal outlined below, and preferably with scanned figures, should be supplied as a plain ASCII file (Wordstar)
5.5 or 7.0 and Microsoft Word for Windows 6.0 are also acceptable, but ASCII is preferred. The language of the , journal is English.

[E] FORMAT OF THE MANUSCRIPT

(I) The Proceedings is published in 'two column format' on A4 page.
(II) The manuscript should be typed double spaced in 12-font size (Arial/Times/New Times Roman) on one side of good quality A4 size paper with one-inch margins. Insert hard returns only at the end of paragraphs. Page number should appear in the upper right hand corner of each page, beginning with the title page. File format for the text are MS-Word, Word Perfect or LaTeX.

Title : 16 pt. font size, bold, starting from the left hand margin, keeping single gap between the lines, first letter of first word capital, others except symbols and proper nouns, in lower case (lc). A short running title should be provided.

Author's Name (s) : 10.5 pt. font size cap letters followed by, 'and' before the last author, 'and' in lc, superscripts for address and Email IDs with symbols like *,$,£ ...in size 8 pt., starting from the left hand margin, and double gap between title and authors. Authors who are fellow of the Academy should write FNASc after their name.

Address : 10.5 pt. font size in italic. India be included from the Indian address also, for foreign papers name of the · ountry is needed in the address. In address should authors avoid writing the short (abbreviated) forms. Address starts from the left hand margin with 'single 'gap between authors' name and address.

Email IDs : 10.5 pt. font size in italic, setting at the left hand margin.

Received : Month, Date, Year ; **Finally revised** : Month, Date Year; **Accepted** : Month, Date, Year, (NASI office will provide)

Arrangement of the text

The text of the paper should be arranged into Abstract, Introduction, Materials and Methods, Results, Discussion, Conclusions, Acknowledgements and References in the format given below.

Abstract (150 words) : Heading setting centre of the column in 9 pt. font size, bold starting with paragraphing and the size of superiors and inferiors in 7 pt.

Keywords : Heading 9 pt. bold starting at left hand or right hand margin as the case be, written within ( ), each word (maximum of 5 words) 9 pt. normal with 'double' gap separated by '/'.

Headings : (Introduction, Materials and Methods, Results and Discussion, Conclusion, other important headings, References) in 10.5 pt. bold set in the centre of the column. For many words, each word to start with first letter 'Cap' and prepositions in 'lc' with double gap.

Subject Matter : 10.5 pt. normal starting with paragraphing superiors and inferiors in 8 pt., gap between the lines single for running matter and double gap after the paragraph.

Equations : 10.5 pt normal italic should be composed in **Corel Equation/Equation Editor.**

Equations centre setting, variables in italics, operators such as log, ln, cos, Im, Re, e, exp in 'lc' and normal. Equation numbers in the right end of the column within ( )
Equation Should be broken where mathematical operations lile+, − and x occur, and aligned after = sign of top line.

Long equations should be broken with different nomenclatures such as

$p = f(x, y, z, t, u, v, w \ldots\ldots\ldots\ldots\ldots)$

$= P_1 + P_2 \pm P_3 \times P_4 + \ldots\ldots\ldots\ldots$ etc. and define P_1, P_2, P_3,.........., very likely it may minimize the errors.

Inferiors and superiors : in 8 pt., and greek letters in 10.5 pt.

Subheadings : 10.5 pt. normal italic, aligned with running matter and running matter be paragraphed.

Sub-subheadings : 10.5 pt. italic, followed by colon':' subject starts just after the sub-subheading.

Tables : Tables should be numbered consecutively using Arabic numerals, have self-explanatory title and submitted separately from the text. Footnotes to tables should be indicated by superscript lower-case letters. Abbreviations should be explained in the footnotes.

Tables be set 9 pt. normal for matter and units and italic for symbols.

Table 1-Title (First-letter capital, other words in lc). No horizontal and vertical lines, except the top and bottom horizontal lines. In text matter it should be referred as Table 1, 2 etc.

Figures : All figures should be numbered consecutively using Arabic numerals. Line drawings and inscriptions should be legible. In case of scanned figures/line drawings, minimum resolution of 800 dpi should be used. All figures should be labeled on the back to indicate figure numbers, top margin and authors. Legends should be brief, self-explanatory, typed on separate page and placed at the end of the text.

Figures be drawn in black colour on Tracing Paper, size preferable (8 cm × 10 cm) for printing in single column size, (15 cm × 12.5 cm) for larger figure printing in double column, letters in New Times Roman, axes be labeled in 10.5 pt., description of the figure be given in figure caption, figures be referred in the text as Fig. 1 (2 etc.), photographs be in good contrast suitable for reproduction. Figures in chemistry should be drawn in CHEMDRAW/ISIS

Units : In the same font size as the subject matter, viz in abstract 9 pt. normal, in the text 10.5 normal. In SI units with standard symbols viz. mass kilogram 'kg', length meter 'm', time second 's', energy Joule 'J', power 'W', conductance Siemen 'S', resistance Ohm 'Ω', and so on.

References : should be indicated in the text by superscript Arabic numerals. The list of references should be arranged in order of their occurrence in the text. References should be given in 9 pt. normal. Authors name starts with 'Surname' followed by ',' and initials. Name separated by ', ' followed by the title of the paper in normal style. Name of the journal in italics following standard abbreviations of the names of periodicals given in the World list of Scientific Periodicals such as Journal of Chemicla Physics (USA) as *J. Chem. Phys. (USA)*. After the name of journal, year; volume number in 'bold', followed by colon ':' then starting and ending page numbers

Examples are given below

Journals :

Chana SJ. Diffraction of plane dilational waves by finite crack. *Quart J Mechanics Appl Math* 1971; **24** : 423-443.

Healy D, Bloor D, Gray D & Cross GH. Stabilized nonlinear optical chromophore alignment in high-Tg guest-host polycarbonate. *J phys D: Appl Phys* 1997; **30** : 3079-3084.

Books : Lakcmore JS. Solid State Physics. Toronto : WB Saunders, 1974.

Gradshteyn, IS & Ryzhik, IM Tables of Integrals, Series and Products, Academic Press : New York 1980, p. 287 .

Abstract in Conference/Symposium : Kumar S, Arora S, Vij DR & Chaturvedi DK. Thermal and optical studies of guest-host polymeric systems, National Conference on Advanced Characterization Technique on Nanomaterials, 2005, Aug. 24-26, Roorkee, India.

Dissertation : Mehra PS. & Sinha MS. Dielectric Dispersion and Absorption in Polar Liquids. D Phil Thesis, University of Allahabad, Allahabad, 1982

Patent : Srivatava N, Singh MM & Ray S. A process for the preparation of tertiary aminoalkoxy derivatives of substituted diaryl-5,6,7,8-tertrahydronaphthyl methane and their salts useful as fertility regulating agents. *Indian Patent 187178, Central Drug Research Institute, Lucknow, 1998.*

Websites : URL of the website should be mentioned e.g., www.nasi.org.in

Graphical Abstract : A graphical abstract of about 50 words on right column and a suitable figure or equation in left column should be provided for the contents page of the journal.

[F] PREPARATION OF ELECTRONIC VERSION (CD)

Ensure that your manuscript files are virus-free. Use only a new CD.

Write the information on the disk label : 1. File name(s). 2. name of Software and version used. 3. Name of corresponding author. 4. Dispatch date

[G] AUTHORS SUGGESTION FOR PROBABLE REFEREES

Authors are encouraged to give 4-5 names of referees.

[H] MISCELLANEOUS

(i) all papers will be screened by a strict refereeing procedure. However, the responsibility for the authenticity of the contents lies with the authors.

(ii) If a paper is recommended for revision, a maximum of 2 months would be given to authors for revising the manuscript, otherwise it would be treated as a fresh communication. The covering letter should indicate the changes made in response to referee's comments.

(iii) The corresponding authors will receive galley proof of the paper from the Academy's Editorial Office. They should return the corrected proof within a week of its receipt. Error free publication is the responsibility of the authors.

(iv) No change in the text of the paper will be made after the matter has been composed by the Press. If it is absolutely essential, a postscript may be added.

(v) Upon acceptance of the paper, authors will be asked to transfer copyright of the paper to the publisher. The transfer will ensure wide dissemination of information.

(vi) **Reprints**; 25 free reprints will be given to the corresponding author for each paper.

(vii) All efforts will be made to publish the paper in about 3-4 months after having received the accepted paper in final form from the author.

(viii) Manuscripts not accepted for publication will not be returned unless specifically requested by the corresponding author.

[I] SUBSCRIPTION RATE OF THE JOURNALS

Annual Subscription for both Sections (See A-Physical Sciences and Sec B-Biological Sciences) : Rs. 500.00; **for each** Rs. 250.00; **Single Copy :** Rs. 100.00, **Foreign Subscription :** (a) for one Section : US $100, (b) for both Sections US $200. **(Air Mall charges included in foreign subscription).**

Kind Attention : Fellows and Members of the National Academy of Sciences, India

(Please fill items and return to the Managing Editor – Proceedings of the National Academy of Sciences, India (Sec A – Physical Sciences; Sec B – Biological Sciences)

The Editorial Boards and Board of Editors of the Journals of the Academy viz. **Proceedings of the National Academy of Sciences, India (Sec A – Physical Sciences)**, **Proceedings of the National Academy of Sciences, India (Sec B– Biological Sciences)** and **National Academy Science Letters,** request its esteemed Fellows and Members to inform their willingness for acting as learned referees for the research papers received for publication in the above Journals They are also requested to suggest other names of subject experts who may be requested for refereeing as per following proforma.

UPDATED DATA OF REFEREES' PANEL FOR THE JOURNALS OF THE NATIONAL ACADEMY OF SCIENCES, INDIA

(I) 1. Name, Designation, Affiliation and ....

Postal Address of the Fellow/Member ....

....

....

(a) Telephone No. (with area code) ....

(b) Fax No. (with area code)..

(c) E-mail Address..

2. State whether a Fellow or Member ....

3. Subject/Sub-disciplines of your expertise in which you are willing to act as Referee.

Sl. No.	Major Disciplines (Such as Physics etc.)	Sub-discipline alonwith super-speciality	Experimental/Theoretical or both
1.		(i) (a) (b)	
2.		(ii) (a) (b)	
3.		(iii) (a) (b)	

(II) Suggestions regarding additional referees

Sl. No.	Name(s) & Address of those whom you suggest for refereeing	His/Her Major Disciplines (such as Physics etc.)	His/Her Sub-disciplines alongwith any Super-specialities	Experimental/Theoretical or Both
1.			(i) (a) (b)	
2.			(i) (a) (b)	
3.			(i) (a) (b)	

Signature of the Fellow/Member

The National Academy of Sciences, India

(Registered under Act XXI of 1860)
Founded 1930

Regd. No. R.N. 35621/78

CONTENTS

The Journal is Abstracted/Indexed in Science Citation Index Expanded (SCIE) also known as SciSearch, and Journal Citation Reports/Science Edition of Thomson Reuters products and Custom Information Services, Thomson Scientific, Philadelphia, PA 19104, USA (http://scientific.thomson.com); CABI, Wallingford, OXON OX 10 8DF, UK (journalreview@cabi.org); Zentralblatt MATH, Franklinstrasse 11, 10587 Berlin/Germany (http://www.zentralblatt-math.org) and others.

Full and free access to Academy journals available on the website http://nasi.iiita.ac.in/library (Courtesy IIIT, Allahabad)